



UNIVERSITAT POLITÈCNICA DE CATALUNYA  
BARCELONATECH

---

Departament d'Enginyeria Electrònica

*INDUCTIVE CONTACTLESS ENERGY TRANSFER  
SYSTEMS FOR RESIDENTIAL AREAS*

Thesis submitted in partial fulfillment of  
the requirement for the PhD Degree issued  
by the Universitat Politècnica de Catalunya,  
in its Electronic Engineering Program.

*Arash Momeneh*

Director: Dr. Miguel Castilla Fernández

July 2016



*Believe in yourself and all that you are. Know that there is  
something inside you that is greater than any obstacle.*

*Christian D. Larson*



---

## Summary

---

In recent years, contactless energy transfer systems have been developed and investigated widely. As evident, the transfer energy is performed without physical connection. This technology is classified according to power level and place of use. However, the most commonly used one is inductive contactless energy transfer system due to its higher efficiency. The inductive contactless system is responsible to deliver the electrical energy to the loads by means of a long winding loop and sliding transformers. In this system, the output converter and load are directly connected to the secondary side of transformer. Moreover, the secondary side transformer has the capability to move along the primary winding loop. According to this capability, and also possibility to construct long contactless system, it can be used as an electrical energy delivery system for mobile receivers. Also, the ICET technologies improve the safety of the final user by means of the elimination of electrical shocks. It is resulted from using a high-frequency resonant transformer which provides electrical isolation. This feature is particularly important in wet environments such as in swimming pools, gardens and bathrooms. Therefore, it is a good alternative system for implementing in the residential area instead of conventional systems.

Implementation of the inductive contactless system in residential area presents several challenges. In this dissertation, several solutions are presented and discussed. In the first chapter, the concept of the contactless energy transfer system is explained. Also, the chapter classifies the contactless system according to the technology and the output power. In chapter two, a new adaptive control algorithm for the fully-controlled contactless energy transfer system is presented. The new adaptive algorithm operates dynamically with the load changes, resulting in maximum efficiency in all the load conditions. Moreover, the mathematical framework of the contactless system with new adaptive algorithm is presented. In chapter three, a partially-controlled inductive contactless system as an alternative to the fully-controlled topology is introduced. The features of the new topology are analyzed by considering several modulation techniques, including frequency modulation, phase modulation and quantum modulation. The

performance of the new topology is evaluated and the best modulation technique is identified. The chapter is finished with the design of the new topology with the best modulation technique. In chapter four, the analysis, design and implementation of a simple and cost-effective technique to supply the residential contactless energy transfer system with multiple mobile loads is presents. The topology is based on the cascaded connection of a closed-loop buck converter and a high frequency resonant inverter operating in open loop which is loaded by several output passive rectifiers. The proposed system includes a sliding transformer to supply the mobile loads, leading to a safe and flexible location of loads. The theoretical analysis and design of the proposed system is based on a mathematical model derived using the first harmonic approximation. Selected experimental results are included to verify the system features. Finally, the dissertation concludes with remarks regarding the results.

---

## Acknowledgment

---

This research has been carried out at the Technical University of Catalonia, Spain, in the group of power electronic and control system (PECS). This thesis could not have been finished without the help and support of many people. I would like to take this opportunity to express my gratitude to them.

First of all, I wish to express my sincere gratitude to my supervisor Dr. Miguel Castilla. I am truly grateful to him for trusting in my ability to complete this work and for his valuable suggestions and ideas during this work. His patience and kindness are greatly appreciated.

I would also like to thank fellow Ph.D. students (Ramon, Javi.M, Mohammad, Javi.T....) for always keeping the spirits high and maintaining a cheerful atmosphere in the PECS lab, I would like to thank Prof. Luis Garcia de Vicuña and Dr. Jaume Miret for their inputs.

Finally, I would like to thank my mother and father, which give me the possibility to continue my education and support me always.



---

## **Confidentiality**

---

This dissertation is the result of my own work in collaboration with the company Optimos Apto B.V., Rotterdam, The Netherlands, with contract number of C-08843 and C-10065. This study has done during 2012 to 2016 and supported by this company. The chapter two of this dissertation cannot be published according to a confidentiality agreement between Technical University of Catalonia and Optimos Apto company till September 2017.



---

# Contents

---

<b>Summary</b>	<b>iii</b>
<b>Acknowledgment</b>	<b>v</b>
<b>Confidentiality</b>	<b>vii</b>
<b>Contents</b>	<b>ix</b>
<b>List of Figures</b>	<b>xiii</b>
<b>List of Tables</b>	<b>xvii</b>
<b>Chapter1</b>	
<b>State-of-the-art and thesis objectives</b>	<b>1</b>
1.1. Historical context and current state.....	3
1.2. Contactless energy transfer system.....	5
1.2.1. Acoustic CET system .....	5
1.2.2. Light CET system .....	6
1.2.3. Capacitive CET system.....	7
1.2.4. Inductive CET system .....	8
1.2.4.1. ICET with cascaded transformer .....	9
1.2.4.2. ICET with multiple secondary transformers .....	9
1.2.4.3. ICET with sliding transformer.....	10
1.3. Low power ICET system.....	11
1.3.1. Induction cookers .....	11
1.3.2. Electrical toothbrushes .....	12
1.3.3. Transcutaneous energy transfer .....	12
1.3.4. Desktop peripherals and mobile phones .....	13
1.4. High power ICET system .....	13
1.4.1. Electrical vehicles and ICET charging .....	13

1.4.2. Industrial transport and automation .....	14
1.4.3. Military and space systems .....	15
1.5. ICET systems for residential areas .....	15
1.5.1. Indoor ICET applications .....	16
1.5.2. Outdoor ICET applications .....	18
1.6. Problem formulation .....	19
1.7. Research objectives and thesis organization .....	21
1.8. Conclusion .....	22

## **Chapter2**

<b>Adaptive control algorithm for the fully-controlled ICET System</b> .....	<b>23</b>
2.1. Introduction .....	25
2.2. Mathematical modeling .....	26
2.2.1. State-space model .....	26
2.2.2. Nominal solution .....	27
2.2.3. Averaged large-signal model .....	27
2.2.4. Sliding mode controller .....	28
2.3. Static $\alpha$ algorithm .....	31
2.4. Basic dynamic $\alpha$ algorithm .....	33
2.5. Load-sensitive dynamic $\alpha$ algorithm .....	36
2.6. Conclusion .....	39

## **Chapter3**

<b>Analysis and design of a partially-controlled ICET system</b> .....	<b>41</b>
3.1. Introduction .....	43
3.2. ICET system under study .....	44
3.3. ICET system with frequency modulation technique .....	45
3.4. ICET System with phase modulation Technique .....	50

3.5. ICET system with quantum modulation technique .....	60
3.6. Design of the resonant transformer .....	66
3.6.1. Effect of the resonant frequency .....	66
3.6.2. Effect of the magnetizing inductance .....	67
3.6.3. Effect of the characteristic impedance .....	69
3.7. Evaluation of the transient response .....	71
3.8. Conclusion .....	75

## **Chapter4**

<b>Simple and cost effective solution for the partially-controlled ICET system</b> .....	<b>77</b>
4.1. Introduction .....	79
4.2. Proposed topology to supply multiple mobile clamps .....	79
4.2.1. Description of proposal .....	80
4.2.2. Discussion on the proposal .....	81
4.3. Mathematical modeling of the proposed topology .....	83
4.3.1. Model of the proposed topology .....	83
4.3.2. Angular resonant frequency .....	84
4.3.3. Output voltage .....	86
4.3.4. Design condition for the reference current .....	86
4.4. Design of the proposed topology .....	87
4.5. Experimental validation and comparison .....	88
4.5.1. Comparison between the conventional and proposed topologies .....	89
4.5.2. Performance in steady state .....	92
4.5.3. Performance in transient state .....	94
4.5.4. Cost comparison .....	95
4.6. Conclusion .....	96

## **Chapter5**

<b>Conclusions and future work</b>	<b>97</b>
5.1. Overview .....	99
5.2. Main results and innovative contributions .....	99
5.3. Outlook and perspectives .....	101

## **Bibliography**

---

# List of Figures

---

## Chapter1

1.1	Classification of CET systems .....	5
1.2	Basic principle of an acoustic CET system .....	6
1.3	Basic principle of a light CET system .....	6
1.4	Basic principle of the capacitive CET system .....	7
1.5	Basic principle of the inductive CET system .....	8
1.6	Basic principle of the inductive ICET with cascaded transformers .....	9
1.7	Basic principle of the inductive ICET with multiple secondary winding .....	10
1.8	Basic principle of the inductive ICET with sliding transformers .....	11
1.9	Electrical vehicles and CET charging system .....	13
1.10	Electrical train with CET rechargeable technology .....	15
1.11	Indoor ICET distribution energy .....	16
1.12	Diagram of the ICET system with various mobile clamps .....	17
1.13	Schematic of the conventional ICET with multiple mobile clamps .....	18
1.14	Control diagram of the conventional topology .....	18
1.15	Outdoor ICET distribution energy .....	19

## Chapter2

2.1	Proposed input sliding-mode control scheme .....	30
2.2	Relation between $\bar{u}_p$ and $\alpha$ in FL/FL condition .....	33
2.3	Flowchart for $\alpha$ generation .....	34
2.4	Main waveforms with dynamic $\alpha$ ( $R_{o1} = R_{o2} = 12.9$ ) .....	34
2.5	Main waveforms with dynamic $\alpha$ ( $R_{o1} = R_{o2} = 129$ ) .....	35
2.6	Main waveforms with static $\alpha$ ( $R_{o1} = 12.9, R_{o2} = 129$ ) .....	35
2.7	Main waveforms with dynamic $\alpha$ ( $R_{o1} = 23.45, R_{o2} = 23.45$ ) .....	35
2.8	$\alpha$ generator and load change detector flowchart .....	36
2.9	Output voltage ( $v_{oi}/10$ ) and $\alpha$ variation. (10% of full load to full load) .....	37
2.10	Output voltage of clamp1 ( $V_{oi}/10$ blue) and $\alpha$ variation (red) .....	37

2.11	Zoom in on Fig.2.10.(a) .....	38
2.12	Transient response of $i_{ref}$ as a function of $\alpha$ . .....	39

### Chapter3

3.1	General diagram of the ICET system with two clamps .....	44
3.2	Schematic of the resonant transformer with sliding transformer and two mobile clamps ...	44
3.3	Electrical circuit representation of the RT system with sliding transformer and two mobile clamps .....	45
3.4	Frequency modulation diagram of the input converter .....	46
3.5	Gain curves for different designs and load combination .....	47
3.6	Gain curves for design 400kHz .....	48
3.7	Phase modulation diagram of the input converter .....	51
3.8	Principal waveforms of the phase modulation .....	51
3.9	Main waveforms of the SRC single-clamp with PM (design 100kHz) .....	52
3.10	Gain of the SRC with PM as a function of $\gamma_2$ for one receiver .....	53
3.11	Input voltage of the resonant tank (top) and input current of the Converter (bottom) for $\gamma_1 = 0.7$ , $\gamma_2 = 0.45$ and $R_o = 176 \Omega$ (design 100kHz).....	55
3.12	Gain curves for design 100 kHz as a function of the parameter $\gamma_2$ for two clamps .....	56
3.13	Gain curves for design 200 kHz as a function of the parameter $\gamma_2$ for two clamps .....	57
3.14	Gain curves for design 1MHz as a function of the parameter $\gamma_2$ for two clamps .....	57
3.15	Gain curves for design 250 kHz as a function of the parameter $\gamma_2$ for two receivers .....	58
3.16	The quantum modulation diagram of the input converter .....	61
3.17	Principal waveforms for the quantum modulation .....	61
3.18	Waveforms with QM control for $R_o = 176 \Omega$ (left) and $R_o = 1760 \Omega$ (right).....	62
3.19	Primary-side resonant current, $i_p$ , and secondary-side current, $i_s$ , for design 100kHz .....	64
3.20	Gain curves for different designs and loads .....	68
3.21	Gain curves for different designs of magnetizing inductance and loads .....	70
3.22	Current waveforms for transformer primary-side (top) and secondary-side (bottom).....	72
3.23	The control scheme of the output DC/AC converters shown in Fig. 3.1 .....	73
3.24	Main waveforms of the complete ICET system .....	74
3.25	Response to step load disturbances in the proposed topology with two high-voltage/high-power clamps .....	75

### Chapter4

4.1	Schematic of the proposed DC/DC converter with multiple mobile clamps .....	80
-----	---	----

4.2	Output waveforms of the resonant inverter .....	81
4.3	Equivalent circuit of the proposed topology .....	83
4.4	Experimental set-up with two mobile clamps .....	88
4.5	Measured output voltage $v_{oi}$ (Top, 10V/div) and resonant current $i_r$ (500 mA, 50 $\mu$ s/div) ...	90
4.6	Measured resonant current $i_r$ and voltage $v_p$ in two load conditions. Full load (top) and 10% full load (bottom) .....	91
4.7	Efficiency as a function of load. Conventional topology (grey), proposed topology (black).	92
4.8	Measured input voltage $v_z$ as a function of load .....	92
4.9	Steady state output voltage $v_{o1}$ , $v_{o2}$ as a function of load demand .....	93
4.10	Experimental results of the output voltage $v_{oi}$ as a function of clamp position along the primary winding loop. ....	93
4.11	Experimental results of the output voltage $v_{oi}$ as a function of clamp air gap .....	93
4.12	Main waveforms of the proposed topology in transient-state .....	95



---

# List of Tables

---

## Chapter2

2.1	Optimal alpha values for several load conditions .....	31
2.2	Searching for the optimal alpha values manually .....	32
2.3	Searching for the optimal alpha values manually with more precision .....	32
2.4	Efficiency in different load conditions .....	39

## Chapter3

3.1	Design of 100kHz for two clamps with FM control .....	49
3.2	Design of 200kHz for two clamps with FM control .....	49
3.3	Design of 400kHz for two clamps with FM control .....	50
3.4	Design 100kHz for one clamp with PM control .....	54
3.5	Design 200kHz for one clamp with PM control.....	54
3.6	Design 1MHz for one clamp with PM control .....	54
3.7	Design 100kHz for two clamps and PM control .....	58
3.8	Design 200kHz for two clamps and PM control .....	59
3.9	Design 250kHz for two clamps and PM control .....	59
3.10	Efficiency results for selected designs operating with the PM and FM .....	60
3.11	QM control with design of 100kHz for two clamps .....	62
3.12	QM control with design of 200kHz for two clamps .....	62
3.13	QM control with design of 1MHz for two clamps .....	63
3.14	QM control with design of 250kHz for two clamps .....	63
3.15	Efficiency results for selected design operating with PM, FM and QM for single clamp ..	65
3.16	Best efficiency results for QM, FM and PM. ....	65
3.17	Comparison between modulation techniques .....	66
3.18	Considered designs for the resonant circuit as a function of the resonant frequency .....	67
3.19	Measured gains and efficiencies for the two clamps RT system .....	69
3.20	New designs for the RT system considering several values of the magnetizing inductance.	69
3.21	Measured gains and efficiency of the designs with variable magnetizing inductance .....	71
3.22	New designs for several values of the characteristic impedance $Z_o$ .....	71
3.23	Measured gains and efficiency for the designs with variable $Z_o$ .....	71

3.24 Proposed parameter values for RT system ..... 72

**Chapter4**

4.1 Circuit parameters for the proposed design ..... 87  
4.2 Circuit parameters for the proposed topology ..... 89  
4.3 Circuit parameters for the conventional topology ..... 90  
4.4 Comparison between conventional and proposed topologies ..... 96

# CHAPTER 1

---

---

## State-of-the- art and thesis objective

---

### Summary

---

1.1 HISTORICAL CONTEXT AND CURRENT STATE .....	3
1.2 CONTACTLESS ENERGY TRANSFER SYSTEM.....	4
1.3 LOW POWER INDUCTIVE CONTACTLESS ENERGY TRANSFER SYSTEM.....	11
1.4 HIGH POWER INDUCTIVE CONTACTLESS ENERGY TRANSFER SYSTEM .....	13
1.5 ICET SYSTEMS FOR RESIDENTIAL AREA .....	15
1.6 PROBLEM FORMULATION .....	19
1.7 RESEARCH OBJECTIVES AND THESIS ORGANIZATION .....	21
1.8 CONCLUSION .....	22

---

This chapter introduces the concept of contactless energy transfer (CET) system. From a historical review to the description of the typical applications, the chapter classifies the CET systems according to the technology and the output power. Likewise, a problem formulation is presented in order to highlight the present unsolved problems for the inductive CET system. Moreover, the main objectives of this thesis also is presented.



## 1.1. HISTORICAL CONTEXT AND CURRENT STATE

In the last decades, the dream of transfer energy without using the cables it seemed out of reach. The people watched the science fiction movies and were being surprised about these phenomena. Nicola Tesla (1856-1943) introduced this technology in 1899-1900. He did several experiments on wireless reception and transmission through the air. For example, he was remote supply of 200 light bulbs through the ground from a distance of about 40 km [1].

After Nicola Tesla for a long time any person did not work on this technology. However, the first reported researches on the so-called energy transport by inductive coupling date from the 1960s [2]. Although this technology has been known for many years, but always remained immature. Nevertheless, the first commercial application as toothbrushes appeared in the 1990s. In the last decade, few companies were interested in constructing these kind of devices. The reasons were probably the doubts on user safety and the lack of standards and regulations.

The first general guidelines were published in 1998 by scientific committee [3]. The focus of these guidelines was avoiding any kind of health risks concerning the exposure of the population to electromagnetic fields. This recommendation makes the restriction for the immersed body proportion, public exposure as a function of the operating frequency and the size of the coils. However, they are not relevant according to [4]. Therein, due to these restrictions the size of the coils for common applications is about 40mm to 100mm which could transfer less than 30mW.

In 2008, the Wireless Power Consortium (WPC) created the protocols related to inductive CET systems. These protocols are created in order to unify the companies work related to the CET technology. Although at that time only eight companies were included in this consortium and were being active in this domain, thanks to its great success nowadays more than 100 companies are in this consortium. Basically the WPC aims to set the standard for interoperable wireless charging [5]. In July 2010, the new standards are prepared which called 'Qi'. These new standards are designed for 5W.

## 1.2. CONTACTLESS ENERGY TRANSFER SYSTEM

Despite the work of Tesla, nowadays the popular way to transfer the energy is conductive wires. Moreover, the reasons for the popularity of energy transfer by electrical conduction are:

- Good efficiency due to small loss
- Low cost for installation and copper guiding material
- Easy to install and convenient to use
- Good tracking of energy flow

However, the cable networks distribute energy all the way from the power plants up to the homes, industrial areas and office buildings. Nevertheless, the energy transfer by electrical conduction has some disadvantages:

- Electrical shocks due to the physical contacts (not safe).
- Electrical wiring is a big problem for many plant engineers or production system designers.
- Installing the wires to rewiring as production lines need to be changed to repair damaged cables and connections, electrical wiring represents an ongoing cost and risk for downtime in manufacturing plants.
- Limits to use the wires in specific places (swimming pool, garden, etc.).
- The miles of electrical wiring that snake around any manufacturing facility, hanging down from ceilings and extending across corridors between equipment, have been viewed as a necessary aspect of industrial automation.

Therefore, in this decade the companies are so interested in replacing the conductive transfer energy by contactless system. In addition, it can be interesting to know about somewhere contactless energy transfer is an ideal application [6]:

- The mobile equipment has to cover long distances
- A variable, extendable track layout is required

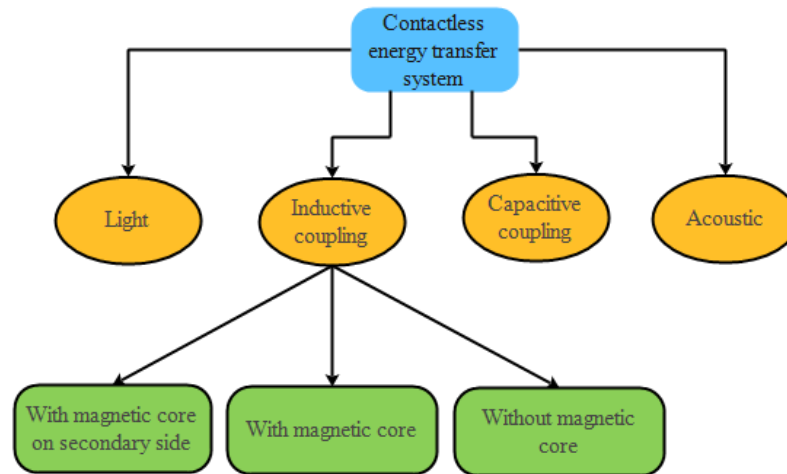


Fig.1.1. Classification of CET systems

- High speeds have to be achieved
- The energy transfer has to be maintenance free
- Additional environmental contaminants are not permitted in sensitive areas
- The operation takes place in wet and humid areas

The CET systems are becoming increasingly feasible as flexible and relatively safe suppliers of energy. This technology can be generally divided into four groups based on the medium used: acoustic, light (optical), capacitive and the largest group of inductive coupled CET systems (see in Fig.1.1). In addition, the CET systems are used in power range from  $\mu\text{W}$  (sensors, actuators, biomedicine, etc.) till several hundred kW (cranes, electrical vehicles, fast battery charging, etc.) [8]–[40].

### 1.2.1. ACOUSTIC CET SYSTEMS

Fig.1.2 shows the basic principle of operation of the acoustic CET system [8]. The power electronic circuits convert the electrical energy into a pressure wave by a transmitting transducer. The produced wave is transferred through a medium (air, living tissue, etc.). After that, it is received by the receiving transducer which is positioned along the path of the sound wave. Finally, the inverse process converts the sound wave into electrical energy. In the final stage, a rectifier with capacitive filter supplies a load. In this technology normally piezoelectric materials are used for transmitting and receiving transducers.

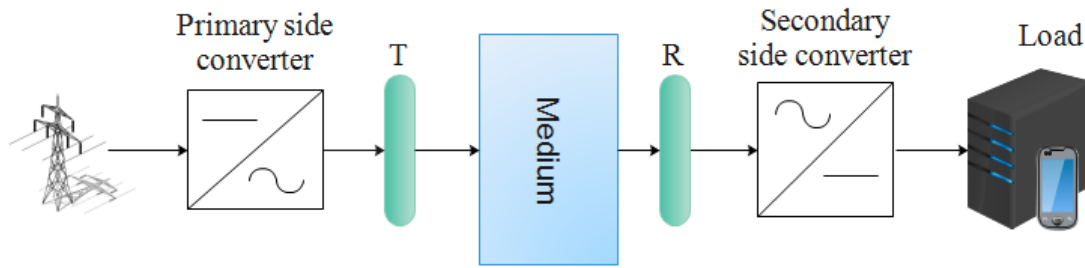


Fig.1.2. Basic principles of an acoustic CET system. The transmitting transducer (T) and the receiver (R).

Typically, the efficiency of the acoustic CET is low in comparison to the other CET systems. However, the efficiency can be notable when the distance between the receiver and transmitter is short [8]-[13]. Some applications such as biomedical (power range up to 100 mW, efficiency up to about 40%) or through-wall application (for example, sensors in nuclear systems) are using this technology [14]-[15].

### 1.2.2. LIGHT CET SYSTEM

Fig.1.3 shows the operation of light or optical CET system. In light CET system, the laser diodes are responsible to generate the optical power beam. This energy is transferred through the medium. Then, the photovoltaic diodes (PV) converts power beam into the electrical energy. Although the optical system is able to transfer massive amounts of energy, the actual application is limited. The main reason is that the efficiency is low in long distances due to its dispersion losses. The power level of this technology is in the range below 1W up to dozens W. Also, the efficiency for optical-electrical conversion is around

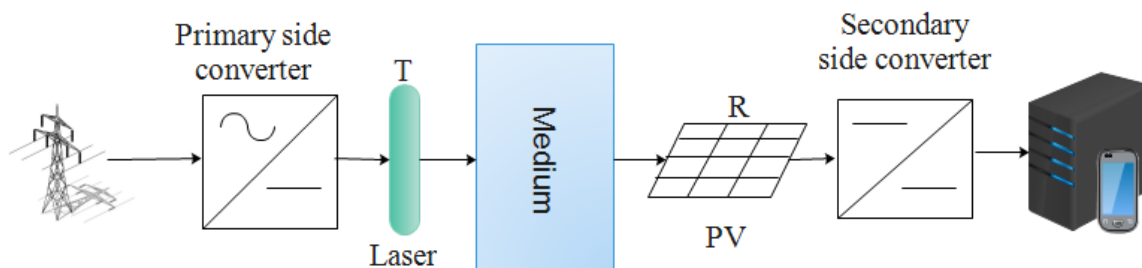


Fig.1.3. Basic principles of a light CET system. The transmitting transducer (T) and the receiver (R).

20% - 50% [10], [16]-[17]. Normally, this technology is employed in spacecraft platforms and terrestrial technologies [16]-[17].

### 1.2.3. CAPACITIVE CET SYSTEM

Fig.1.4 illustrates the operation principle of capacitive CET system. It consists of a high frequency primary resonant converter, two primary and secondary plates, output converter and capacitive filter. When secondary side plates are placed additionally to the primary side ones, the alternating electrical field is produced. Therefore, the current is flowing through them and the energy is transferred to the load without any direct electrical connection. As a consequence of this principle of operation, freedom of movement for secondary side plates is obtained. Also, an inductor (not shown in the figure) is normally connected in series with the secondary coupling plates. This inductor increases the output power and regulates the equivalent coupling capacitor. Finally, a full bridge rectifier with capacitive filter is implemented to supply the load. Generally, to provide electrical isolation and increasing the coupling capacitance, the surface of the coupling metal plates is coated with dielectric materials [18]-[20].

As a consequence of employment an electrical field in this technology, surroundings becomes less of an issue. Moreover, the electromagnetic interference (EMI) is reduced thanks to the constrained nature of the electric field between the plates. In this system, the

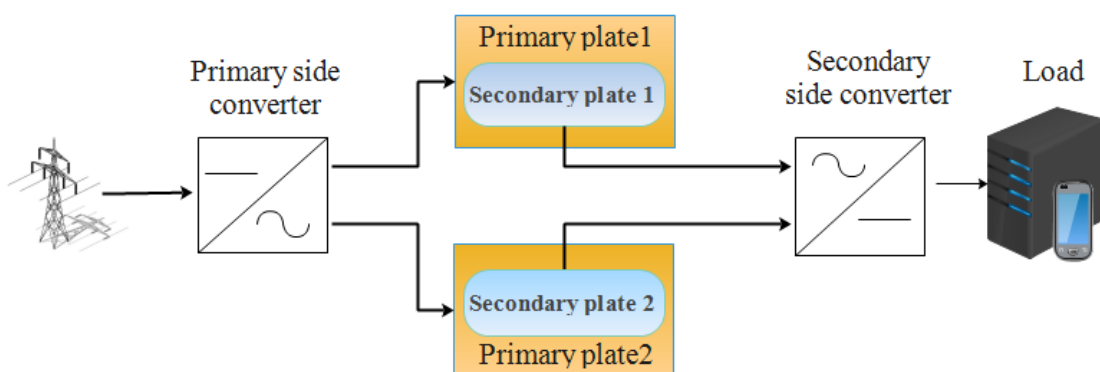


Fig.1.4. Basic principle of the capacitive CET system.

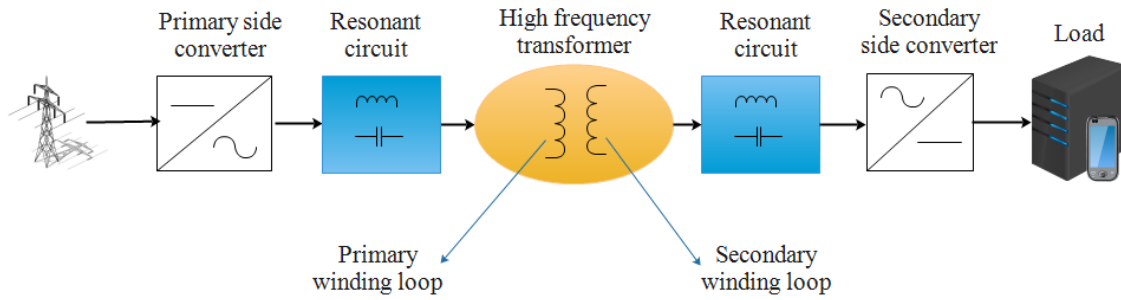


Fig.1.5. Basic principle of the inductive CET system.

power level and efficiency is in the range of 5-50 W and 50%, respectively [11]-[13]. The applications are mainly in soccer playing robots, mobile phones, sensors for respiratory devices, bio potential measurement system, etc. [19]-[20].

#### 1.2.4. INDUCTIVE CET SYSTEM

The basic principle of the inductive contactless energy system (ICET) is shown in Fig.1.5. The resonant converter in the primary side is responsible to convert the DC voltage into a high frequency AC voltage. Then, the high frequency AC energy is transferred via high frequency transformer to the secondary side receiver. Note that the direct electrical connection between the primary and secondary side does not exist. Therefore, the load can be a movable (linearly or/and rotating). Also, as a consequence of this property electrical shock can be eliminated. Normally, a diode rectifier with capacitive filter is implemented as a secondary side converter. Nevertheless, an active rectifier is used in some applications for stabilizing DC or AC loads [22]-[33].

The ICET system can be implemented by different transformer cores. These transformers are chosen according to the power range and air gap length. Therefore, several ICET systems such as cascaded transformers, multiple secondary side winding and sliding transformer with long primary winding can be formed.

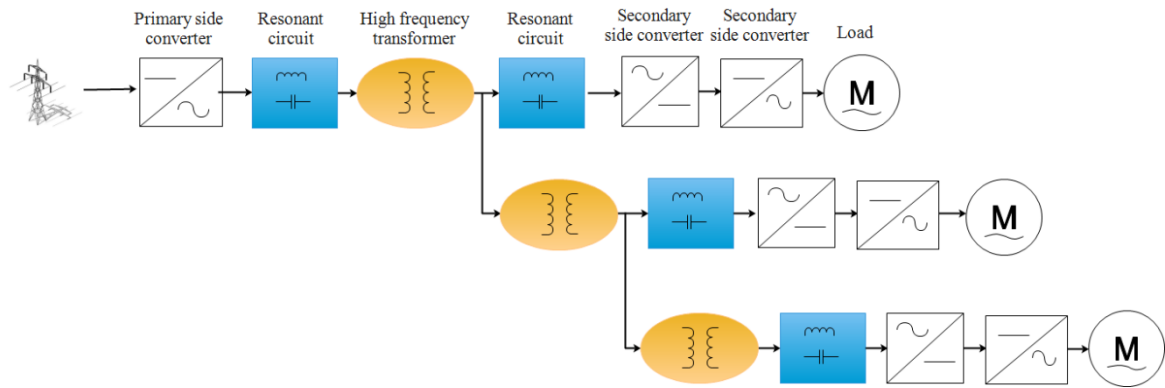


Fig.1.6. Basic principle of the inductive ICET with cascaded transformers.

### 1.2.4.1. ICET WITH CASCADED TRANSFORMERS

Fig.1.6 illustrates the basic principle of ICET with cascaded transformer. The DC/AC power converter in collaboration with resonant elements generates the square voltage waveform. The range of this square voltage is about 200-600 V and 20-60 kHz. The produced voltage is used to supply the primary winding of rotatable transformer located on the first axis of the robot. Then, voltage is converted by secondary AC/DC/AC power converters. The secondary side converters are using PWM technique to generate variable frequency AC voltage for supply three-phase motors. As evident from the figure, the secondary side of each transformer is connected to the primary side of the second rotatable transformer located on the second joint of the robot. In this system, several transformers can be added to create the arrangement of an AC bus throughout the robot. Usually, this topology applies to robots [21]-[25] and multilayer optical disc [26] where the output power rang for these devices are 10-20 kW [21].

### 1.2.4.2. ICET WITH MULTIPLE SECONDARY WINDING

In Fig.1.7 the ICET with multiple secondary winding is illustrated. The secondary side of the primary transformer is equipped with multiple winding. From the figure, this topology gives the possibility to supply several isolated loads [27]-[28]. Moreover, the secondary side of this system is implemented by AC/DC/AC or AC/AC active converters to meet the required energy.

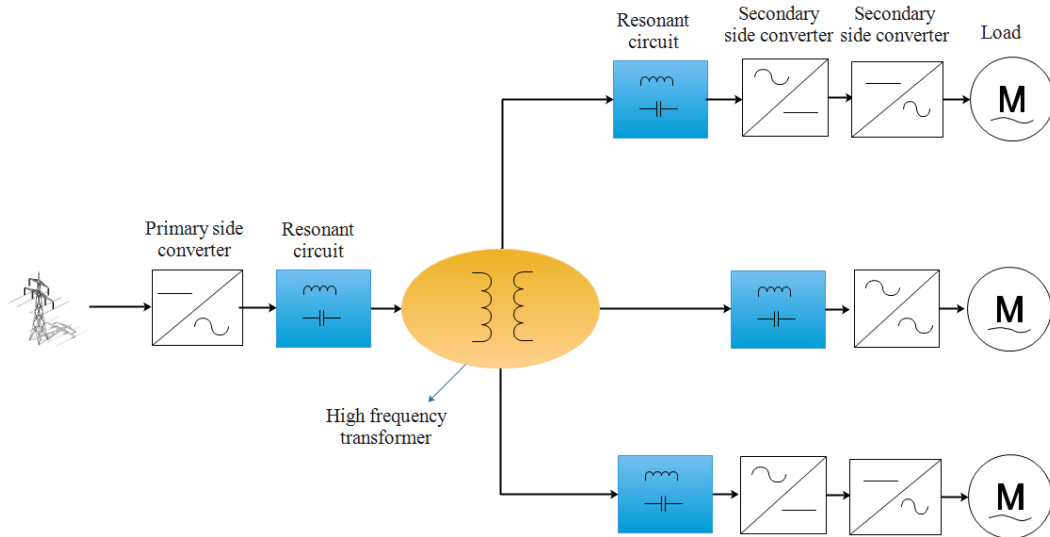


Fig.1.7. Basic principle of the inductive ICET with multiple secondary winding.

Nowadays, several companies have been working on this technology. For example, ‘ABB’ has developed WISA factory to communication and wireless power supply system for sensors and actuators [29]-[31]. In this factory, a coreless single winding which constructed as a frame is implemented in the primary side. This primary winding is coupled with multiple secondary windings to feed sensors and actuators. The application is mainly airborne radar systems which uses a rotating transformer with double parallel connected secondary windings for power supply [32].

### 1.2.4.3. ICET WITH SLIDING TRANSFORMER

Fig.1.8 shows ICET system with a long primary winding loop and sliding transformer. Normally, the ICET system with sliding transformers are used in some application in which long distance is required [34]-[35]. Generally, two types of geometry are used in this technology for the primary winding loop including long linear and circular. In this system, the output converter and load are directly connected to the secondary side of transformer. Moreover, the secondary side transformer has the capability to move along the primary winding loop. According to this capability, and also the possibility to construct long contactless, it can be used as an electrical energy delivery system for mobile receivers [35]. The core materials are chosen depending on the application. Usually, the amorphous or nano crystalline magnetic materials are preferable.

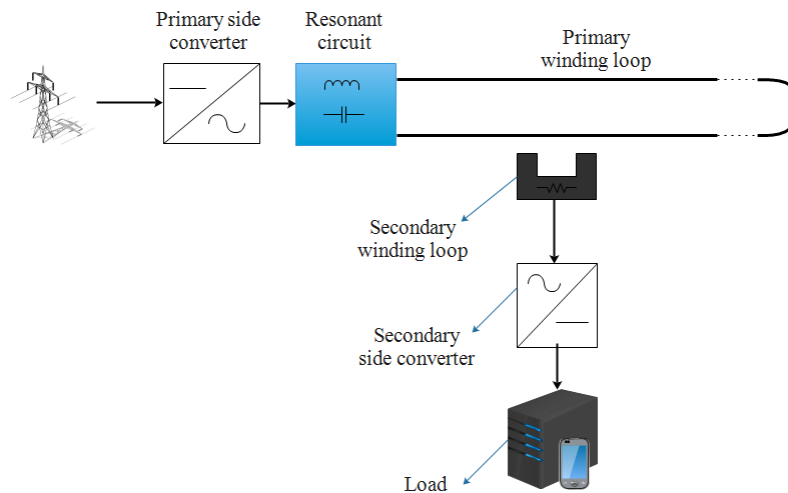


Fig.1.8. Basic principle of the inductive ICET with sliding transformers.

The length of primary winding loop in this system is in the range of 1-70 m and the power range is about 1-200kW [36]-[37].

### 1.3. LOW POWER ICET SYSTEM

According to a large number of ICET applications, it can be classified into low and high power ICET system. The low power ICET applications are the widespread group of applications which works with low power energy. Furthermore, the ranges of power transfer in these applications are between 1W to 20W. Nowadays, there are many companies that have come up with innovative solutions of powering or charging consumer electronic devices using ICET. A few of these companies are Witricity, Powermat Fujitsu etc. Moreover, this technology can be used in different devices as tooth brush, inductive cooker, bio-medical application, desktop peripherals and mobile phones, etc. Below some of these applications are explained in detail.

#### 1.3.1. INDUCTION COOKERS

Although it seems that induction cookers are a new application, the initial researches and patents date from the early 1900s. Moreover, first induction cookers were implemented in the 1970s by the Westinghouse Electric Corporation [42]. Nowadays, several companies are working on this application, such as Bosch, Miele, Siemens, Electrolux, etc. In this application, the primary coil produces the magnetic field. This magnetic field creates Eddy

current in the secondary side, resulting the heating Joule effect. The output power of this application is in the range of 1 to 2 kW and the operating frequency is about 20 kHz to 50 kHz.

### **1.3.2. ELECTRIC TOOTHBRUSHES**

Shock proof devices are the most popular applications of ICET. This feature can be implemented in some devices which are used in a wet environment or even immersed in water. The first rechargeable toothbrushes were made in 1990s. In this application the primary and secondary side are fully isolated therefore can protect users from electrical shocks (for example Sonicare electrical toothbrushes by Philips [43]). Generally, the ferromagnetic core is used in this system, resulting in high coupling between the coils. The range of operation frequency is around 10 kHz and the transferred power energy is between 10 to 15W.

### **1.3.3. TRANSCUTANEOUS ENERGY TRANSFER**

The medical domain is one of the best research areas of ICET systems. Thanks to the diversity and the advantages of this technology, it can be used to supply surgically implemented devices. In the medical domain, this technology is specifically called transcutaneous energy transfer (TET) systems. For example, TET systems can be used in heart assist devices to circumvent left ventricular dysfunctions [44]. Normally, standard way to supply heart assist devices has been wire which passed through the skin. However, this way develops additional risks associated to the apparition of infections. To solve this problem, a resonant converter with special transformer has been designed in [45]. The power range in this application is 10W and the operating frequency is 205.1 kHz. In addition, another TET system which was designed for implementable artificial heart is in [46]-[47]. In this application the power transfer is 20W and frequency is 50 kHz.

### **1.3.4. DESKTOP PERIPHERALS AND MOBILE PHONES**

The ICET technology is so popular in the mobile phones domain. The first ICET prototype for recharge a mobile phone was proposed in [49]-[50] early 2000s. There are many manufactures which are interested in this domain. For example, A4 Tech produces an application called battery-free optical mouse which is the present desktop application [51]. This application is supplied by ICET system and is working in the range of 1W. Also, the HP Touchstone is used to recharge the phone and the Palm device [52]. The range of transfer power is 5W and the connection to the computer is via the USB. On the other hand, the first CET table was proposed by Fulton Innovation for supplying multiple fixed devices [53]. There are several products in this market, which are operating similarly. For example, eZone charger [54], MojoPad [55], Powermat product line [56]. The power transfer in these applications are less than 5W and only can supply low power devices.

## **1.4. HIGH POWER ICET SYSTEM**

High power CET systems have also a large number of applications. Moreover, better efficiency (in high power) and safety are two clear reasons for the popularity of this technology. The range of power transfer in this system is between some kilowatts to hundreds of kilowatts. The high power contactless power transfer has found applications in people movers, industrial transport and automation, mining, military and aviation, electric vehicles, etc. Below some of these applications will be introduced.

### **1.4.1. ELECTRICAL VEHICLES AND ICET CHARGING**

The idea of electrical vehicles (EV) is an old idea. In the 1900s with the beginning of automotive era this idea arose [57]. However, with the advent combustion engine in the early 20<sup>th</sup> century, the EVs went out of the market. Nowadays, due to global warming and the idea of environmentally friendly, this application came back to the markets. Although this technology initially had a lot of technical problems, with the development of cost-effective and fast charging battery it can be an alternative for the conventional vehicles.

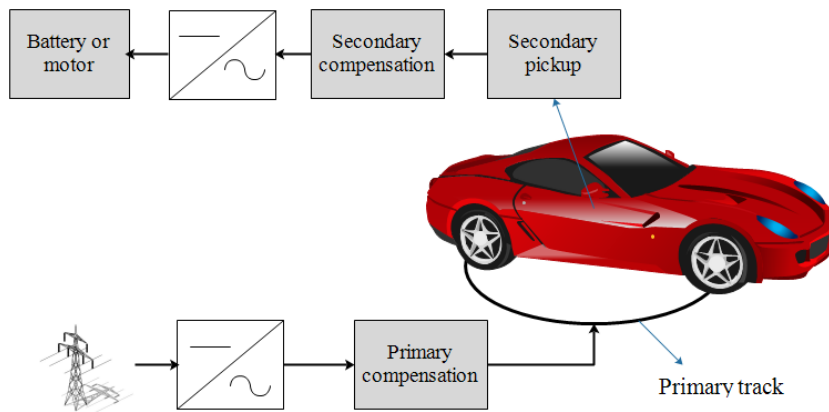


Fig.1.9. Electrical vehicles and ICET charging system.

The standard way for charge replenishment of EVs has been via conductive wires between the charging station and vehicle. However, this common way has some disadvantages such as inconvenience source, electrical shocks in wet and damp conditions and no easy automation. According to the mentioned problems, the ICET system can be used as an alternative system for the battery charging.

Fig.1.9 shows the ICET technology for charge replenishment of the vehicle. In primary side the power converter in collaboration with primary compensation is responsible to supply the primary track. In the secondary side the transformer is directly connected to the secondary compensation, power converter and battery. The charging process is started when the vehicle is placed on the primary winding. The energy is transferred towards the secondary winding and then it makes charging replenishment of EVs.

Fig.1.10 illustrates the principle of operation of the electrical train with ICET technology for charge replenishment. The charging process is similar to the electrical vehicles. The primary windings are located in the railway and secondary winding is located in the cabins. By implement this technology, the train can be recharged statically or dynamically.

#### 1.4.2. INDUSTRIAL TRANSPORT AND AUTOMATION

ICET system can be used in industrial environment as a transporter or platform system [59]. This application can be installed as overhead or floor. The principle of operation of this

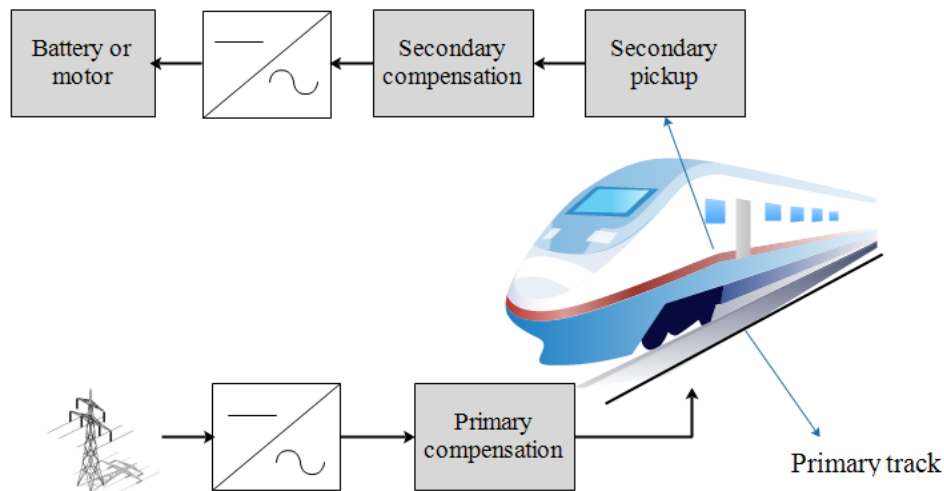


Fig.1.10. Electrical train with ICET rechargeable technology.

system is so similar to ICET with sliding transformers. In other words, the long primary winding loop is implemented as a primary side and the secondary side is a sliding transformer. Furthermore, the contactless system is a good alternative in undergrounds with high risk of explosion [60].

### 1.4.3. MILITARY AND SPACE SYSTEMS.

Several applications of ICET systems have been presented for military and space system area. In a military application where the sealing of compartments is vital, the contactless energy transfer can be used as an alternative supply system. Also, a satellite rotary connection has been proposed [61] for space application.

## 1.5. ICET SYSTEMS FOR RESIDENTIAL AREA

Nowadays, with the advancement of technology and entry the technology into the residential area, the development and investigation on this issue seems essential. In the previous section, several ICET applications have been explained which are possible to use in residential areas, for example, electrical toothbrush, induction cooker, ICET charging, etc. Generally, according to the place of use of the residential ICET applications, it is possible to



Fig.1.11. Indoor ICET distribution energy.

classify these applications in two groups. The first group is indoor ICET applications and the second one is outdoor ICET applications. Below these applications are explained.

### 1.5.1. INDOOR ICET APPLICATIONS

This section introduces some ICET applications which can be used in the interior parts of the building. In this case, many low power ICET products can be mentioned. For example, a toothbrush in the toilet or ICET charging in privet room and etc. The number of these applications are so high, but it is interesting to note that the companies have paid a little attention to the distribution of energy by the ICET system in residential areas. Hence, the focus of this thesis is related to this issue.

Fig.1.11 shows the distribution of energy in the residential area with ICET system. From the figure, the primary winding in collaboration with sliding transformer is responsible to transfer the energy from the source to the loads. The primary winding is located around the flat and give the possibility of movement to the sliding transformers along the primary winding. The new distribution system is a good alternative for conventional one, due to its

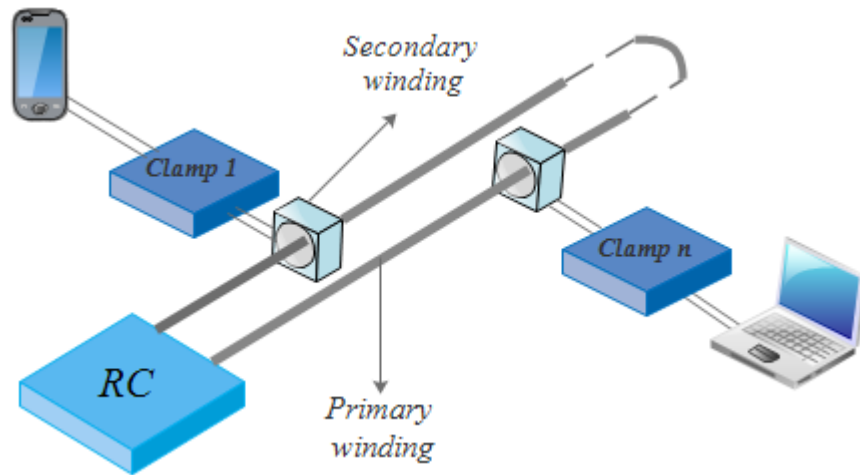


Fig.1.12. Diagram of the ICET system with various mobile clamps

benefits such as movable plugs and elimination of electrical shocks. These features are significant in humid environments such as indoor swimming pool and bathroom.

A diagram of the reference topology to supply residential loads is shown in Fig.1.12. This system consists of a resonant converter (RC), a primary winding loop, secondary side transformer frequency and various mobile clamps. The RC is responsible to generate a high-frequency AC voltage to supply the mobile loads through the long primary winding loop of the sliding transformer. This feature offers the possibility to construct long ICET systems for mobile clamps.

Fig.1.13 illustrates the electrical representation of the conventional topology to supply the residential loads. It consists of a series resonant network connected in series with the primary side of  $n$  sliding transformers excited by the full-bridge resonant inverter. The secondary side of each clamp is formed by an active full-bridge rectifier and a capacitive filter. The magnetizing inductances of the high frequency transformers are modelled by parallel equivalent inductors ( $L_{m1}, \dots, L_{mn}$ ). Note that in the primary side, the (small) leakage inductance of the transformer is absorbed by the large discrete inductance ( $L_r$ ). The secondary side leakage inductance ( $L_{s1}$ ) is included in the schematic.

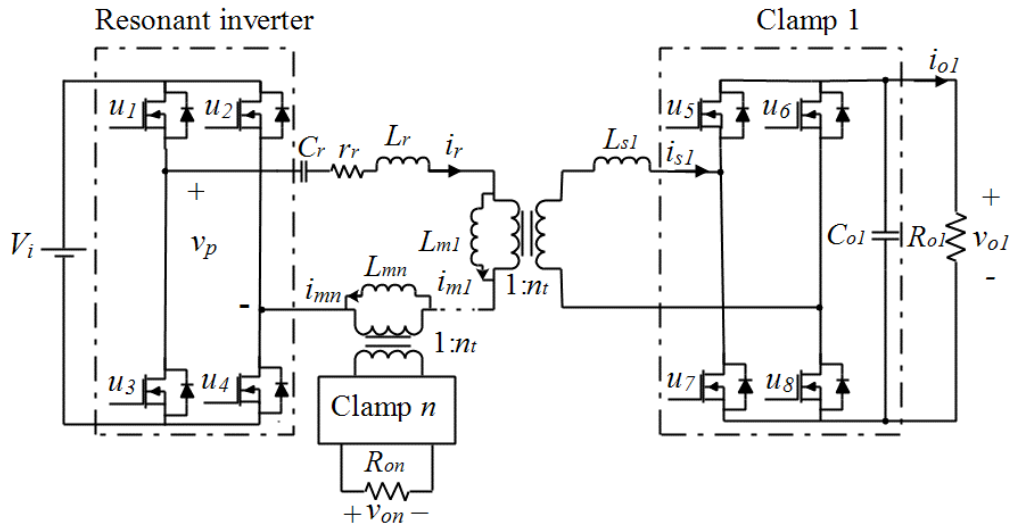


Fig.1.13. Schematic of the conventional ICET with multiple mobile clamps.

Fig.1.14. shows the control diagram of the conventional approach to supply multiple mobile loads. From the figure, there are a primary side control and several secondary side controls (depending on the number of loads). Several control approaches could be applied to the primary side resonant inverter to regulate the resonant current. However, several challenges are introduced as a consequence of using a long primary winding loop, which is explained in section 1.6. Moreover, the secondary side controllers are used to regulate the output voltages against changes in the input and output powers. More details on these controllers can be found in [80], [81].

### 1.5.2. OUTDOOR ICET APPLICATIONS

In general, outdoor applications include all type of ICET systems which are used in exterior parts (parking and garden) of residential area. Usually, these areas are exposed to the rain and humidity. Hence, this area needs a safe electrical system against the electrical accidents. The ICET system is a good choice thanks to the electrical shock proof.

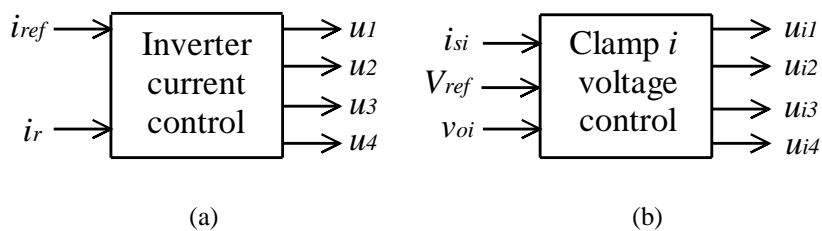


Fig. 1.14. Control diagram of the conventional topology: (a) resonant inverter control and (b) clamps control

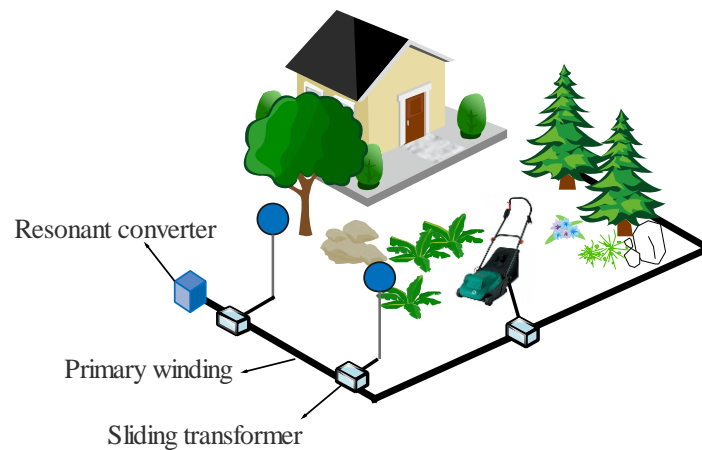


Fig.1.15. Outdoor ICET distribution energy.

Fig. 1.15 shows the outdoor ICET energy distribution system in garden application. According to the figure, several movable loads can be supplied with this system. Therefore, some loads such as a grass cutter has more possibility for movement. Also, the position of the lampposts in the garden could be changed as desired place.

## 1.6. PROBLEM FORMULATION

The performance of ICET systems has been extensively studied from different perspectives such as high efficiency DC/DC converter [62]-[63], magnetic shield [64], analyzing and modeling of coupling system [65]-[69], control method and proper system design [70]-[72], and high efficiency coupling [73]. It should be mentioned that these achievements are applicable only to the single clamp system. In fact, there are many unsolved problems to apply these methods to a multiple clamp system.

Feeding multiple loads is one of the interesting advantages besides eliminating the last wire. The practical application scenario here is a long winding loop with sliding transformers supplying power for various electronic devices such as wearable devices, mobile phones, and laptops. The characteristics of these devices are normally different in size, power requirement and charging conditions. Therefore, to supply the aforementioned devices, several challengeable problems should be solved. Over the past few years, several research

studies have done to address such a multiple clamp system from different perspectives [74]-[82]. In [74] the coupled mode theory has been used to explore the effect of multiple loads on power transfer efficiency. A new circuit model for an ICET system with multiple load has been presented in [75]. Moreover, [76] presented a new method to design the circuit parameters with several clamps. [77] discussed the power distribution for a system with two mobile clamps. Reference [78] and [79] discussed the optimal load analysis and effect of coupling between multiple clamps, respectively.

Despite of numerous publications in the field of ICET systems with multiple clamps, few attempts have been made to bring this technology into the residential area where the distribution system is traditionally based on copper cables and fixed point sockets [80]-[82]. In fact, this distribution system is a very good technical solution to the supply of fixed and heavy loads such as refrigerators, washing machines, air conditioning, etc. However, for residential mobile loads such as laptops and mobile phones, ICET technology will drastically improve flexibility. Note that this kind of loads includes internal post-regulators (they are active loads), so that excellent output voltage regulation is not strictly required for ICET systems in this particular case.

In this application as a consequence of the long primary winding loop and the mobile load flexibility, the information about the load consumption is not available in the primary side of the full bridge inverter. This problem can be solved by using a wireless communication system. However, this design decision will drastically increase both the system cost and the bandwidth communication required to send output side data to the primary side control. Therefore, the design and implementation of the control system that provides a high efficiency without communication system can be considered as a complex trend.

Several approaches can be adopted to regulate the inverter current including constant and variable input reference current( $i_{ref}$ ) [80]- [81]. By using constant  $i_{ref}$ , high efficiency can be only reached at full load conditions [80]. With variable  $i_{ref}$ , the efficiency is improved for low load conditions, but at the expense of increasing the complexity of the current control loop. In [81], the current reference is online updated by estimating the load consumption through indirect measures. On the other hand, the output voltages in the conventional

topology depend on the load conditions, so that a separated control system is required for each clamp. Although, the output voltage can be correctly regulated, the cost of the system is drastically increased in the case of high number of clamps (because of the sensing circuit, control system and driver needed by each active full-bridge rectifier). To sum-up, the conventional topology to supply multiple loads is complex and expensive.

## 1.7. RESEARCH OBJECTIVES AND THESIS ORGANIZATION

In this section the main objectives of this thesis are introduced. The main focus of this thesis is the application of the ICET system with multiple clamps in residential area. According to the mentioned problems, several challenges are identified which will be address in this thesis. The main objectives are listed below:

- ✚ *Adaptive control algorithm for the fully-controlled ICET topology with multiple clamps:* As mentioned before, the ICET system with long primary loop has an efficiency problem (especially in low load condition) as a consequence of lack of communication channel to inform the resonant converter about the load consumption. Therefore, the adaptive control algorithm is essential to update the reference input current without communication line. Few studies have been done to address this problem, while this problem should be considered as an important issue in residential applications. A new adaptive control algorithm to improve the efficiency problem will be presented in chapter 2. This control algorithm is based on the characteristics of the input control signal it estimates the load consumption without using a communication channel.
  
- ✚ *Analysis and design of a partially-controlled ICET system with multiple clamps:* In this application, several control approaches can be implemented to control the primary resonant converter. The main control techniques include frequency, phase and quantum modulation. These control techniques, have benefits and drawbacks which should be considered in the implementation of this application. In chapter 3, these control approaches will be analyzed and compared. Moreover, the design of the resonant elements and the high frequency transformer will be presented.

✚ *Simple and cost-effective design for partially controlled ICET system:* The conventional topology is a complex system due to the need for an especial control algorithm. This complexity raises by increasing the number of clamps. On the other hand, the conventional topology is an expensive system as a consequence of the high number of required control systems. In this case, for input side and each clamp the separated control system is necessary. Thus, the design of a simple and cost-effective system to supply the multiple loads could be an interesting issue. In chapter4, a new simple and cost-effective topology of a partially controlled ICET system will be presented.

✚ *Build a prototype to validate the theoretical analysis:* To validate the theoretical results, a high frequency DC/DC resonant converter prototype with two clamps has been built and tested. The maximum power and efficiency of the prototype is around 10W and 80%, respectively. The experimental results will be presented in chapter 4.

## **1.8. CONCLUSION**

The current application of CET systems and also several classifications of the ICET systems have been introduced in this chapter. Moreover, the state-of-the-art relevant to an ICET system with multiple clamp has been presented. According to these studies, several unsolved problems can be mentioned. In fact, the main focus of this thesis is to find the best solutions for these problems. These solutions will be presented in detail in the next chapters.

---

# Adaptive control algorithm for the fully-controlled ICET System

---

## Summary

---

2.1 INTRODUCTION .....	25
2.2 MATHEMATICAL MODELING.....	26
2.3 STATIC $\alpha$ ALGORITHM.....	31
2.4 BASIC DYNAMIC $\alpha$ ALGORITHM.....	33
2.5 LOAD-SENSITIVE DYNAMIC $\alpha$ ALGORITHM .....	36
2.6 CONCLUSION .....	39

---

The conventional ICET system without a communication line only has a good efficiency at full load condition. In this system, the resonant converter cannot be informed about the load consumption. Therefore, at low load conditions, the value of input reference current cannot be updated. This chapter presents a new adaptive control algorithm for fully-controlled ICET system with multiple clamps. The new adaptive algorithm operates dynamically with the load changes, resulting in maximum efficiency in all the load conditions. In addition, a mathematical framework of the contactless system with new adaptive algorithm is presented. Moreover, the operation of the new control system with load step changes is analyzed and tested.



## 2.1. INTRODUCTION

As mentioned above, in residential area, the implementation of the ICET system with long primary winding loop and sliding transformer introduces several challenges. The most challenging aspect is the lack of communication line to inform the resonant converter about the load consumption. This problem could be solved by using a wireless communication system. However, this design drastically increases the system cost due to the high bandwidth communication required to send output side data to the primary side controller. Therefore, the system without communication is preferable.

In the system without communication, the control scheme is based on estimating the load consumption. In [80], the estimation of the load consumption is based on the nominal component values. This method is not accurate due to the tolerance of the components and the temperature effect during operation. Moreover, the complex control method should be applied to the primary side inverter to obtain the maximum efficiency. In [81] the estimation is based on the power matching in the resonant tank. This method is so complex and the estimation is almost wrong due to the lack of precise measurement of the real power. Also, the presented algorithm is only applicable for one clamp situation. By adding more number of clamps, the estimation gets wrong. The last negative point is that the impact of load step changes is not evaluated.

This chapter presents a new adaptive algorithm for supply multiple clamps. The presented algorithm is based on the estimation of the load consumption by using an indirect information from the primary control signal. The proposed algorithm is applicable to the multiple mobile clamp and it deals with the load step changes. The mathematical foundation and simulation results of the proposed control will be presented in the following sections.

The main contributions of this chapter are: 1) the large-signal averaged model, which is very useful to devise the control scheme for ICET system with multiple clamps and 2) an adaptive control algorithm which provides excellent properties such as fast transient response and high efficiency in all the load conditions

## 2.2. MATHEMATICAL MODELING

The purpose of this section is to present the mathematical framework of the contactless system with the new adaptive algorithm. In this release, the averaged model of the system is presented. Also, some explanation about  $u_p$  maximum is presented. Note that in this study the effect of the magnetizing and leakage inductances are neglected. With this approximation, the mathematical modeling is strongly simplified. Its impact will be examined in the discussion of the simulation results.

### 2.2.1. STATE-SPACE MODEL

The topology of the conventional ICET system was shown in Fig 1.13. The topology consists of a series resonant tank (neglecting the parasitic inductances) with multiple active output rectifiers and output filters. This topology is controlled using quantum modulation; see [81] for more details. Using this modulation technique, the state-space model of the conventional topology can be presented as follows:

$$\frac{di_r}{dt} = \frac{1}{L_r} \left[ V_i u_p \text{sgn}(i_r) - r_r i_r - v_{cr} - \sum_{j=1}^{n_{cl}} \frac{v_{oj}}{n_j} u_{sj} \text{sgn}(i_{oj}) \right], j = 1, 2, \dots, n \quad (2-1)$$

$$\frac{dv_{cr}}{dt} = \frac{1}{C_r} \cdot i_r \quad (2-2)$$

$$\frac{dv_{oj}}{dt} = \frac{1}{C_{oj}} \left[ \frac{i_r u_{sj}}{n_j} - \frac{v_{oj}}{R_{oj}} \right] \quad (2-3)$$

where  $V_i$ ,  $i_r$  and  $v_{cr}$  are the input voltage, resonant inductor current and resonant capacitor voltage, respectively.  $v_o$  is the output voltage and  $C_r$  and  $L_r$  are resonant elements. The primary and secondary control signals ( $u_p$ ,  $u_s$ ) are discrete-time variables which show the selected mode of operation:  $u=1$  corresponding to energizing mode and  $u=0$  to de-energizing mode.

The state-space model equations are discontinuous and then not directly applicable to the control design. Therefore, below some assumptions are considered to derive a control dynamic model.

### 2.2.2. NOMINAL SOLUTION

According to the standard design, the resonant variables are nearly pure sinusoidal signals. In addition, slow variations are expected in the amplitude and phase of these signals in comparison with the switching period [83]. In steady state, the resonant inductor current and capacitor voltage can be expressed as

$$i_r = I_r \sin \omega_0 t \quad (2-4)$$

$$v_{cr} = V_{cr} \sin(\omega_0 t - \varphi) \quad (2-5)$$

where  $i_r$  and  $v_{cr}$  are fast variables and  $I_r$  and  $V_{cr}$  are slow variables. It should be noticed that the state variables using quantum modulation operate exactly at resonant frequency (i.e.,  $\omega = \omega_0$ ). Therefore, the phase angle of the resonant current is forced to be always zero.

### 2.2.3. AVERAGED LARGE-SIGNAL MODEL

Note that as a consequence of longer time scale of output filter in comparison with the resonant tank the ripple associated with output filter variables can be neglected. Therefore, the output voltage  $v_o$  is approximated by means of its time-varying averaged value. Then by averaging (2-1), (2-2) and (2-3) over a half switching period the resulting averaged model is:

$$\frac{d\bar{i}_r}{dt} = \frac{4}{\pi^2 L_r} \left( u_p V_i - r_r \bar{i}_r - \sum_{j=1}^{n_{cl}} \frac{\bar{v}_{oj}}{n_j} u_{sj} \right) \quad (2-6)$$

$$\bar{v}_{cr} = \frac{\omega_0 L_r}{\cos \varphi} \bar{i}_r \quad (2-7)$$

$$\frac{d\bar{v}_{oj}}{dt} = \frac{1}{C_{oj}} \left[ \frac{\bar{i}_r u_{sj}}{n_j} - \frac{\bar{v}_{oj}}{R_{oj}} \right] \quad (2-8)$$

where  $\bar{i}_r$  and  $\bar{v}_{cr}$  are defined as:

$$\bar{i}_r = \frac{2}{\pi} I_r \quad (2-9)$$

$$\bar{v}_{cr} = \frac{2}{\pi} V_{cr} \quad (2-10)$$

#### 2.2.4. SLIDING MODE CONTROLLER

Sliding mode control is an elegant non-linear method to control a chosen error-defined function (and its weighted derivatives) to zero. The elegance is hidden in the fact that actually the main objective of sliding mode control is to be sure that from any system state the next time step brings the state closer to the required state. The error convergence to zero is only a direct consequence of the last objective.

Essentially, the sliding mode control defines a switching surface that divides the state-space into two subspaces with different dynamic behavior. A proper control law causes the dynamics of the converter in both subspaces to drive in the direction of the switching surface and to remain on the surface, once the system state reaches the surface, for all subsequent time.

The main requirement in the design is that the control should satisfy the reaching condition, which, besides, guarantees the existence of a sliding regime in the switching surface  $S$ . The often used reaching condition is given by:

$$S \cdot \frac{dS}{dt} < 0 \quad (2-11)$$

which allows for the determination of the control strategy:

$$u = \begin{cases} u^+, & \text{for } S > 0 \\ u^-, & \text{for } S < 0 \end{cases} \quad (2-12)$$

For the construction of a sliding mode controller, it is necessary to formulate a candidate sliding surface. In our case the candidate sliding surface for input side is defined as (see Fig.2.1):

$$S_p = \left[ I_{ref} + \alpha \frac{\omega_c}{s + \omega_c} (u_p) \right] - \bar{i}_r \quad (2-13)$$

where  $\alpha$  is a control gain and  $u_p$  is the primary control signal. Moreover, for the output-side sliding surface can be expressed as:

$$S_{sj} = v_{ojref} - \bar{v}_{oj} \quad (2-14)$$

By inserting (2-13) and (2-14) in (2-6) and (2-8), it is possible to derive the expressions for the control signals as follows:

$$u_p \approx \sqrt{\frac{1}{\alpha V_i} \sum_1^j \frac{v_{oj}^2}{R_{oj}}} \quad (2-15)$$

$$u_{sj} \approx \frac{1}{\alpha u_p} \cdot \frac{v_{ojref}}{R_{oj}} \quad (2-16)$$

Equations (2-15) and (2-16) are fundamental to understand how the system works as they show clearly the operation of the variable  $\alpha$  algorithm. According to these equations, we can mention that:

- The value of  $u_p$  and  $u_{sj}$  increases by reducing the  $\alpha$  value.
- It is interesting to see that the value of  $u_p$  has a maximum value. This phenomenon happens when  $u_{sj}$  arrives to 1, the secondary control saturates (the corresponding



Table.2.1. Optimal alpha values for several load conditions.

Loads	$P_{o1}$	$P_{o2}$	$P_{ot}$	$\alpha_{\min}(\text{OL})$	$\bar{u}_p$	$i_{peak}(\bar{i}_p)$	$I_{\max}(i_{o1}, i_{o2})$	$i_{peak}-i_{\max}$
FL / FL	1000	1000	2000	16	0.6269	14.7	11.4	3.3
FL / 10%FL	1000	100	1100	23	0.3815	13.4	11.5	1.9
55%FL/ 55%FL	550	550	1100	12.5	0.5	9.6	6.3	3.3
10%FL/ 10%FL	100	100	200	17	0.1571	5.1	1.2	3.9

### 2.3. STATIC $\alpha$ ALGORITHM

In this section the principle of operation of the static  $\alpha$  algorithm in different load conditions is evaluated. The main purpose of this section is to show the operation and limitations of static  $\alpha$  algorithm and find the optimum value for  $\alpha$  in different load conditions. Note that in this section the value of  $\alpha$  is chosen in open loop ( $\alpha$  is not used and the value of  $\alpha$  is fixed manually). It should be also mentioned that a converter with two clamps is considered for all the simulation results.

Fig.2.1. shows the schematic of the proposed input sliding mode control system based on (2-13). According to the figure,  $u_p$  is filtered to eliminate the ripple and noise. Then, the filtered signal goes into  $\alpha$  generator block in order to produce the optimal  $\alpha$ . Finally, the optimal  $\alpha$  is multiplied by  $\bar{u}_p$  and produces the reference current  $i_{ref}$ .

Table.2.1 shows the information about the correct operation (without output voltage distortion and optimum  $\alpha$ ) of the system in several load conditions. As it can be seen, the results are achieved in open loop and the optimum  $\alpha$  for several load conditions is different. According to Table.2.2, the maximum necessary  $\alpha$  in which the system could operate correctly (no optimum) for all the load conditions is 23. The  $\bar{u}_p$  is changing as a function of the load condition and it seems that it is the key factor to predict the load consumption.

According to Table.2.2, the maximum  $\bar{u}_p$  is achieved with optimum value of primary side current ( $\bar{i}_r$ ). In fact, the control system should automatically find the maximum  $\bar{u}_p$  in order to arrive to the optimum value for primary side current. The idea is to first run the

Table.2.2. Searching for the optimal alpha values manually.

Load conditions	$\alpha$	$\bar{u}_p$	Comments
FL/FL	17	0.6127	More $\bar{u}_p$ than necessary
FL/FL	16	0.6300	Optimum (minimum) $\bar{u}_p$
FL/FL	15	0.6178	Distortion on $v_{o1}$ and/or $v_{o2}$
10%FL/10%FL	18	0.1567	More $\bar{u}_p$ than necessary
10%FL/10%FL	17	0.1601	Optimum (minimum) $\bar{u}_p$
10%FL/10%FL	16	0.1386	Distortion on $v_{o1}$ and/or $v_{o2}$
FL/10%FL	24	0.3812	More $\bar{u}_p$ than necessary
FL/10%FL	23	0.3851	Optimum (minimum) $\bar{u}_p$
FL/10%FL	22	0.3754	Distortion on $v_{o1}$ and/or $v_{o2}$
55%FL/55%FL	13.5	0.4860	More $\bar{u}_p$ than necessary
55%FL/55%FL	12.5	0.5007	Optimum (minimum) $\bar{u}_p$
55%FL/55%FL	11.5	0.4702	Distortion on $v_{o1}$ and/or $v_{o2}$

Table.2.3. Searching for the optimal  $\alpha$  values manually with more precision.

Loads	$\alpha$	Output distortion	$\bar{u}_p$	$\bar{u}_p - \bar{u}_p(-)$	Loads	$\alpha$	Output Distortion	$\bar{u}_p$	$\bar{u}_p - \bar{u}_p(-)$
FL / FL	15.8	No	0.6344	0.0014	10%FL/FL	24.1	No	0.3810	0.0008
FL / FL	15.7	No	0.6358	0.0012	10%FL/FL	23.9	No	0.3818	0.0012
FL / FL	15.6	No	0.6370	0.0011	10%FL/FL	23.7	No	0.3830	0.0012
FL / FL	15.5	No	0.6381	0.0003	10%FL/FL	23.5	No	0.3842	0.0005
FL / FL	15.4	Yes	0.6384	0.0002	10%FL/FL	23.3	Yes	0.3847	0.0011
FL / FL	15.3	Yes	0.6386	-0.0026	10%FL/FL	23.1	Yes	0.3858	-0.0007
FL / FL	15.2	Yes	0.6360		10%FL/FL	22.9	Yes		
10%FL/10%FL	18.2	No	0.1557	0.0012	55%FL/55%FL	12.8	No	0.4965	0.0020
10%FL/10%FL	17.9	No	0.1569	0.0011	55%FL/55%FL	12.7	No	0.4985	0.0014
10%FL/10%FL	17.6	No	0.1580	0.0010	55%FL/55%FL	12.6	No	0.4999	0.0016
10%FL/10%FL	17.3	No	0.1590	0.0007	55%FL/55%FL	12.5	No	0.5015	0.0007
10%FL/10%FL	17.0	Yes	0.1597	0.0002	55%FL/55%FL	12.4	Yes	0.5022	0.0009
10%FL/10%FL	16.7	Yes	0.1599	-0.0003	55%FL/55%FL	12.3	Yes	0.5031	-0.0027
10%FL/10%FL	16.4	Yes	0.1596		55%FL/55%FL	12.2	Yes	0.5004	

system with the maximum necessary initial value of  $\alpha$  (see Table.2.1) then reduce  $\alpha$  and searching for maximum  $\bar{u}_p$  in order to find the optimum primary side current.

Table.2.3 is an extension of Table.2.2 with more detailed information. As it can be seen, maximum  $\bar{u}_p$  is achieved at optimal value of  $\alpha$ , but a distortion of the output voltage is observed at this optimal  $\alpha$  value. Fig.2.2 shows the relation between  $\bar{u}_p$  and  $\alpha$  for FL/FL condition. According to the Fig.2.2, the starting point of  $\alpha$  should be 16 and this value should

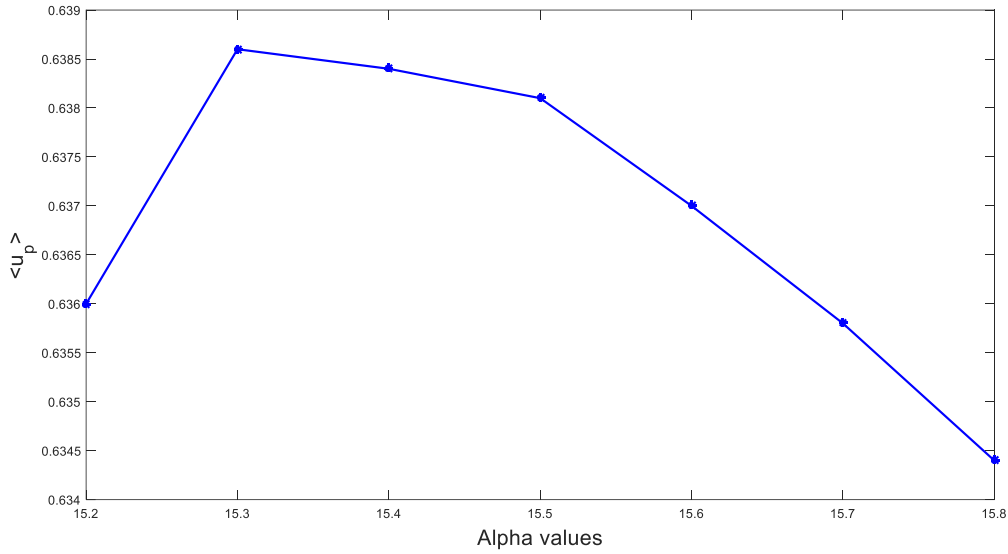


Fig.2.2. Relation between  $\bar{u}_p$  and  $\alpha$  in FL/FL condition.

be reduced in order to climb to the peak value of  $\bar{u}_p$ . The problem is that the output voltage is distorted for the peak value of  $\bar{u}_p$ . One possible solution to avoid this distortion is to stop the searching for  $\alpha$  when the error between the current value of  $\bar{u}_p$  and its previous value is lower than a certain threshold. According to Table.2.3, this threshold could be 0.001. By using this new searching algorithm, the solution for  $\alpha$  is 15.5 for FL/FL condition. This value for  $\alpha$  guarantees the minimum  $\alpha$  with no distortion in the output voltage.

## 2.4. BASIC DYNAMIC $\alpha$ ALGORITHM

The purpose of this section is to present the dynamic  $\alpha$  algorithm for a system with two clamps. In previous section, the static  $\alpha$  algorithm was presented and discussed. In this section, by applying the new adaptive algorithm, we try to solve the previous problems and then to guarantee the maximum efficiency for all the load conditions.

Fig.2.3 shows the flowchart to find the optimal  $\alpha$  ( $\alpha_{op}$ ). According to the flowchart,  $\alpha$  has an initial value  $\alpha_{max}= 24$ , in order that the system starts working without distortion for any load condition..  $\alpha$  is reduced step by step (-0.1) by the counter and the current  $u_p$  is compared with the previous one ( $\bar{u}_p(-)$ ). If  $u_p$  is smaller than  $u_p(-)$ , then the flowchart finds the maximum  $u_p$  (see Fig. 2.2). In addition,  $\alpha$  comes back to one step before and it

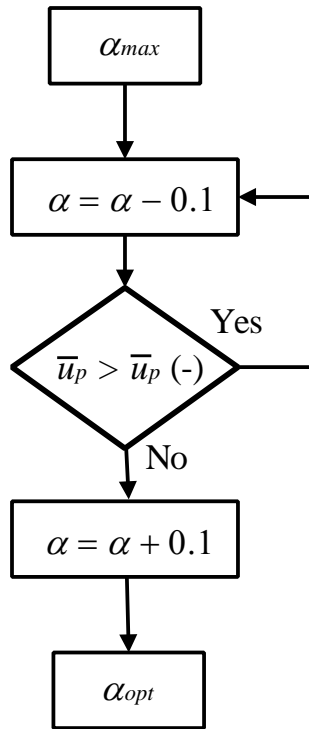


Fig.2.3. Flowchart for  $\alpha$  generation.

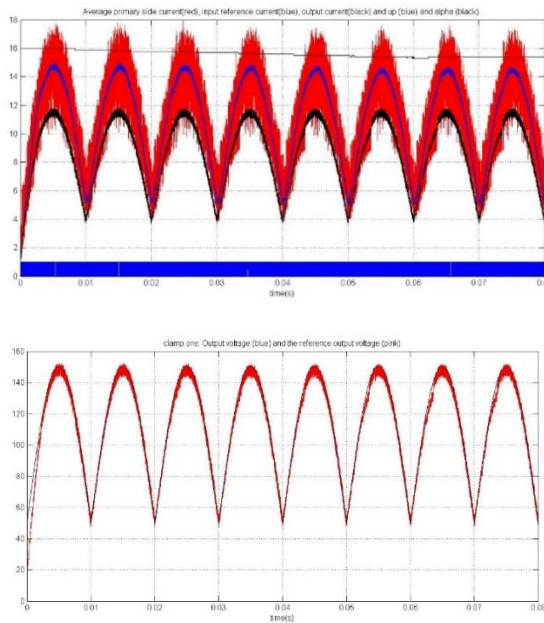


Fig.2.4. Main waveforms with dynamic  $\alpha$  ( $R_{o1} = R_{o2} = 12.9$ ). Top: average primary side current (red), input reference current (blue), output current (black),  $u_p$  (blue) and  $\alpha$  (black). Bottom: output voltage (red) and reference output voltage (black).

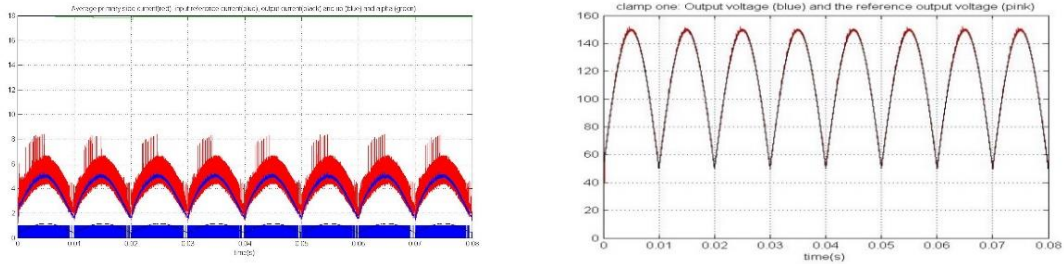


Fig.2.5. Main waveforms with dynamic  $\alpha$  ( $R_{o1}=R_{o2}=129$ ). Left: average primary side current (red), input reference current (blue), output current (black),  $u_p$  (blue) and  $\alpha$  (green). Right: output voltage (red) and reference output voltage (black).

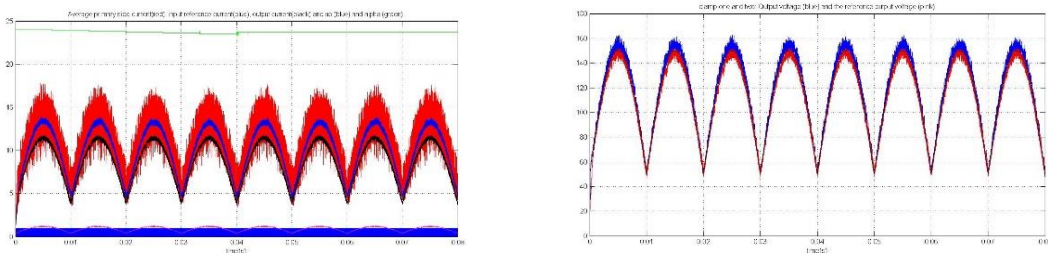


Fig.2.6. Main waveforms with static  $\alpha$  ( $R_{o1}=12.9$ ,  $R_{o2}=129$ ). Left: average primary side current (red), input reference current (blue), output current (black),  $u_p$  (blue) and  $\alpha$  (green). Right: output voltage (red and blue) and reference output voltage (black).

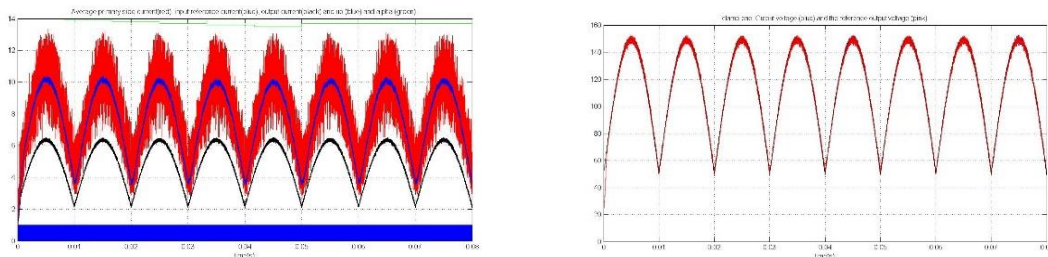


Fig.2.7. Main waveforms with dynamic  $\alpha$  ( $R_{o1}=23.45$ ,  $R_{o2}=23.45$ ). Left: average primary side current (red), input reference current (blue), output current (black),  $u_p$  (blue) and  $\alpha$  (green). Right: output voltage (red) and reference output voltage (black).

waits in this value. This step back level guarantees the correct operation of the system without output voltage distortion.

Fig.2.4 shows the main waveforms of the converter in FL/FL condition. From the figure,  $\alpha$  is reduced step by step (-0.1) and finally finds the maximum  $\bar{u}_p$  in 15.2 then comes back one step before and waiting on 15.3. As it can be seen, the output voltage has some distortion, but it could be acceptable for residential application.

Fig.2.5, Fig.2.6 and Fig.2.7 show the main waveforms of the converter for several load conditions. As it can be seen, the system finds correctly the maximum  $\bar{u}_p$  in all the cases. The system operates correctly with fix load and the maximum efficiency can be achieved. The next step is to design the system for load step changes. The current algorithm has no possibility to detect the load changes. Therefore, a new  $\alpha$  generator process should be considered to detect the load step changes.

## 2.5. LOAD-SENSITIVE DYNAMIC $\alpha$ ALGORITHM

Fig.2.8 shows the  $\alpha$  generator flowchart to find the optimal  $\alpha$  ( $\alpha_{op}$ ) including load change detection. In comparison with previous flowchart (Fig.2.3) the algorithm has a new input ( $\bar{i}_r$ ) to find the load changes. According to the figure, two coefficients are introduced ( $\beta, \gamma$ ). By determining these coefficients, the algorithm can detect the load changes in all the load conditions. In our study the values of these two coefficients are achieved by trial and error method. Three different modes can be defined for the new  $\alpha$  generator system as shown in Fig.2.9.

- Searching mode (SM): In this mode the system is searching for optimum  $\alpha$ .

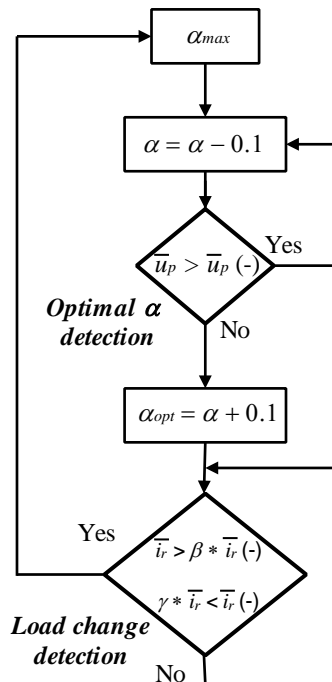


Fig.2.8.  $\alpha$  generator and load change detector flowchart.

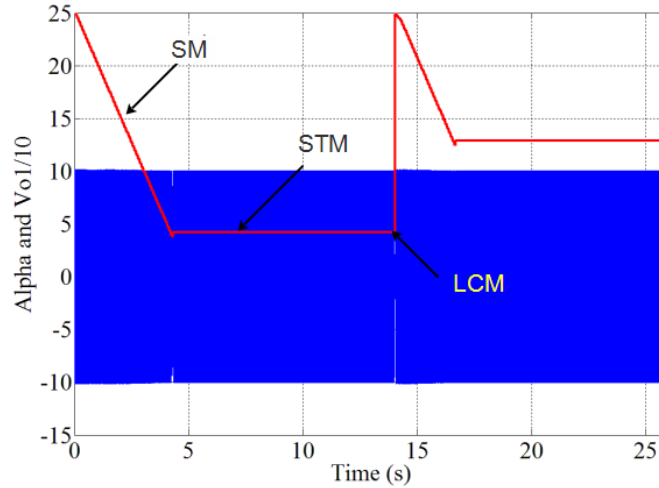


Fig.2.9. Output voltage (blue,  $v_{o1}/10$ ) and  $\alpha$  variation (red). (10% of full load to full load).

- Standby mode (STM): This mode will happen after finding the optimal  $\alpha$ . In this mode the value of  $\alpha$  is fixed.
- Load change mode (LCM): in this mode the load change is detected and the value of  $\alpha$  increases as the maximum value.

Fig.2.10. shows the operation of the adaptive algorithm during the load step changes. The figure illustrates two different load step change situations (10% of full load to full load, full load to 10 % full load). According to the figure, the algorithm is correctly detecting the load change at 14s and then updating  $\alpha$  as the initial value. The new algorithm is satisfying the desired behavior for finding the optimal  $\alpha$  and also detects the load changes.

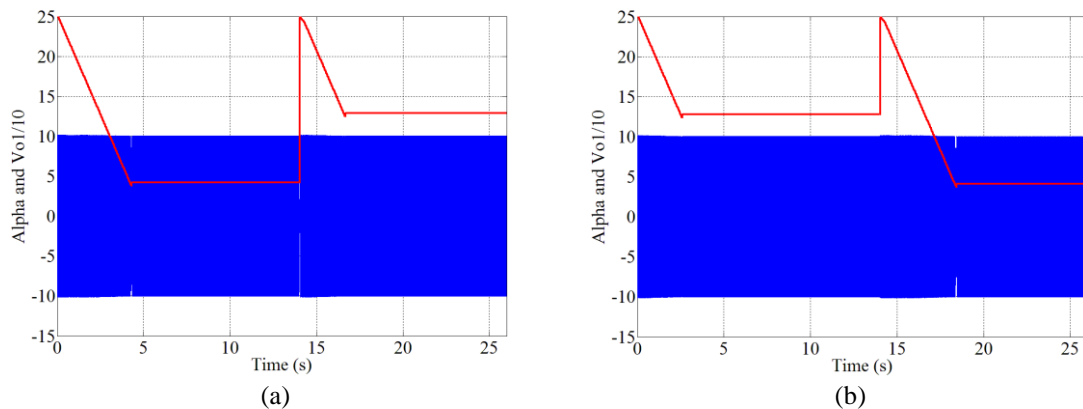


Fig2.10. Output voltage of clamp1 ( $V_{o1}/10$  blue) and  $\alpha$  variation (red). (a):10% of full load to full load, (b): full load to 10 % full load). ( $\beta = 1.1$ ,  $\gamma = 1.03$ ).

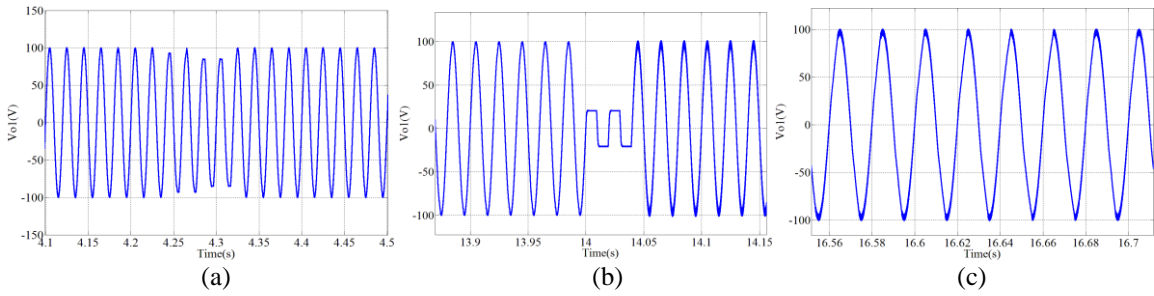


Fig.2.11. Zoom in on Fig.2.10.(a). (a): Output voltage distortion during the first transition from searching mode to standby mode, (b): Transient response due to load change, (c): Output voltage distortion during the second transition from searching mode to standby mode.

Fig. 2.11 is a zoom-in of Fig. 2.10(a). It clearly shows the output voltage distortion during the transitions between operational modes. As expected, the output waveform during load step changes has distortion which is the natural response of the system. This interval is short and the control system quickly eliminates it.

Fig.2.12 shows the performance of the dynamic  $\alpha$  algorithm to regulate the reference current. From the figure,  $i_{ref}$  is reducing during the SM (according to the  $\alpha$  step changes) and finally arrives to the optimal value. Then, during STM keeps the optimal value till the load step change is happening. After that, the reference current is updated and the process for SM is started again. It should be noticed that the optimal value always can be achieved in this control algorithm therefore the maximum efficiency is reached in all the load conditions.

An efficiency comparison between the conventional and proposed control systems is presented in Table.2.4. From the table, the maximum efficiency in both cases is achieved in FL/FL condition as 97%. As it was mentioned in section 1.6, in the conventional control system, the fixed reference input current is selected accordance with the maximum efficiency which is obtained in FL/FL condition. Therefore, in this load condition, the same results are expected for both control configurations. However, by reducing the load value, the efficiency in the conventional topology is drastically reduced while the proposed control system has the efficiency always more than 93% in all the load conditions. This improvement is more obvious in low load condition. For example, in 10%FL/ 10%FL condition, the proposed

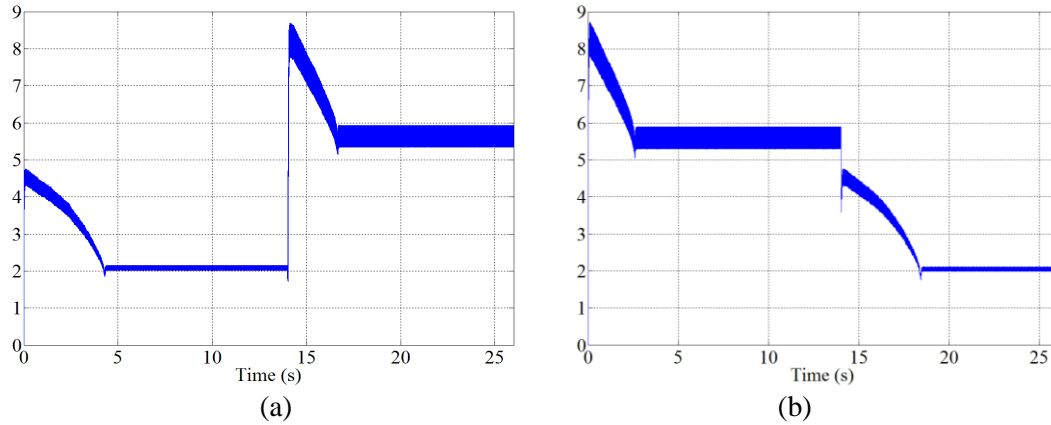


Fig.2.12. Transient response of  $i_{ref}$  as a function of  $\alpha$ . (a):10%full load to full load, (b): full load to 10 %full load).

Table.2.4. Efficiency in different load conditions.

Loads	$P_{o1}$ (W)	$P_{o2}$ (W)	$P_{tot}$ (W)	Conventinal Eff.(%)	$\alpha$ algorithm Eff. (%)
FL / FL	1000	1000	2000	97	97
FL / 10%F1	1000	100	1100	65	95
55%FL/ 55%FL	550	550	1100	62	94
10%FL/ 10%FL	100	100	200	47	93.2

control system improves the efficiency in nearly 46.2 points compared to the conventional result. This improvement is a consequence of the adaptive reference input current which is updated by changing the load conditions.

## 2.6. CONCLUSION

A new adaptive control algorithm for the contactless system with multiple mobile loads has been presented in this chapter. The presented control system operates by using indirect information about the load conditions. The estimation of the load consumption is obtained by measuring and filtering the input control signal. The new control algorithm can guarantee the maximum efficiency for all the load conditions. Therefore, make the possibility to have a contactless system with a long primary winding loop with high efficiency. Moreover, a theoretical tool for the analysis of the proposed control algorithm has been introduced. The

averaged large-signal model is obtained based on the space-state model of the system. Then, the control design procedure is applied to the averaged model. The proposed control algorithm is detecting the optimal value of the reference input current in all the load conditions. Also, the control system can update the value of the reference input current during the load step changes. An efficiency more than 93% is achieved in all the load conditions

---

# Analysis and design of a partially-controlled ICET system

---

## Summary

---

<b>3.1 INTRODUCTION.....</b>	<b>43</b>
<b>3.2 ICET SYSTEM UNDER STUDY.....</b>	<b>44</b>
<b>3.3 ICET SYSTEM WITH FREQUENCY MODULATION TECHNIQUE.....</b>	<b>45</b>
<b>3.4 ICET SYSTEM WITH PHASE MODULATION TECHNIQUE .....</b>	<b>50</b>
<b>3.5 ICET SYSTEM WITH QUANTUM MODULATION TECHNIQUE.....</b>	<b>60</b>
<b>3.6 DESIGN OF THE RESONANT TRANSFORMER.....</b>	<b>66</b>
<b>3.7 EVALUATION OF THE TRANSIENT RESPONSE .....</b>	<b>71</b>
<b>3.8 CONCLUSION .....</b>	<b>75</b>

---

This chapter presents a partially-controlled ICET system as an alternative to the conventional fully-controlled topology. The features of the new topology are analyzed by considering several modulation techniques, including frequency modulation (FM), phase modulation (PM) and quantum modulation (QM). The performance of the new topology is evaluated and the best modulation technique is identified. The chapter ends with the design of the new topology with the best modulation technique.



### 3.1. INTRODUCTION

The ICET with the fully-controlled system was presented in [80]-[83]. As mentioned in chapter one, the conventional system with fully-controlled algorithm is complex and expensive. Therefore, to find a simple and cost effective product, this study has been done. In this study, a partially-controlled ICET system as an alternative to the conventional fully-controlled topology is presented [84]. The features of the new topology are analyzed by considering several modulation techniques, including frequency modulation (FM), phase modulation (PM) and quantum modulation (QM). Note that, in this chapter, the presented control systems for FM and PM are operating in open loop and QM is operating in closed loop without access to the load information ( $v_o, i_o \dots$ ). This is done to facilitate the generation of the driving signals for the switches in the QM, which are in general more complicated compared to FM and PM techniques.

The chapter also presents a detailed design process for the resonant transformer. The effects of several parameters such as resonant frequency, magnetizing inductance and characteristic impedance are considered in the design process. The proposed design improves the system efficiency and guarantees a unity gain. Then, the evaluation of the complete system under several load conditions and load step changes is presented. The achieved result shows the excellent performance of the proposed system in steady-state and transient state.

The main contributions of this chapter are: 1) a new topology to supply ICET system with multiple clamps, 2) the identification of the best control technique for the proposed topology, 3) the design procedure of the resonant components that fulfill the desired specifications in terms of system efficiency and voltage gain, 4) the performance evaluation of the complete system, including input PFC stage, resonant inverter and load post-regulators.

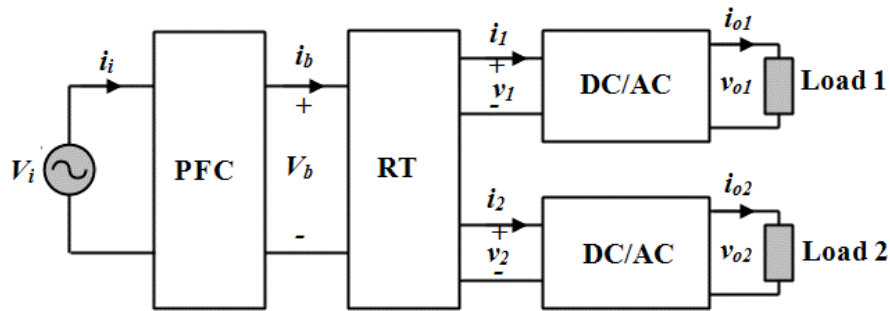


Fig.3.1. General diagram of the ICET system with two clamps.

### 3.2. ICET SYSTEM UNDER STUDY

Fig.3.1 shows the general configuration of the ICET system with multiple clamps. This topology consists of a power factor converter (PFC), a resonant transformer (RT) and two mobile clamps with output converters. The system is connected to a single-phase input voltage source ( $V_i$ ) with  $230 V_{rms}$  and 50 Hz frequency. The RT is the key element in this system and it is responsible to eliminate the direct electrical connection between the input source and the loads. The input PFC and the output DC/AC inverters are conventional topologies. They are using a closed-loop control system with the aim of providing a unity power factor and well-regulated output voltages.

Fig.3.2 illustrates the schematics of the RT system with sliding transformer and two mobile clamps. The input DC voltage ( $V_b$ ) is inverted into a high frequency AC voltage ( $v_p$ ) by means of the inverter (INV). A high frequency resonant voltage is delivered to the mobile

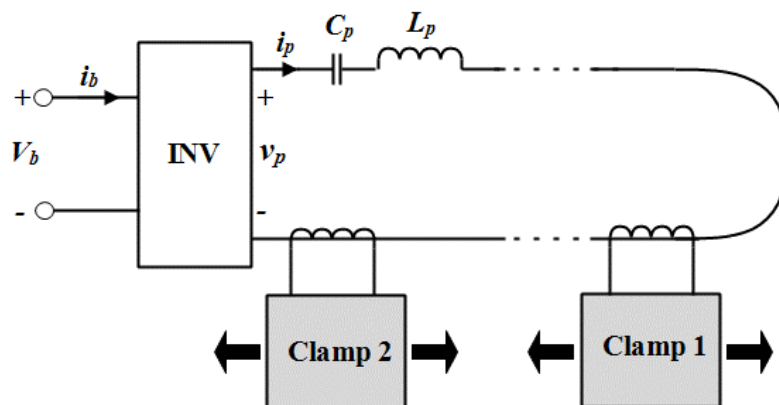


Fig. 3.2. Schematic of the resonant transformer with sliding transformer and two mobile clamps.

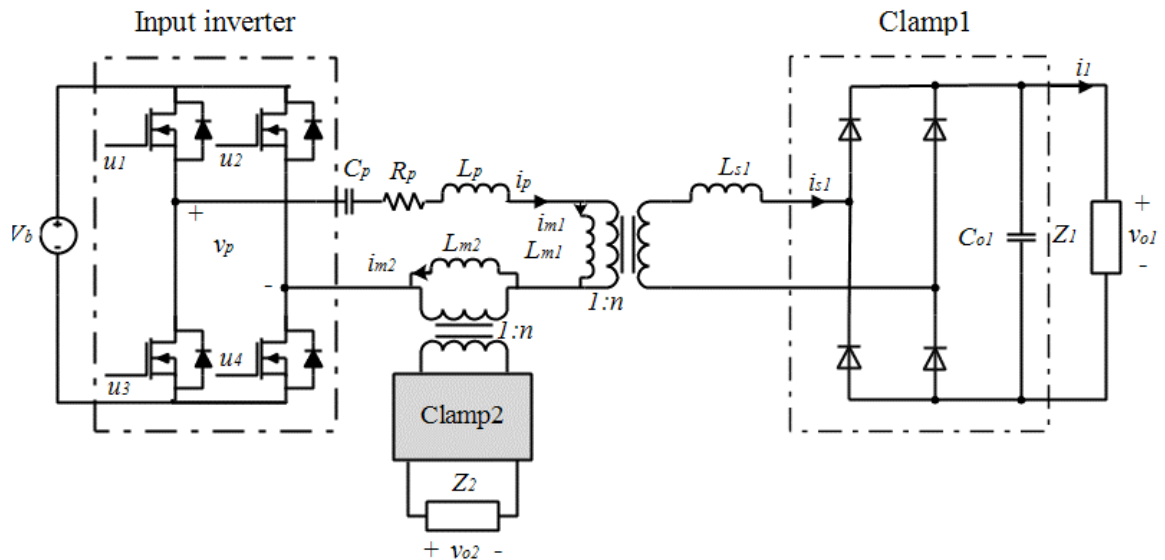


Fig.3.3. Electrical circuit representation of the RT system with sliding transformer and two mobile clamps

clamps via a series resonant circuit and a long primary winding loop through the sliding transformer. As explained in chapter 1, the mobile clamps have the possibility to move along the primary winding loop.

Fig.3.3 illustrates the electrical circuit representation of the RT system with two mobile clamps. Note that the transformer is modeled by three parasitic elements: a parasitic resistor ( $R_p$ ), a magnetizing inductance ( $L_m$ ) and an output leakage inductance ( $L_s$ ). The (small) input leakage inductance is absorbed by the discrete primary side inductance ( $L_p$ ). It is interesting to note that the magnetizing inductance has a small value in this application ( $50\mu\text{H}$ ). This fact will have a significant impact on the RT operation as will be explained below. In this model, two transformers are connected in series at the input side and in parallel with the corresponding loads at the output side. This is a consequence of the primary winding loop shown in Fig.3.2.

### 3.3. ICET SYSTEM WITH FREQUENCY MODULATION TECHNIQUE

During the last decades, the frequency modulation technique has been studied in the literature [84]-[90]. This control technique has been applied for different topologies such as parallel, series and series-parallel converters. Generally, the series resonant (SRC) topology has been applied to the ICET system with multiple clamps due to its benefits [90]. In series

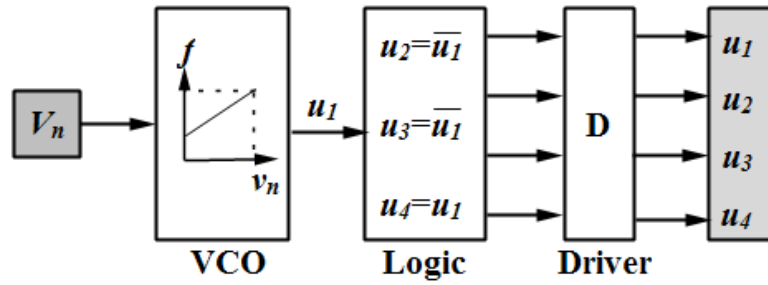


Fig.3.4. Frequency modulation diagram of the input converter.

resonant converter, operation above resonance frequency is preferred because it offers higher efficiency [90]. Therefore, the regulation of the output voltage against load variation can be achieved by varying the switching frequency. This principle of operation can be applied to multiple mobile clamps in order to achieve a fixed output voltage for different load conditions. Note that the specification for the output voltage is 450V and the loads will be varied from  $176\Omega$  (full load) to  $1760\Omega$  (10% full load).

Fig.3.4 depicts the configuration of the frequency modulator. Note that this scheme is an open loop control system, which does not require the measure of any signal from the resonant circuit. In other words, the control input of the modulator is maintained constant for a specified number of clamps and a particular design of the resonant circuit components. This open loop operation is not really a problem since the input PFC and the output converters operate in closed loop. In the ICET system with sliding transformer, the loads are moving along the distance of the primary loop. Thus, the system is notably simplified by assuming that the resonant converter operates in open loop (with no need to measure the voltage around the mobile loads).

Fig.3.5 shows the gain curves of the designs 100kHz, 200kHz and 1MHz. Each figure has three curves corresponding to different load combination (see details at figure caption). The frequency axis is normalized as a function of the resonant frequency, i.e.,  $f_s / f_o$ , where  $f_o = 1 / 2 \pi (\text{sqrt} (L_p * C_p))$ . In view of these figures, the following comments can be made:

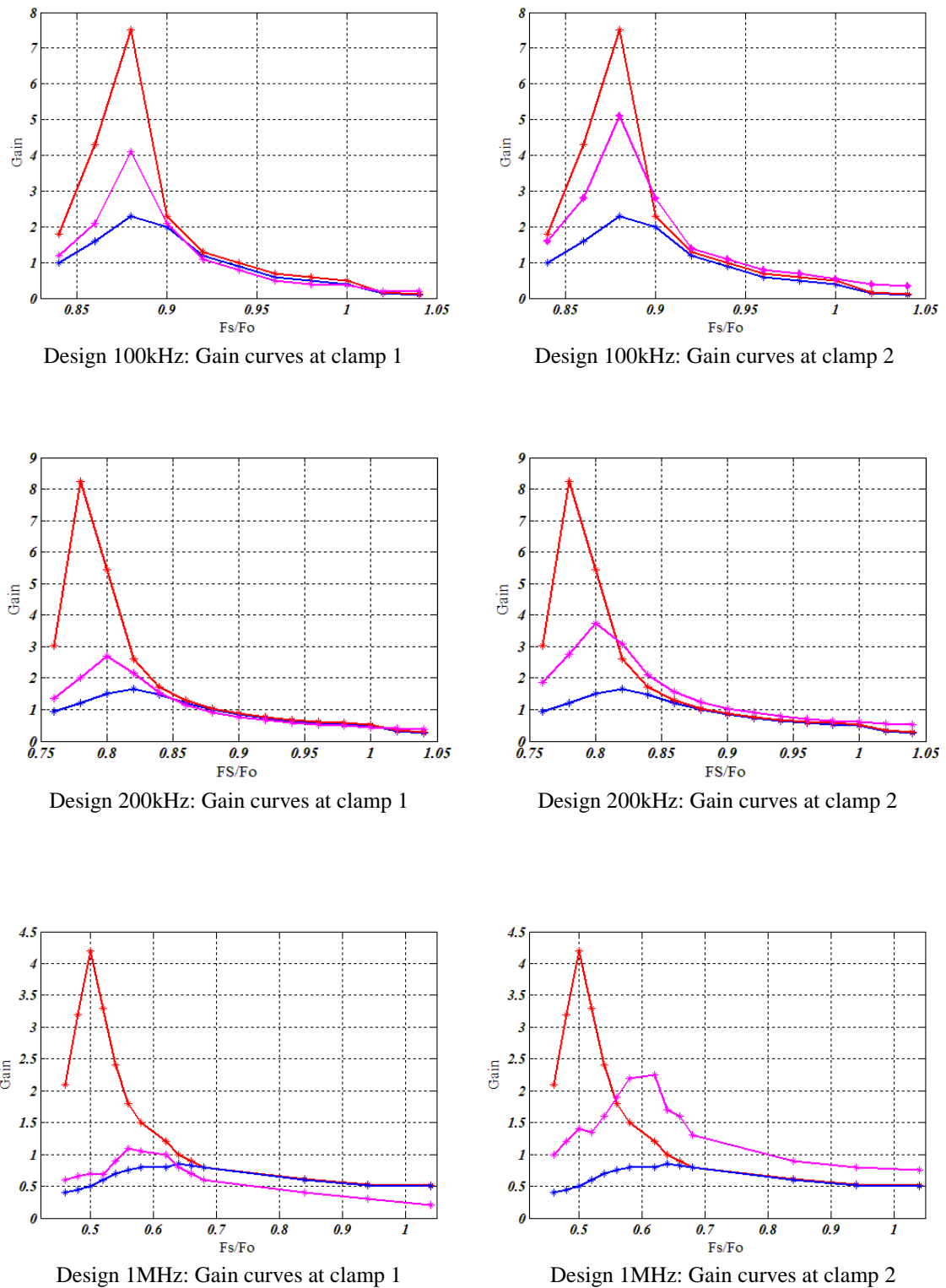


Fig.3.5. Gain curves for different designs and load combination. Blue:  $R_{o1}=R_{o2}=176$ , Red:  $R_{o1}=R_{o2}=1760$ , Pink:  $R_{o1}=176, R_{o2}=1760$ . Note that 176 corresponds to full load and 1760 to 10% of full load.

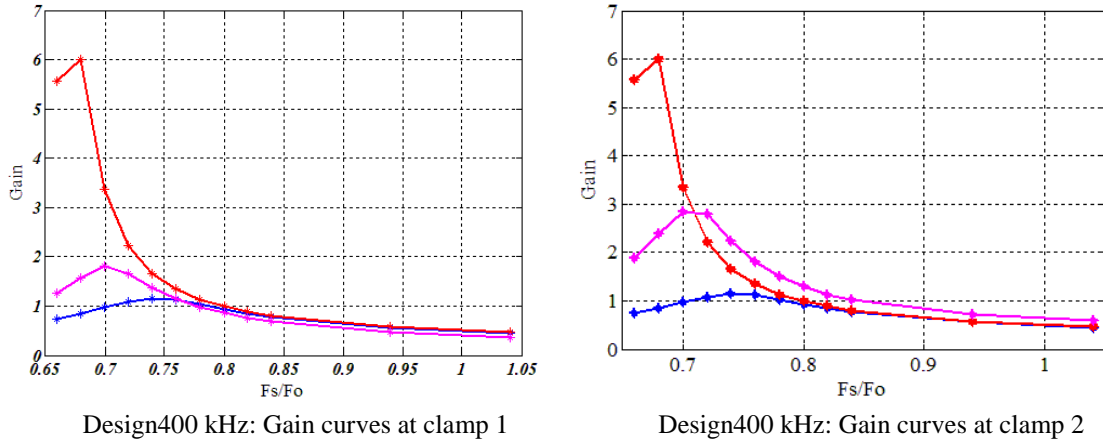


Fig.3.6. Gain curves for design 400kHz. Blue:  $R_{o1}=R_{o2}=176$ , Red:  $R_{o1}=R_{o2}=1760$ , Pink:  $R_{o1}=176, R_{o2}=1760$ .

- With design 100kHz, the peak of the gain curves is placed in the same location ( $f_s/f_o = 0.88$ ). This is the limit point between capacitive (ZCS) and inductive (ZVS) operating region. The gain = 1 is in the inductive region at  $f_s/f_o = 0.94$ , as desired. The gain is nearly constant at  $f_s/f_o = 0.94$  (small output voltage variation is expected for the entire range of load resistors).
- With design 200kHz, the peak of the gain curves varies with the load resistors. Fortunately, the gain = 1 point is always located in the inductive region (i.e., ZVS can be guaranteed for all the load range). This point can be identified as  $f_s/f_o = 0.88$ . A higher output voltage variation is expected in this case for  $f_s/f_o = 0.88$ , in comparison with design 100kHz results.
- With design 1MHz, we can identify several problems: 1) the gain = 1 cannot be achieved for all the considered loads, 2) when gain = 1 is achieved, the frequency variation necessary to obtain this gain is high. This suggests that a closed-loop regulator is necessary to maintain this gain. Note that, in design 100kHz and 200kHz, the modulator can operate in open loop fixing the frequency as  $f_s/f_o = 0.94$  and  $f_s/f_o = 0.88$ , respectively.

The next step is to find a new design with the maximum possible switching frequency and gain = 1 for all the considered loads. Fig.3.6 shows the gain curves for the design 400kHz. We choose  $f_s/f_o = 0.8$  as the constant switching frequency with gain = 1. A certain output

voltage variation is expected in this design (see, for example, the gain at  $f_s/f_o = 0.8$  in the clamp2 for  $R_{o1} = 176$ ,  $R_{o2} = 1760$ ).

The output voltages ( $v_{o1}$  and  $v_{o2}$ ), switching frequency ( $f_s$ ), average input current ( $i_i$ ), efficiency ( $\eta$ ) and total output power ( $P_t$ ) is presented in Table.3.1, Table.3.2 and Table.3.3 for the following load conditions: Full load, 50 % full load, and 10 % full load. Note that, the design 1MHz is not considered in this study. This design does not accomplish the output voltage specifications. As evident from the tables, the maximum efficiency is achieved in design 400kHz. Therefore, for the open-loop FM system, we have identified a design trade-off between efficiency and voltage deviation (as a function of load).

Table.3.1. Design of 100kHz for two clamps with FM control.

Design	$R_{o1}$ ( $\Omega$ )	$R_{o2}$ ( $\Omega$ )	$v_{o1}/V_b$	$v_{o2}/V_b$	$i_i$ (A)	$f_s$ (kHz)	$\eta$ (%)	$P_t$ (W)
100kHz	176	176	0.924	0.924	5.16	94.2	84.61	1964.7
100kHz	176	325	0.887	0.980	4.04	94.2	80.22	1458.4
100kHz	176	1760	0.859	1.082	3.02	94.2	72.46	984.78
100kHz	325	325	0.934	0.934	3.01	94.2	73.99	1005.6
100kHz	325	1760	0.8984	1.027	2.11	94.2	61.69	585.8
100kHz	1760	1760	0.978	0.9	1.29	94.2	37.96	220.4

Table.3.2. Design of 200kHz for two clamps with FM control.

Design	$R_{o1}$	$R_{o2}$	$v_{o1}/V_b$	$v_{o2}/V_b$	$i_i$ (A)	$f_s$ (kHz)	$\eta$ (%)	$P_t$ (W)
200kHz	176	176	0.994	0.994	5.45	177	92.83	2276.7
200kHz	176	325	0.950	1.090	4.30	177	89.04	1723.1
200kHz	176	1760	0.911	1.249	3.16	177	80.63	1135.7
200kHz	325	325	1.014	1.014	3.14	177	83.79	1184
200kHz	325	1760	0.947	1.141	2.07	177	71.53	666.3
200kHz	1760	1760	1.038	1.038	1.15	177	47.99	248.3

Table.3.3. Design of 400kHz for two clamps with FM control.

Design	$R_{o1}$	$R_{o2}$	$v_{o1}/V_b$	$v_{o2}/V_b$	$i_i$ (A)	$f_s$ (kHz)	$\eta$ (%)	$P_t$ (W)
400kHz	176	176	0.928	0.928	4.48	325	98.44	1984.6
400kHz	176	325	0.865	1.072	3.59	325	94.33	1523.9
400kHz	176	1760	0.859	1.297	2.73	325	85.01	1044.3
400kHz	325	325	0.972	0.972	2.71	325	89.30	1089
400kHz	325	1760	0.893	1.150	1.80	325	75.55	611.9
400kHz	1760	1760	0.991	0.911	0.96	325	52.32	226.04

### 3.4. ICET SYSTEM WITH PHASE MODULATION TECHNIQUE

Phase modulation (PM) is another possibility to control the state of the full-bridge inverter switches ( $S_1$ ,  $S_2$ ,  $S_3$ , and  $S_4$ ) [91]-[94]. In this section, the characteristics of the SRC with multiple clamp are analyzed for different designs. As mentioned in previous section, the specification for the output voltage is 450V and the loads will be varied from 176 $\Omega$  (full load) to 1760 $\Omega$  (10% full load). Advantages and limitations of PM are revealed through simulation results. In particular, the efficiency and voltage deviations are compared to the results obtained with FM.

Fig.3.7 illustrates the implementation of the PM. The principle of operation of this modulator is shown in Fig 3.8. From the figure, a ramp signal is compared with two control parameters  $\gamma_1$  and  $\gamma_2$  to generate the state of the full-bridge inverter switches. The ramp signal is synchronized with the zero crossing points of the resonant current,  $i_p$ . In this way, the modulator is robust to the variation of the resonant tank components (due to tolerance, age, temperature...). In other words, possible changes in these values are immediately known by the modulator by means of the online measuring of the resonant current. The parameter  $\gamma_1$  defines the time delay between the resonant current and the input voltage to the resonant tank. This delay guarantees ZVS operation for all the load range. The parameter  $\gamma_2$  is used to choice the desired output voltage.

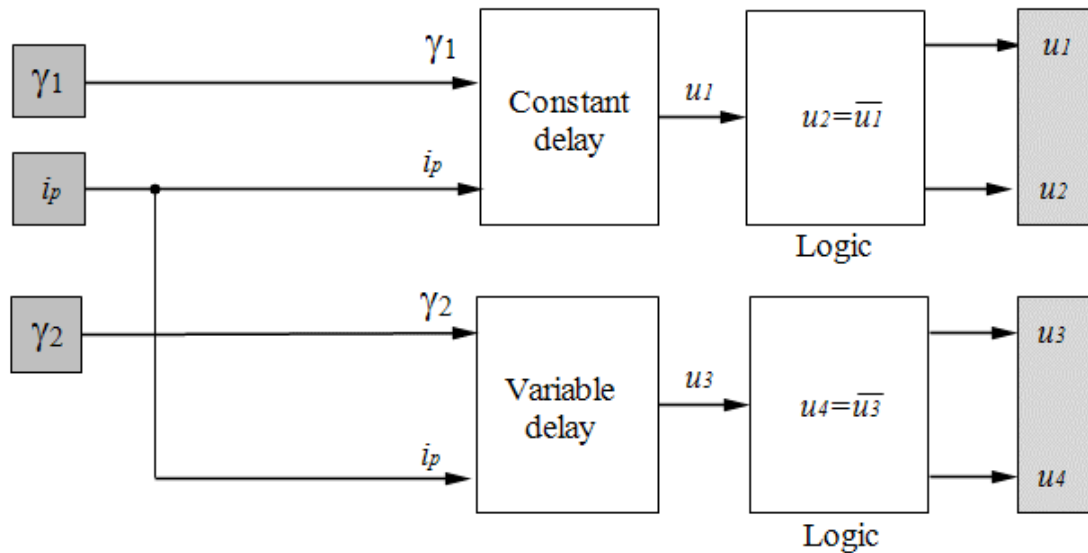


Fig.3.7. Phase modulation diagram of the input converter.

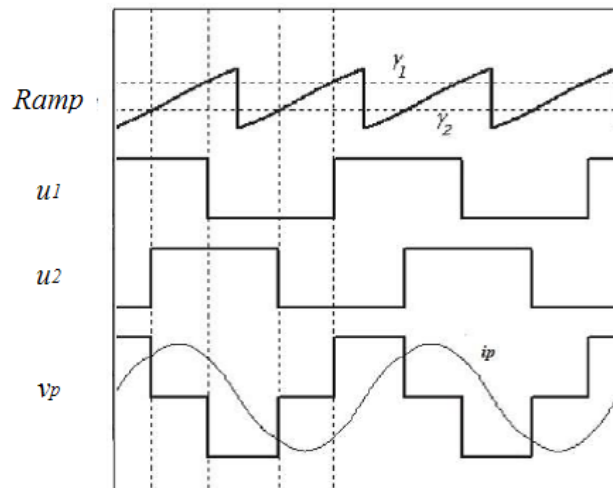


Fig3.8. Principal waveforms of the phase modulation.

Fig.3.9 shows the main waveforms of the SRC single-clamp with PM for two values of  $\gamma_1, \gamma_2$  and output resistor. Note that the time delay between the input voltage and the resonant current is fixed due to the constant value of  $\gamma_1$ . This point can be easily observed by measuring the time delay between the zero to top value of the input voltage and the zero crossing point in the resonant current. Note that the variation of  $\gamma_2$  produces a change in the duration of the zero voltage interval of the input voltage. In general, the output voltage reduces as the zero voltage interval increases.

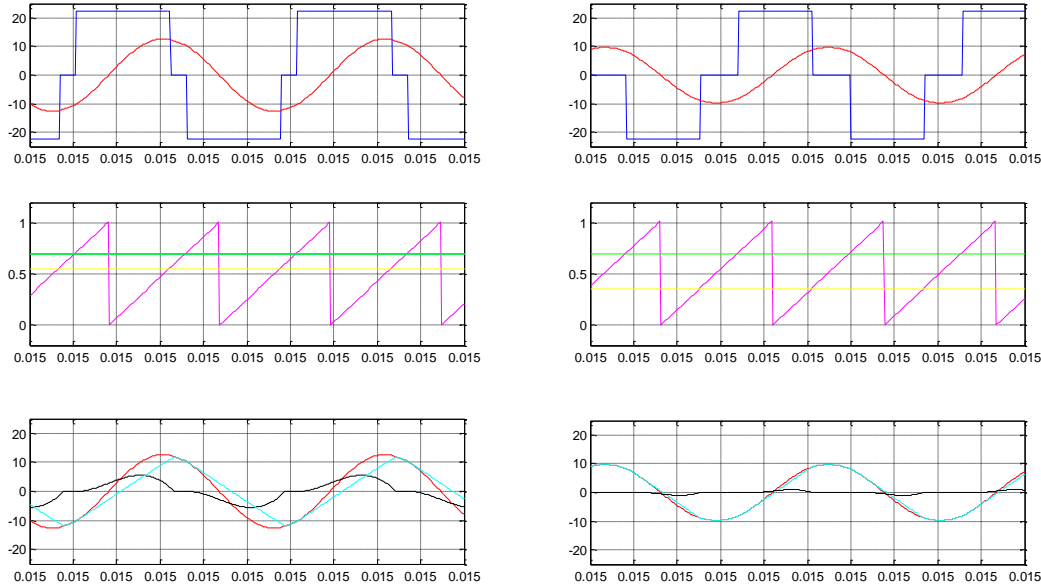


Fig. 3.9. Main waveforms of the SRC single-clamp with PM (design 100kHz). (Left)  $\gamma_1 = 0.7$ ,  $\gamma_2 = 0.55$  and  $R_o = 176 \Omega$ . (Right)  $\gamma_1 = 0.7$ ,  $\gamma_2 = 0.35$  and  $R_o = 1760 \Omega$ . Blue:  $0.05 \cdot \text{input voltage}$ , red: resonant current, pink: ramp signal, green:  $\gamma_1$ , yellow:  $\gamma_2$ , light blue: magnetizing current, black: secondary side current

Fig.3.10 shows the gain curves of the SRC with PM. Each graph corresponds to a particular design (100 kHz, 200 kHz, or 1000 kHz) and a fixed value for  $\gamma_1$  (0.7, 0.75, or 0.85). The gain curves are depicted as a function of the parameter  $\gamma_2$  (from 0.35 to 0.7). As state above, the parameter  $\gamma_1$  defines the time delay between the resonant current and the input voltage to the resonant tank. In particular, the time delay decreases as  $\gamma_1$  increases. This parameter also has a certain influence on the voltage gain. In general, the output voltage increases as the parameter  $\gamma_1$  increases. On the other hand, the parameter  $\gamma_2$  is normally used to choice the desired output voltage. Note that the output voltage increases as the parameter  $\gamma_2$  increases.

What is even more important is to observe that the gain curves are load dependent. If we fix a constant value for  $\gamma_1$  and  $\gamma_2$ , the output voltage varies with the load resistor. This is probably the main limitation of the SRC with PM. Remember that with FM, the output voltage is practically independent of the load when the gain is around 1. In PM, it is possible to achieve gain = 1 in all the considered designs by varying  $\gamma_1$  and  $\gamma_2$ . This means that open loop operation is not allowed in PM. Therefore, a closed-loop control should be designed in order to get the specified output voltage.

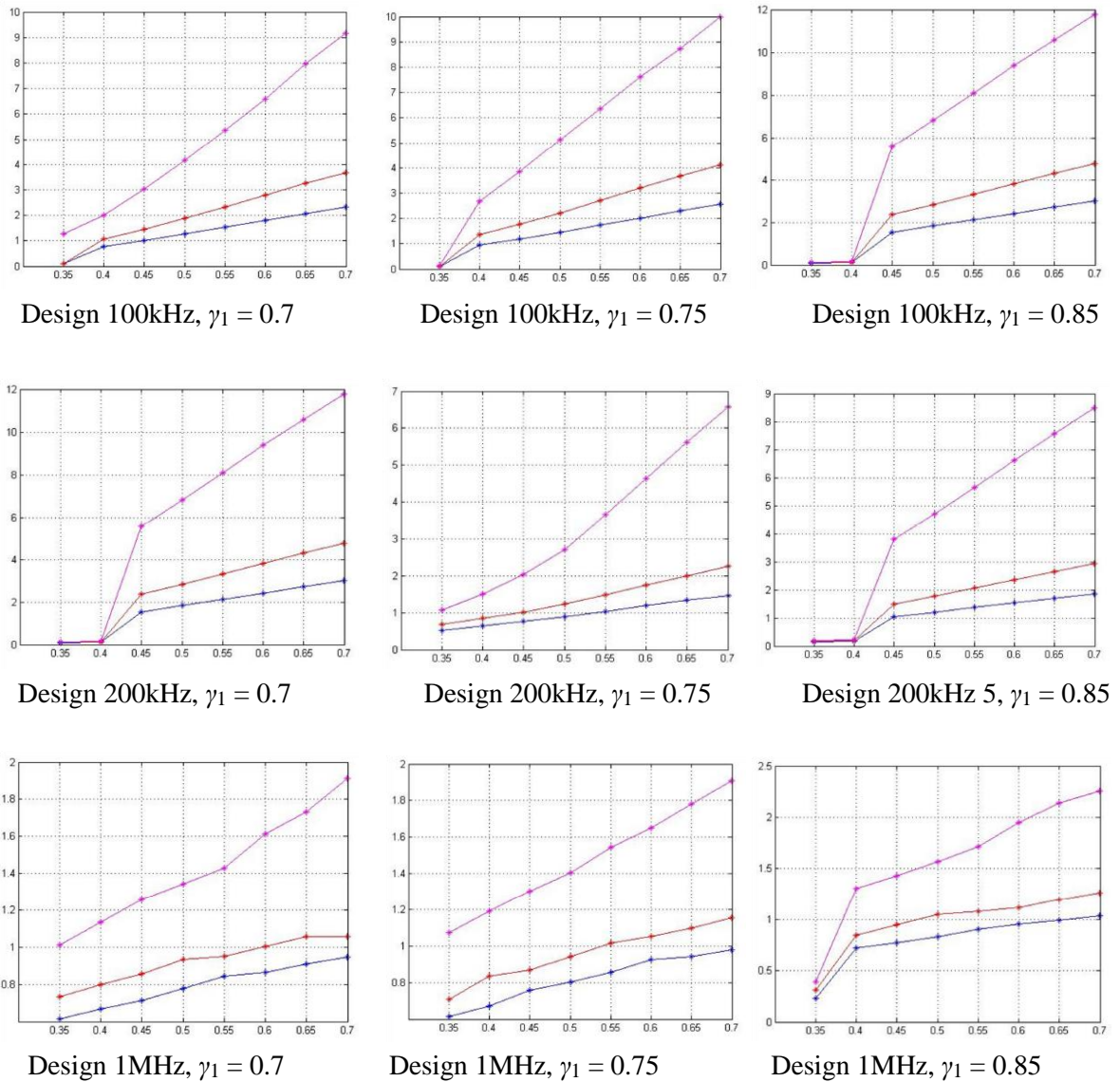


Fig.3.10. Gain of the SRC with PM as a function of  $\gamma_2$  for one clamp. Blue:  $R_o = 176 \Omega$  (FL), Red:  $R_o = 352\Omega$  (50% FL) Pink:  $R_o = 1760 \Omega$  (10% FL).

Below we will analyze the features of the SRC with PM and  $\gamma_1 = 0.7$  (constant value from now on) in Table 3.4, 3.5 and 3.6 for one clamp. We have chosen this value due to the output voltage is in general lower with  $\gamma_1 = 0.7$  and thus it is easier to achieve the desired gain = 1 (note that it is not always possible to obtain gain = 1 with  $\gamma_1 = 0.75$  or 0.85). It is interesting to note that, in general, better efficiency is achieved with PM in comparison with the results obtained with FM (except of design 1MHz).

Table.3.4. Design 100kHz for one clamp with PM control.

$\gamma_1$	$\gamma_2$	load	$v_o/V_b$	$i_i$	$f_s/f_o$	$P_{out}$	$\eta$ % PM	$\eta$ % FM
0.7	0.45	full	1.0062	3.06	1	1164.9	84.6	62.1
0.7	0.40	50% full	1.0776	1.93	0.99	667.97	76.0	47.5
0.7	0.35	10% full	1.2653	0.87	0.98	184.21	47.0	29.8

Table.3.5. Design 200kHz for one clamp with PM control.

$\gamma_1$	$\gamma_2$	load	$v_o/V_b$	$i_i$	$f_s/f_o$	$P_{out}$	$\eta$ % PM	$\eta$ % FM
0.7	0.55	full	1.0391	3.02	1	1242.3	91.4	83.5
0.7	0.45	50% full	1.0178	1.52	1	595.92	87.1	74.1
0.7	0.35	10% full	1.0651	0.45	1	130.52	64.0	41.2

Table.3.6. Design 1MHz for one clamp with PM control.

$\gamma_1$	$\gamma_2$	load	$v_o/V_b$	$i_i$	$f_s/f_o$	$P_{out}$	$\eta$ % PM	$\eta$ % FM
0.7	0.70	full	0.9458	2.55	1.08	1029.2	89.7	93.6
0.7	0.60	50% full	1.0044	1.51	0.99	580.40	85.5	88.2
0.7	0.35	10% full	1.0129	0.41	0.98	118.04	64.0	59.1

Fig.3.11 shows the main reason behind these results. The figure shows the input voltage of the resonant tank and the input current of the converter with the PM and FM. Note that, in PM, the input current is zero during the 0V interval of the input voltage. In FM, the input current is always continuous (no zero current interval is present). The average current flowing from the source is nearly the same in both modulation techniques given that the input and output voltages and the output resistor coincide in both cases. However, the average positive current and the average negative current are higher in FM, thus producing higher conduction losses and lower efficiency in the converter. In design 1MHz, the switching frequency is so high (10 times higher than in design 100kHz) that the difference between the average positive current in both modulation techniques is negligible. The same argument is valid for the average negative current. In this discussion, “average positive current” means the averaged value of only the positive current; the negative current is not considered (it is assumed to be zero) when calculating the averaged positive current. A similar definition can be used for “average negative current”. In this case, the positive current is assumed to be zero.

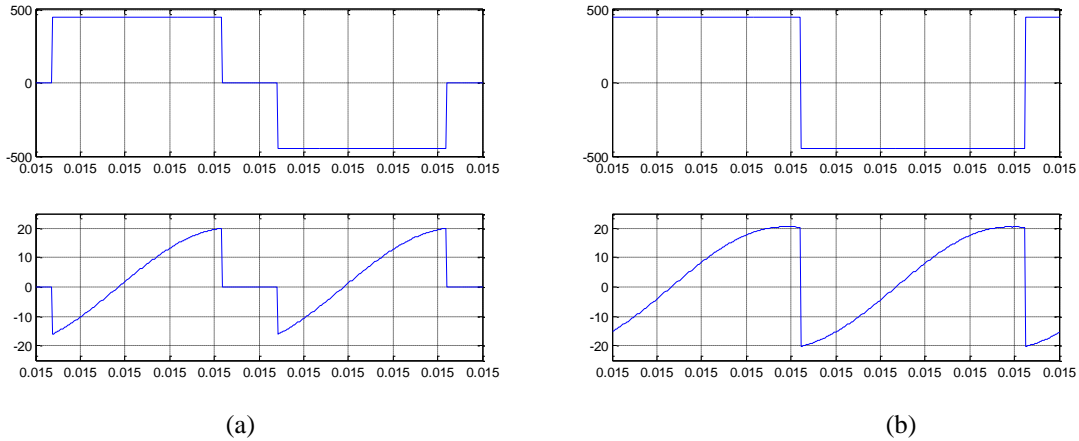


Fig.3.11. Input voltage of the resonant tank (top) and input current of the converter (bottom) for  $\gamma_1 = 0.7$ ,  $\gamma_2 = 0.45$  and  $R_o = 176 \Omega$  (design 100kHz): (a) PM, (b) FM.

Fig.3.12, Fig.3.13 and Fig3.14 show the gain curves of the two-clamps SRC with PM. For design 100kHz, the gain curves are depicted in Fig.3.12. In this case, the gain = 1 is reached for all the considered loads. The parameter  $\gamma_1$  is fixed at 0.7 and  $\gamma_2$  is modified in order to get different output voltages. For design 200kHz, the gain curves are shown in Fig.3.13. The gain = 1 is also reached for all the considered loads. However, in this case, the parameter  $\gamma_1$  must be varied according to the load in order to get the desired gain = 1. In fact, if  $\gamma_1$  is maintained at 0.7 in design 200kHz, the gain is lower than 1 for several load combinations. For design 1MHz, the gain curves are depicted in Fig.3.14. In this design, it is not possible to guarantee a gain = 1 for all considered loads. Note that  $\gamma_1$  has been increased from 0.7 to 0.95 with the aim to enlarge the gain, but even in this situation the gain is lower than 1 in some cases.

This low gain feature for design 200kHz was previously observed in the two-clamped SRC with FM. In that case, the problem was solved by reducing the natural switching frequency  $f_o$  from 1 MHz to 400 kHz. In fact, design 400kHz was the design with highest switching frequency and gain = 1 in FM. In the case of PM, it is not possible to get gain = 1 with design 400kHz. The gain is lower than 1 for some load combinations due to  $\gamma_1$  is chosen lower than 1 (i.e., the resonant circuit does not operate at maximum gain in order to guarantee ZVS for all the load range). Actually, it has been found that it is necessary to reduce the natural switching frequency below 400 kHz to achieve unity gain. In fact, the design with highest switching frequency and gain =1 in PM is design 250 kHz.

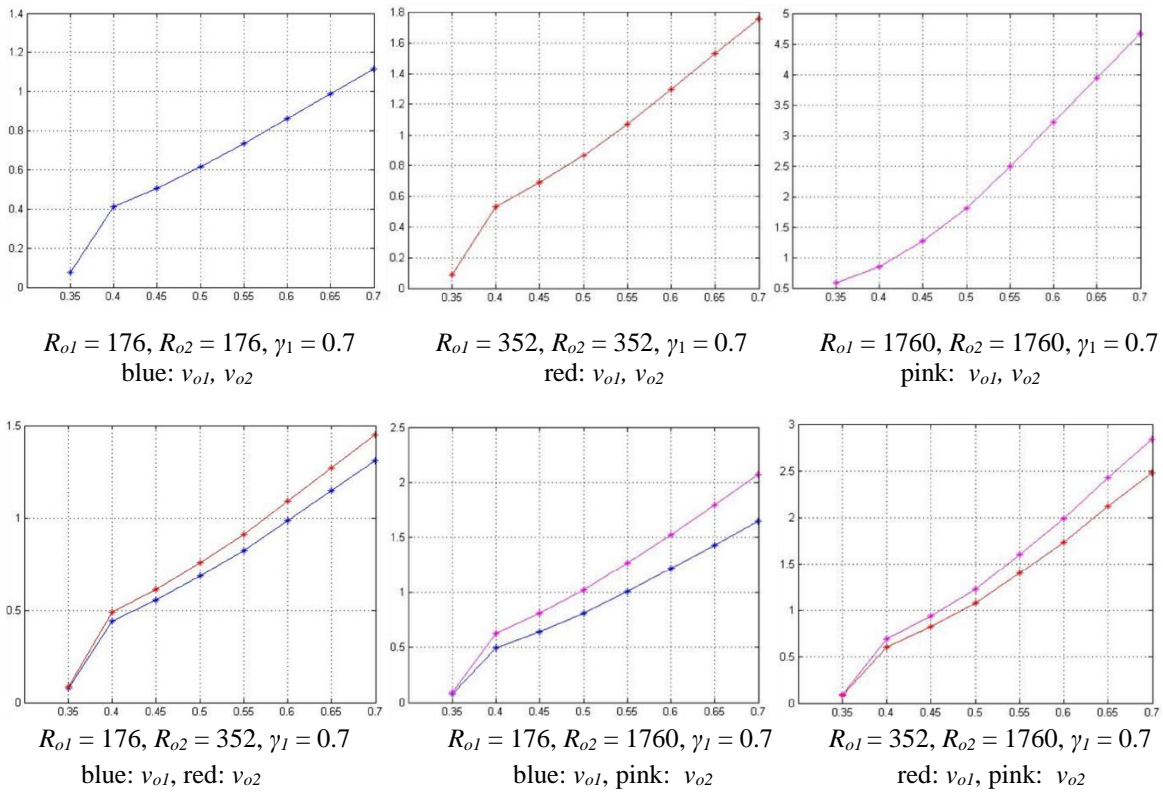


Fig.3.12. Gain curves for design 100 kHz as a function of the parameter  $\gamma_2$  for two clamps.

The gain curves for design 250 kHz are shown in Fig.3.15. Note that design 250kHz is a valid design. It provides a gain = 1 for all the load range with the highest switching frequency. As a negative point, both control parameters  $\gamma_1$  and  $\gamma_2$  must be online calculated to get the desired gain (i.e., complex control implementation).

Table.3.7, Table.3.8 and Table.3.9 present the information about gain, efficiency, input current and total power of the proposed system with phase modulation technique. These results are obtained in several design conditions. As evident, design 250kHz has more efficiency. Therefore, in this study it can be considered as the best design for PM technique.

It should be mentioned that the following results are measured operating the two-clamp SRC in open loop. The parameters  $\gamma_1$  and  $\gamma_2$  are tuned manually in order to get a gain as near as possible to 1. In a real scenario, this converter with PM must be operated in closed-loop.

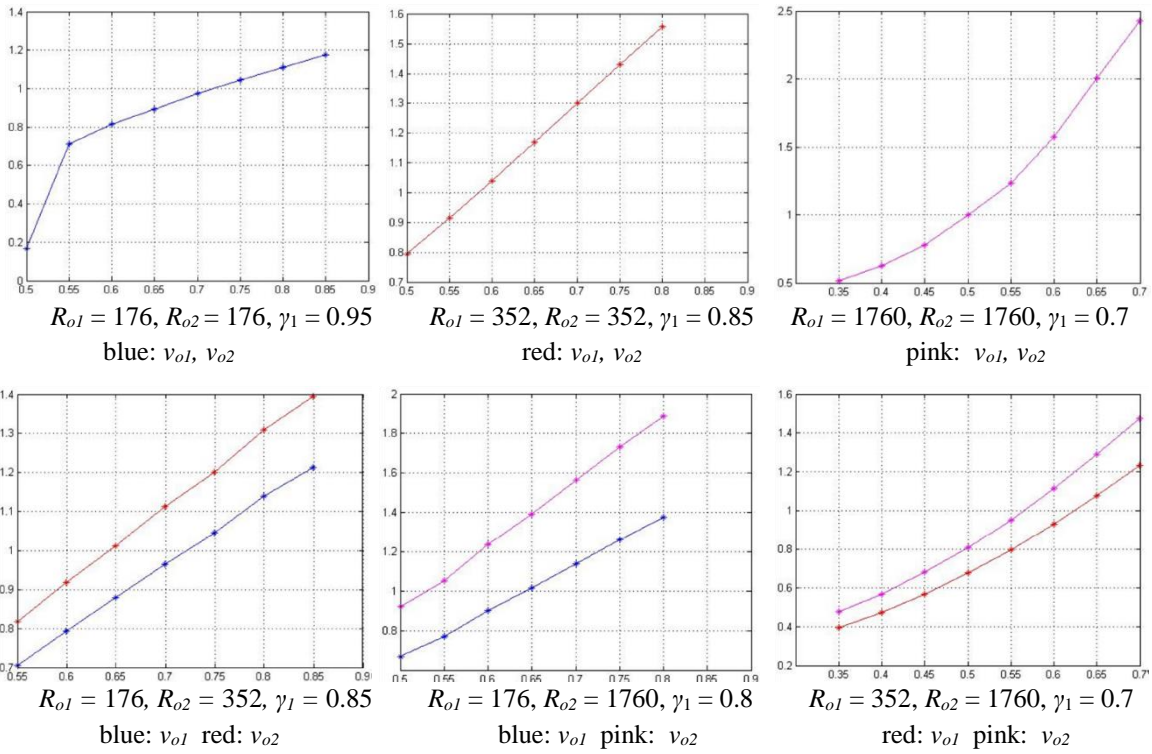


Fig.3.13. Gain curves for design 200 kHz as a function of the parameter  $\gamma_2$  for two clamps.

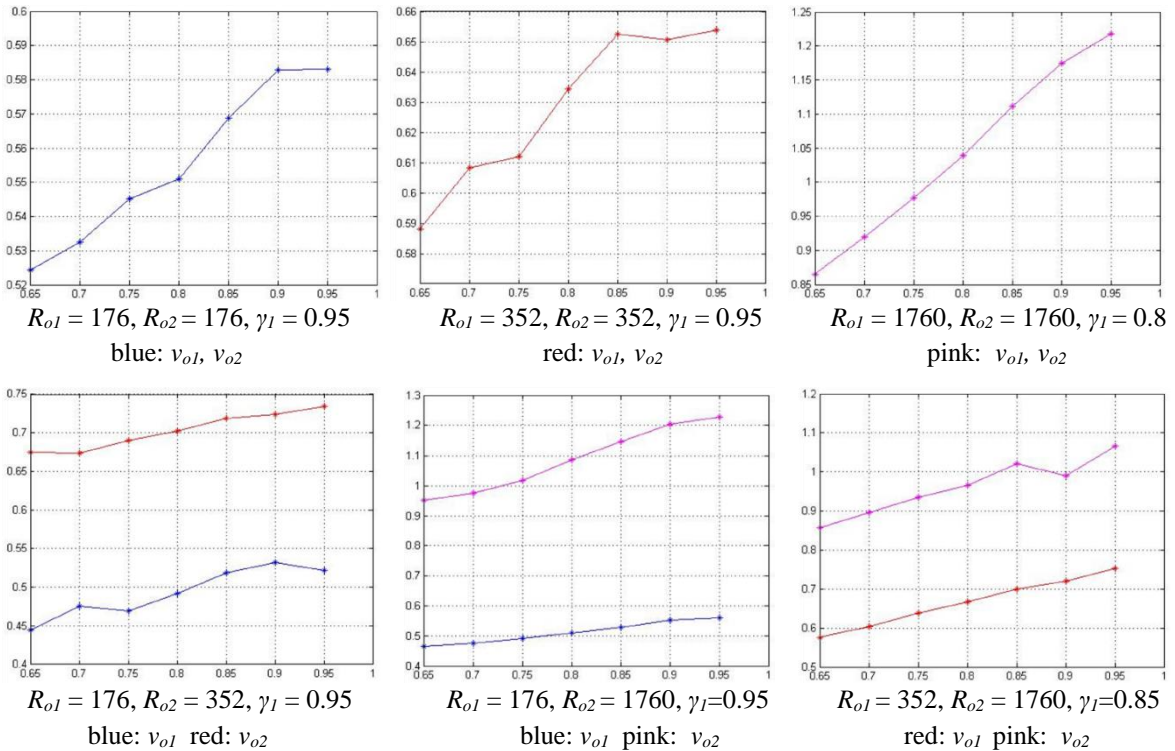


Fig3.14. Gain curves for design 1MHz as a function of the parameter  $\gamma_2$  for two clamps.

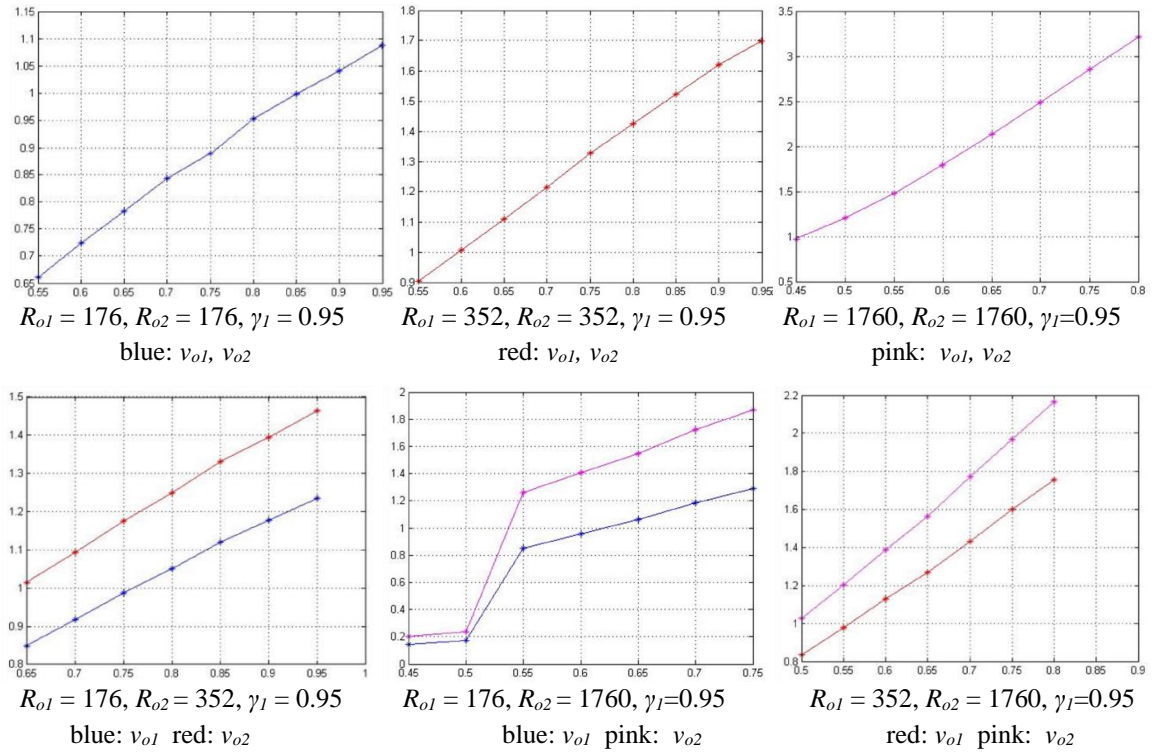


Fig.3.15. Gain curves for design 250 kHz as a function of the parameter  $\gamma_2$  for two clamps.

Table.3.7. Design 100kHz for two clamps and PM control.

Design	$R_{o1}$	$R_{o2}$	$\gamma_1$	$\gamma_2$	$v_{o1}/V_b$	$v_{o2}/V_b$	$i_i$ (A)	$f_s/f_o$ (kHz)	$\eta$ (%)	$P_t$ (W)
100kHz	176	176	0.7	0.65	0.99	0.99	5.62	0.93	89.17	2255.3
100kHz	176	325	0.7	0.65	0.92	1.02	3.98	0.93	87.79	1572.4
100kHz	176	1760	0.7	0.52	0.92	1.16	2.92	0.93	85.89	1128.7
100kHz	325	325	0.7	0.53	0.99	0.99	2.95	0.93	84.94	1127.7
100kHz	325	1760	0.7	0.47	0.93	1.07	1.81	0.93	77.26	629.29
100kHz	1760	1760	0.7	0.42	1.02	1.02	0.96	0.93	55.41	239.41

Table.3.8. Design 200kHz for two clamps and PM control.

Design	$R_{o1}$	$R_{o2}$	$\gamma_1$	$\gamma_2$	$v_{o1}/V_b$	$v_{o2}/V_b$	$i_i$ (A)	$f_s/f_o$ (kHz)	$\eta$ (%)	$P_t$ (W)
200kHz	176	176	0.95	0.72	1	1	5.42	0.88	94.34	2301.1
200kHz	176	325	0.85	0.67	0.93	1.07	3.95	0.88	93.03	1653.8
200kHz	176	1760	0.8	0.58	0.83	1.14	2.33	0.89	89.85	942.15
200kHz	325	325	0.85	0.58	0.98	0.98	2.68	0.88	91.62	1105
200kHz	325	1760	0.7	0.58	0.89	1.07	1.49	0.89	87.60	587.41
200kHz	1760	1760	0.7	0.5	1	1	0.74	0.88	69.10	230.11

Table.3.9. Design 250kHz for two clamps and PM control.

Design	$R_{o1}$	$R_{o2}$	$\gamma_1$	$\gamma_2$	$v_{o1}/V_b$	$v_{o2}/V_b$	$i_i$ (A)	$f_s/f_o$ (kHz)	$\eta$ (%)	$P_t$ (W)
250kHz	176	176	0.95	0.85	1	1	5.4	0.86	94.7	2301.1
250kHz	176	325	0.95	0.7	0.91	1.09	3.92	0.86	92.75	1636.3
250kHz	176	1760	0.95	0.53	0.81	1.21	2.23	0.86	92.01	923.34
250kHz	325	325	0.95	0.59	1	1	2.78	0.85	91.97	1150.6
250kHz	325	1760	0.85	0.52	0.9	1.11	1.52	0.86	88.85	607.44
250kHz	1760	1760	0.8	0.45	1	1	0.72	0.86	71.02	230.11

To facilitate the efficiency comparison between PM and FM, Table.3.10 collects the efficiency results obtained with these modulation techniques in the two-clamped SRC system. The efficiency results are presented as a matrix form which shows the achieved results for different load conditions. The load condition for each element of the matrix is defined below:

$$\eta(\%) = \begin{bmatrix} \text{FL/FL} & \text{FL/50\%FL} & \text{FL/10\%FL} \\ 50\%FL/FL & 50\%FL/50\%FL & 50\%FL/10\%FL \\ 10\%FL/FL & 10\%FL/50\%FL & 10\%FL/10\%FL \end{bmatrix}$$

Table.3.10. Efficiency results for selected designs operating with the PM and FM. (\*) maximum frequency for which gain = 1 is reached in FM, (\*\*) maximum frequency for which gain = 1 is reached in PM.

Design	PM	FM
100 kHz	$\eta(\%) = \begin{bmatrix} 89.17 & 87.79 & 85.89 \\ 87.79 & 84.94 & 77.26 \\ 85.89 & 77.26 & 55.41 \end{bmatrix}$	$\eta(\%) = \begin{bmatrix} 84.61 & 80.22 & 72.46 \\ 80.22 & 84.94 & 61.69 \\ 72.46 & 61.69 & 37.96 \end{bmatrix}$
200 kHz	$\eta(\%) = \begin{bmatrix} 94.34 & 93.03 & 89.85 \\ 93.03 & 91.62 & 87.60 \\ 89.85 & 87.60 & 69.10 \end{bmatrix}$	$\eta(\%) = \begin{bmatrix} 92.83 & 89.04 & 80.63 \\ 89.04 & 83.79 & 71.53 \\ 80.63 & 71.53 & 47.99 \end{bmatrix}$
400 kHz (*)	-	$\eta(\%) = \begin{bmatrix} 98.44 & 94.33 & 85.01 \\ 94.33 & 89.30 & 75.55 \\ 85.01 & 75.55 & 52.32 \end{bmatrix}$
250kHz (**)	$\eta(\%) = \begin{bmatrix} 94.70 & 92.75 & 92.01 \\ 92.75 & 91.97 & 88.85 \\ 92.01 & 88.85 & 71.02 \end{bmatrix}$	-

### 3.5. THE ICET SYSTEM WITH QUANTUM MODULATION TECHNIQUE

The quantum modulation with only energizing mode produces a high gain in the SRC with low magnetizing inductance [82]. Therefore, in an open loop control system, the unity gain can never be achieved for SRC topology with two different load conditions. Thus, voltage regulation with a closed-loop system is necessary in this case. This section introduces a QM implementation with both energizing and free resonant modes that allows to achieve unity gain for all the load conditions [95]-[97]. The advantages and limitations of this new modulator are highlighted by comparing the performance with the FM and PM configurations.

Fig.3.16 shows the closed-loop control system based on the QM technique. A direct measurement of the output voltage is not available in this ICET system, then the output voltage is estimated by rectifying and filtering the transformer voltage at the primary side. This voltage is called  $v_r$  from now on. The estimation of the output voltage is compared with the reference  $V_{ref}$  (the desired output voltage) in order to decide between energizing and free resonant modes. The updating of these modes is synchronized with the zero crossing of the current  $i_p$ .

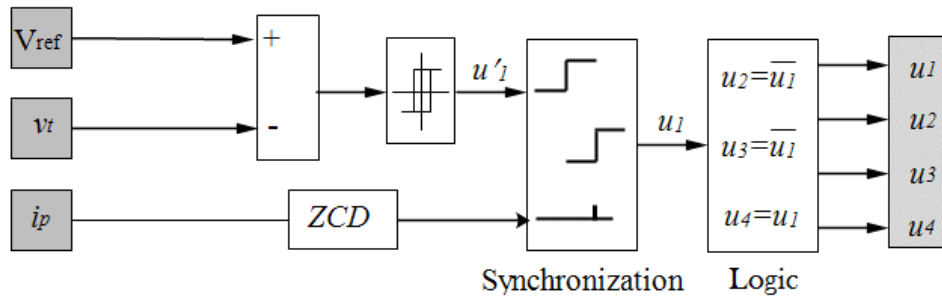


Fig.3.16. Quantum modulation diagram of the input converter.

Fig.3.17 illustrates the principle of operation of the quantum modulator technique. According to the figure, the signal  $u'_1$  is synchronized with the zero current detection of the resonant current  $i_p$ . The resulting signal  $u_1$  is used to drive the switches ( $S_1$  to  $S_4$ ).

Fig.3.18 shows the main waveforms for maximum ( $176 \Omega$ ) and minimum ( $1760 \Omega$ ) loads. In both figures, the estimation is close to the reference voltage (500 V in this case). It should be noticed that the peak value of  $v_t$  tracks the output voltage with a smaller error. This error can be identified as the voltage in the parasitic elements of the system ( $R_p$ , output diodes). Assuming that the error is low and nearly constant for all the loads, the reference voltage can be adjusted to compensate it (we need  $v_o = 450$  V, then we choose  $V_{ref} = 500$  V in order to compensate the voltage across the parasitic elements). The following results in Table.3.11, Table.3.12, Table.3.13 and Table.3. 14 are measured operating the two-clamp SRC with the new QM configuration.

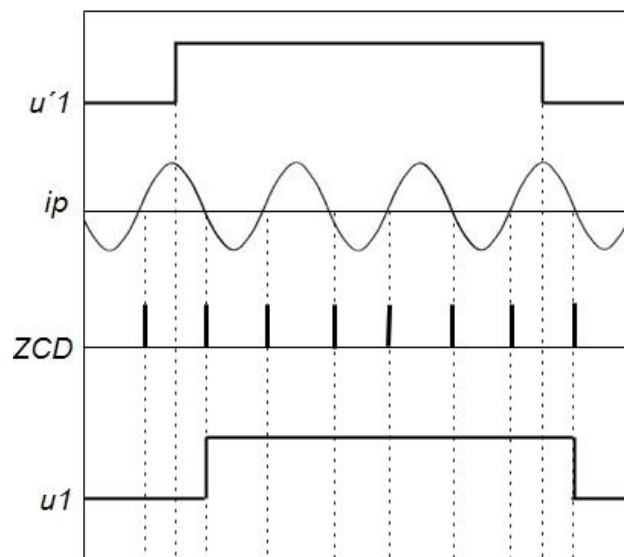


Fig.3.17. Principal waveforms for the quantum modulation.

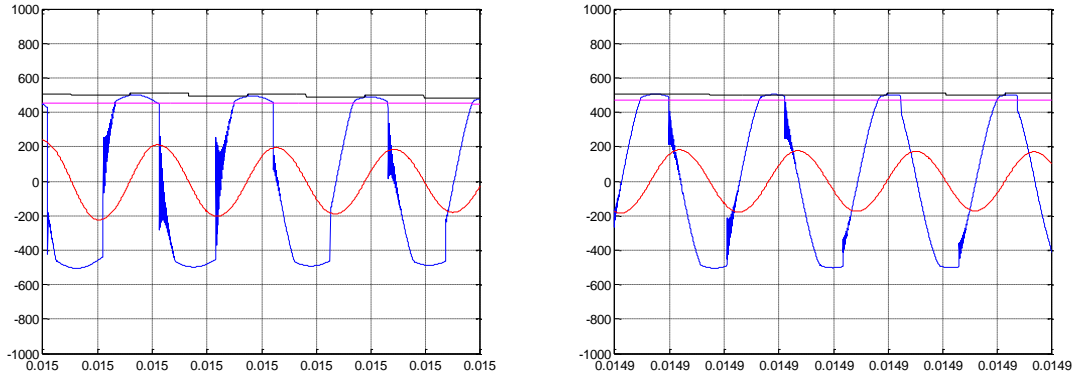


Fig.3.18. Waveforms with QM control for  $R_o = 176 \Omega$  (left) and  $R_o = 1760 \Omega$  (right). Blue: transformer input voltage ( $v_i$ ), red:  $10*i_p$ , pink:  $v_o$ , black: estimation of the converter output voltage.

Table.3.11. QM control with design of 100kHz for two clamps.

Design	$R_{o1}$	$R_{o2}$	$v_{o1}/V_b$	$v_{o2}/V_b$	$i_i$ (A)	$f_s/f_o$ (kHz)	$\eta$ (%)	$P_t$ (W)
100kHz	176	176	1.037	1.037	6.40	0.88	85.81	2474.6
100kHz	176	325	0.989	1.105	4.95	0.88	82.4	1827.8
100kHz	176	1760	0.910	1.203	3.34	0.88	74.35	1119.3
100kHz	325	325	1.050	1.050	3.68	0.88	76.55	1268.5
100kHz	325	1760	0.965	1.155	2.34	0.88	65.28	689.20
100kHz	1760	1760	1.068	1.068	1.35	0.87	43.2	262.47

Table.3.12. QM control with design of 200kHz for two clamps.

Design	$R_{o1}$	$R_{o2}$	$v_{o1}/V_b$	$v_{o2}/V_b$	$i_i$ (A)	$f_s/f_o$ (kHz)	$\eta$ (%)	$P_t$ (W)
200kHz	176	176	0.989	0.989	5.49	0.83	91.10	2250.8
200kHz	176	325	0.944	1.1	4.33	0.80	88.20	1721.4
200kHz	176	1760	0.820	1.248	2.71	0.80	78.13	952.84
200kHz	325	325	1.023	1.023	3.17	0.80	84.27	1204.1
200kHz	325	1760	0.905	1.185	1.91	0.80	73.34	632.73
200kHz	1760	1760	1.046	1.046	1.03	0.80	54.05	251.77

Table.3.13. QM control with design of 1MHz for two clamps.

Design	$R_{o1}$	$R_{o2}$	$v_{o1}/V_b$	$v_{o2}/V_b$	$i_i$ (A)	$f_s/f_o$ (kHz)	$\eta$ (%)	$P_t$ (W)
1MHz	176	176	0.799	0.799	3.35	0.655	92.63	1396.4
1MHz	176	325	0.690	0.996	2.67	0.615	92.98	1118.5
1MHz	176	1760	0.553	1.346	1.51	0.606	82.45	560.30
1MHz	325	325	0.843	0.843	2.01	0.615	90.93	817.65
1MHz	325	1760	0.575	1.223	1.26	0.519	63.89	362.26
1MHz	1760	1760	0.928	0.928	0.71	0.505	61.85	198.17

Table.3.14. QM control with design of 250kHz for two clamps.

Design	$R_{o1}$	$R_{o2}$	$v_{o1}/V_b$	$v_{o2}/V_b$	$i_i$ (A)	$f_s/f_o$ (kHz)	$\eta$ (%)	$P_t$ (W)
250kHz	176	176	0.964	0.964	5.27	0.80	90.17	2138.4
250kHz	176	325	0.891	1.061	3.89	0.80	89.17	1561
250kHz	176	1760	0.804	1.266	2.56	0.79	80.56	928.15
250kHz	325	325	1.013	1.013	3.066	0.80	85.57	1180.7
250kHz	325	1760	0.877	1.193	1.81	0.79	75.67	616.37
250kHz	1760	1760	1.035	1.035	0.977	0.79	56.06	246.50

Fig.3.19 shows the impact of the modulation technique on the principle of operation of the single-clamp SRC. In fact, we are comparing the transformer primary- and secondary-side currents in QM, FM and PM for full load and 10% full load conditions. It is evident that QM produces a significant ripple in the resonant currents which is not noticeable in the FM and PM. The main reason is that the control input in QM can take only discrete values. In other words, the QM can only decide if the next mode is energizing or free resonant, but this decision is maintained during at least a half resonant period. It is interesting to note that the duration of a control cycle in QM increases with  $R_o$ . Thus the control frequency of QM is lower as  $R_o$  increases, thus enlarging the ripple in the main waveforms. Quite the opposite, in FM and PM, the control inputs (switching frequency and phase, respectively) are continuous variables and no amplitude modulation (or ripple) is observed in the currents.

The efficiency comparison of several modulation techniques for single clamp situation is given in Table.3.15. It is clear that for design 100kHz and 200kHz the best results are obtained with PM. Also design 1Mhz results are better than design 100kHz results. However, the best results comparing the three designs are obtained with design 1MHz. Clearly the best efficiency is achieved with the higher switching frequency (design 1MHz). For full load, QM and FM has superior efficiency than PM in design 1MHz.

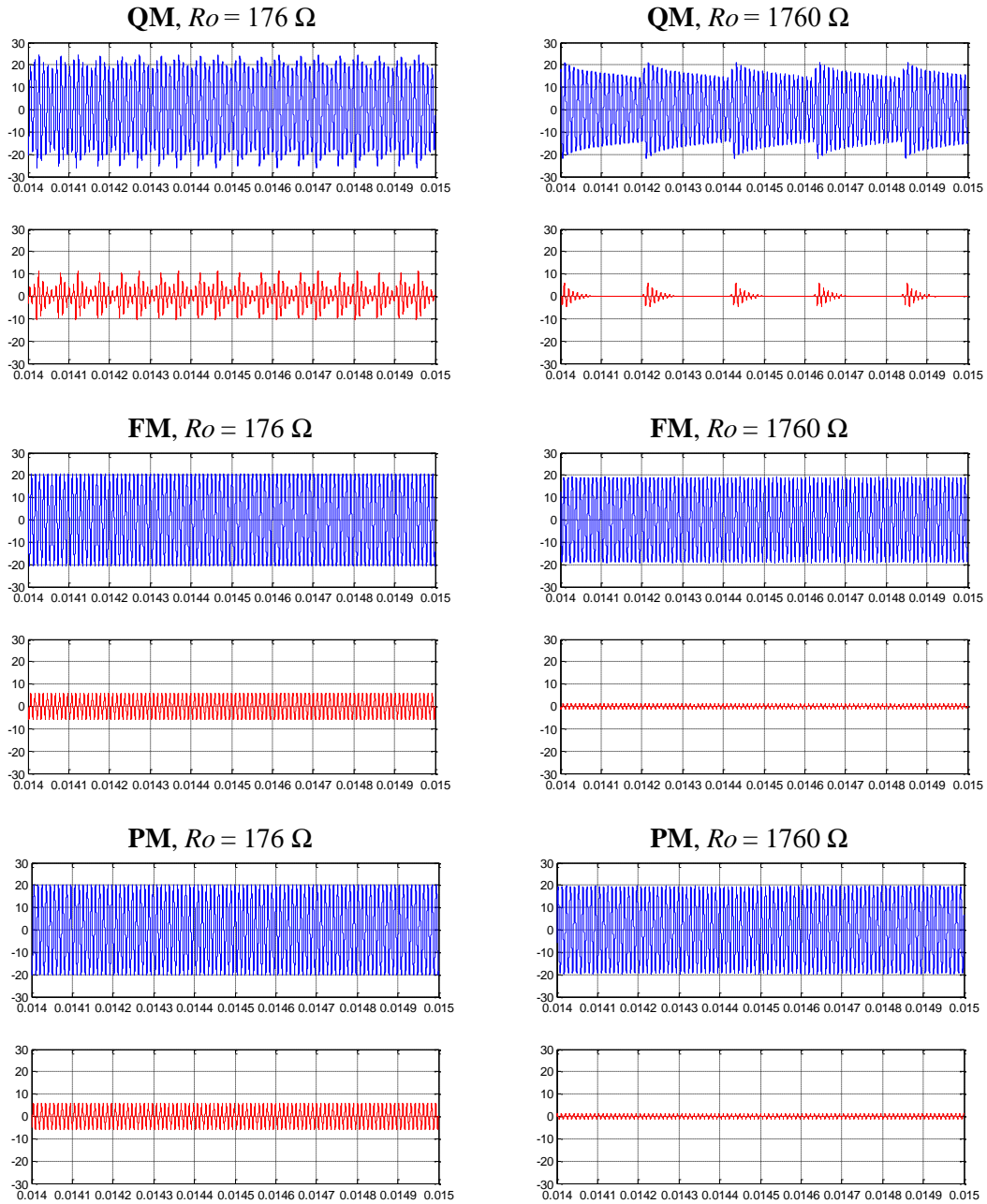


Fig.3.19. Primary-side resonant current,  $i_p$  (blue), and secondary-side current,  $i_s$  (red), for design 100kHz.

Table.3.15. Efficiency results for selected design operating with PM, FM and QM for single clamp.

Design	Load	$\eta$ % QM	$\eta$ % FM	$\eta$ % PM
100kHz	full	78.0	62.1	84.6
100kHz	50% full	69.3	47.5	76.0
100kHz	10% full	34.6	29.8	47.0
200kHz	full	88.4	83.5	91.4
200kHz	50% full	81.0	74.1	87.1
200kHz	10% full	49.9	41.2	64.0
1Mhz	full	93.7	93.6	89.7
1Mhz	50% full	87.6	88.2	85.5
1Mhz	10% full	51.6	59.1	64.0

Table3.16. Best efficiency results for QM, FM and PM. (\*) maximum frequency for which gain = 1 is reached in FM, (\*\*) maximum frequency for which gain = 1 is reached in QM and PM

Design	QM	FM	PM
400 (*)		$\begin{bmatrix} 98.44 & 94.33 & 85.01 \\ 94.33 & 89.30 & 75.55 \\ 85.01 & 75.55 & 52.32 \end{bmatrix}$	
250 (**)	$\begin{bmatrix} 90.17 & 89.17 & 80.56 \\ 89.17 & 85.57 & 75.67 \\ 80.56 & 75.67 & 56.06 \end{bmatrix}$		$\begin{bmatrix} 94.70 & 92.75 & 92.01 \\ 92.75 & 91.97 & 88.85 \\ 92.01 & 88.85 & 71.02 \end{bmatrix}$

To facilitate the efficiency comparison between QM, FM and PM, Table.3.16 collects the best efficiency results obtained with these modulation techniques in the two-clamped SRC converter.

According to Table.3.17 and Fig.3.19, it is evident that the ripple of resonant current in FM is less than QM. Moreover, the FM has more efficiency in full load condition in comparison with the PM and QM. Also, a unity gain for all the load conditions is achieved in open loop for FM while the QM and PM in practice need a closed-loop control. Moreover, the complexity and cost of QM and PM are higher than FM as a consequence of the implementation of the closed-loop systems. Therefore, FM is the preferred option to be used in the partially-controlled ICET system because of its superior performance compared to PM and QM alternatives.

Table.3.17. Comparison between modulation technique.

Modulation	Resonant Current ripple	Efficiency in full load	Unity gain in open loop	Cost and complexity
FM	Low	98.44	Achieved	Low
QM	High	90.17	No achieved	High
PM	Low	94.7	No achieved	High

### 3.6. DESIGN OF THE RESONANT TRANSFORMER

In this section, the design process of the resonant transformer for FM control is presented in detail. The design process includes three subsections which analyzes the effects of the resonant frequency, magnetizing inductance, and characteristic impedance.

#### 3.6.1. EFFECT OF THE RESONANT FREQUENCY

Table.3.18 shows several designs for the resonant circuit as a function of the resonant frequency. The characteristic impedance ( $Z_o$ ) is maintained constant. In this section, the main goal is to achieve unity gain for both mobile clamps while the resonant frequency is considered as a variable in the designs.

Fig.3.20 shows the gain curves of the RT system with two mobile clamps. These figures also include the value of the control input ( $f_s/f_o$ ) required to obtain nearly unity gain in each particular design. As can be seen, by increasing the resonant frequency the maximum gain is reduced and also shifted to the left side (i.e. to lower frequency). In other words, the maximum gain for different designs is achieved in different control input values ( $f_s/f_o$ ). It is worth mentioning that unity gain is not achieved for full load conditions with design 1MHz. Thus, this design is no further considered in the study. According to the figure, for the other designs (100kHz, 200kHz, 400kHz), the output gain can be maintained nearly constant at the desired value ( $v_o/V_b=1$ ) for all the load conditions using the specified control input.

Table3.18: Considered designs for the resonant circuit as a function of the resonant frequency.

Design	$Z_o(\Omega)$	$\omega_o(\text{rad/s})$	$L_p(\mu\text{H})$	$C_p(\text{nF})$
100 kHz	200	$2\pi.100\text{k}$	318.3	7.96
200 kHz	200	$2\pi.200\text{k}$	159.1	3.98
1MHz	200	$2\pi.1000\text{k}$	31.8	0.8
400kHz	200	$2\pi.400\text{k}$	79.5	1.98

Table.3.19 lists the measured gains and efficiencies in the several designs. Note that the gain experiences a certain deviation as the resonant frequency rises. Also, the efficiency increases when the resonant frequency rises. However, the improvements in efficiency are more significant in comparison with the negative deviation in gain, thus the best design is 400kHz.

### 3.6.2. EFFECT OF THE MAGNETIZING INDUCTANCE

Table.3.20 shows the designs for the RT system considering several values of the magnetizing inductance. The magnetizing inductance has a direct relation to the length of the primary winding loop and also the parasitic resistor ( $R_p$ ). Thus, by increasing the length of the primary winding loop, the values of both the magnetizing inductance and the parasitic resistance are increased. In this section, the resonant frequency is 400 kHz and also the characteristic impedance is fixed at 200 ohms.

Fig.3.21 illustrates the gain curves for different designs of the magnetizing inductance and loads. It is interesting to note that nearly unity gain is reached for the three considered designs. More interesting are the measured gain and efficiency results shown in Table.3.21. Although the natural frequency ( $f_o$ ) is 400 kHz for the three designs, the control input ( $f_s/f_o$ ) should be reduced in order to guarantee the desired nearly unity gain as the magnetizing inductance ( $L_m$ ) and the parasitic resistor ( $R_p$ ) increase. The table also lists the switching frequency for the three designs. This switching frequency reduces as the values of  $L_m$  and  $R_p$  increases. This is a particular phenomenon noticed in the series resonant circuit topology with low  $L_m$ . In this topology, the measured efficiency increases by  $L_m$  and  $R_p$ ; see Table.3.21. From design 400k\_025 to design 400k\_050, the efficiency increases 4.44 points which could be considered a notably increment. From design 400k\_50 to design 400k\_100, the efficiency

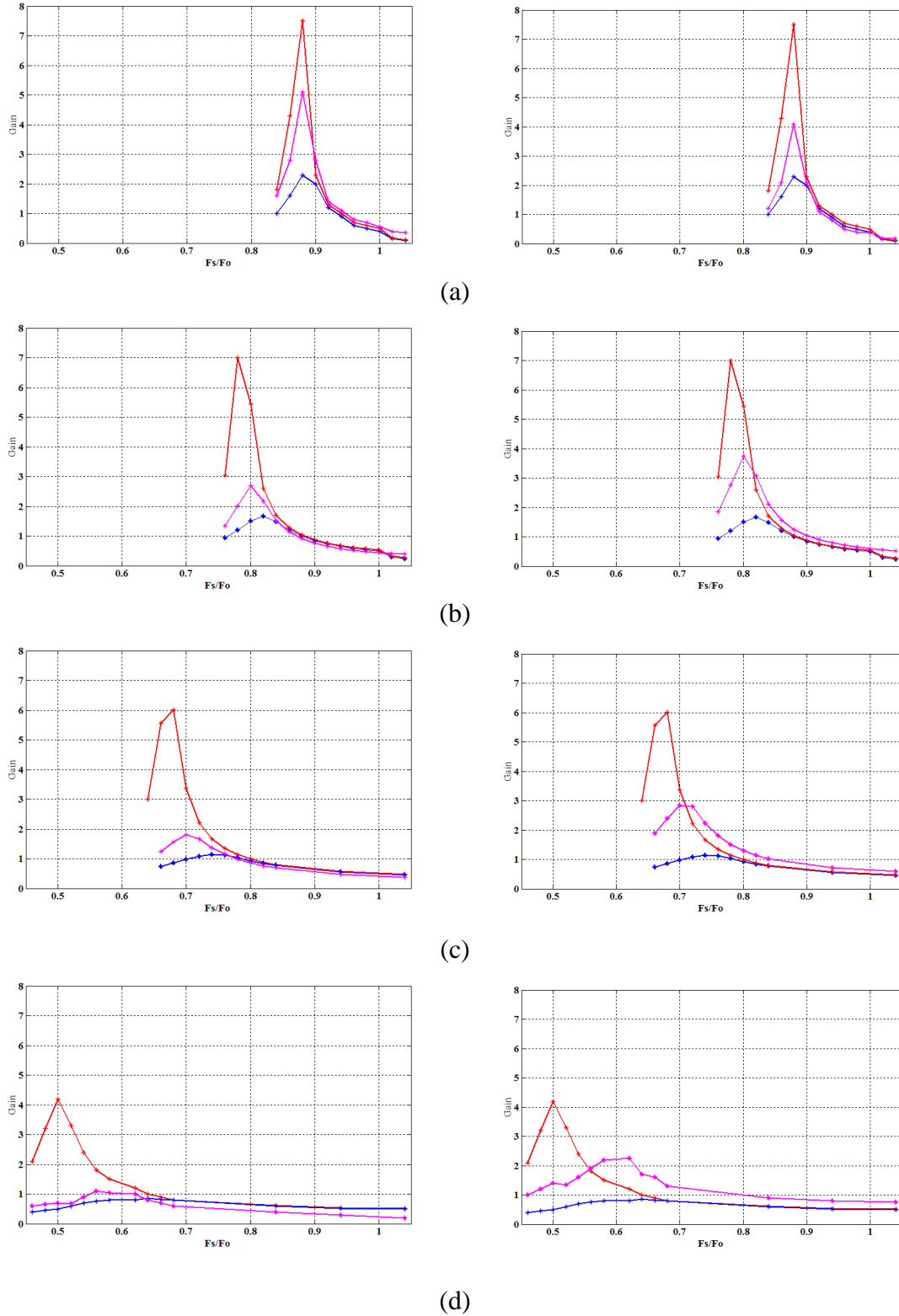


Fig.3.20. Gain curves for different designs and loads. Blue:  $R_{o1}=R_{o2}=176$ , Red:  $R_{o1}=R_{o2}=1760$ , Pink:  $R_{o1}=176$ ,  $R_{o2}=1760$ .  $v_{o1}$  (left),  $v_{o2}$  (right). (a): design 100k, (b): design 200k, (c): design 400k, (d): design 1M.

Table.3.19: Measured gains and efficiencies for the two clamps RT system.

Design	$f_s/f_o$	$R_{o1}$ ( $\Omega$ )	$R_{o2}$ ( $\Omega$ )	$v_{o1}/V_b$	$v_{o2}/V_b$	$\eta$ (%)
100kHz	0.935	176	176	0.92	0.92	84.6
	0.935	176	1760	0.86	1.08	72.5
	0.935	1760	1760	0.98	0.98	48.0
200kHz	0.88	176	176	0.99	0.99	92.8
	0.88	176	1760	0.91	1.25	80.6
	0.88	1760	1760	1.04	1.04	58.0
400kHz	0.80	176	176	0.93	0.93	98.4
	0.80	176	1760	0.86	1.30	85.0
	0.80	1760	1760	0.99	0.99	62.3

Table.3.20. New designs for the RT system considering several values of the magnetizing inductance.

Design	$f_o$ (kHz)	$Z_o$ ( $\Omega$ )	$L_p$ ( $\mu$ H)	$C_p$ (nF)	$L_m$ ( $\mu$ H)	$R_p$ ( $\Omega$ )
400k_025	400	200	79.5	1.98	25	0.5
400k_050	400	200	79.5	1.98	50	1
400k_100	400	200	79.5	1.98	100	2

only increases 0.64 points. Taking into account that the last design requires a cable with double length, it could be concluded that the design 400k\_50 is a better design (high efficiency and short cable length).

### 3.6.3 EFFECT OF THE CHARACTERISTIC IMPEDANCE

Table.3.22 shows two designs with different characteristic impedance. The resonant frequency and magnetizing inductance are chosen as 400 kHz and 50  $\mu$ H respectively. Note that the switching frequency is reduced in order to guarantee the desired nearly unity gain as  $Z_o$  decreased.

Fig.3.22 depicts the current waveforms of transformer primary-side ( $i_p$ ) and secondary-side ( $i_s$ ). It is interesting to see that the primary-side current in the design 400k\_Z200 is nearly sinusoidal. By reducing  $Z_o$ , the harmonic content of this current rises. Note that the secondary side current operates in discontinuous conduction mode in both cases. This is produced by the low magnetizing inductance. However, the zero current interval is larger in the low impedance design, which again causes a higher harmonic content in this current. Table.3.23. lists the measured gain and efficiencies for these designs. It is clear to see that

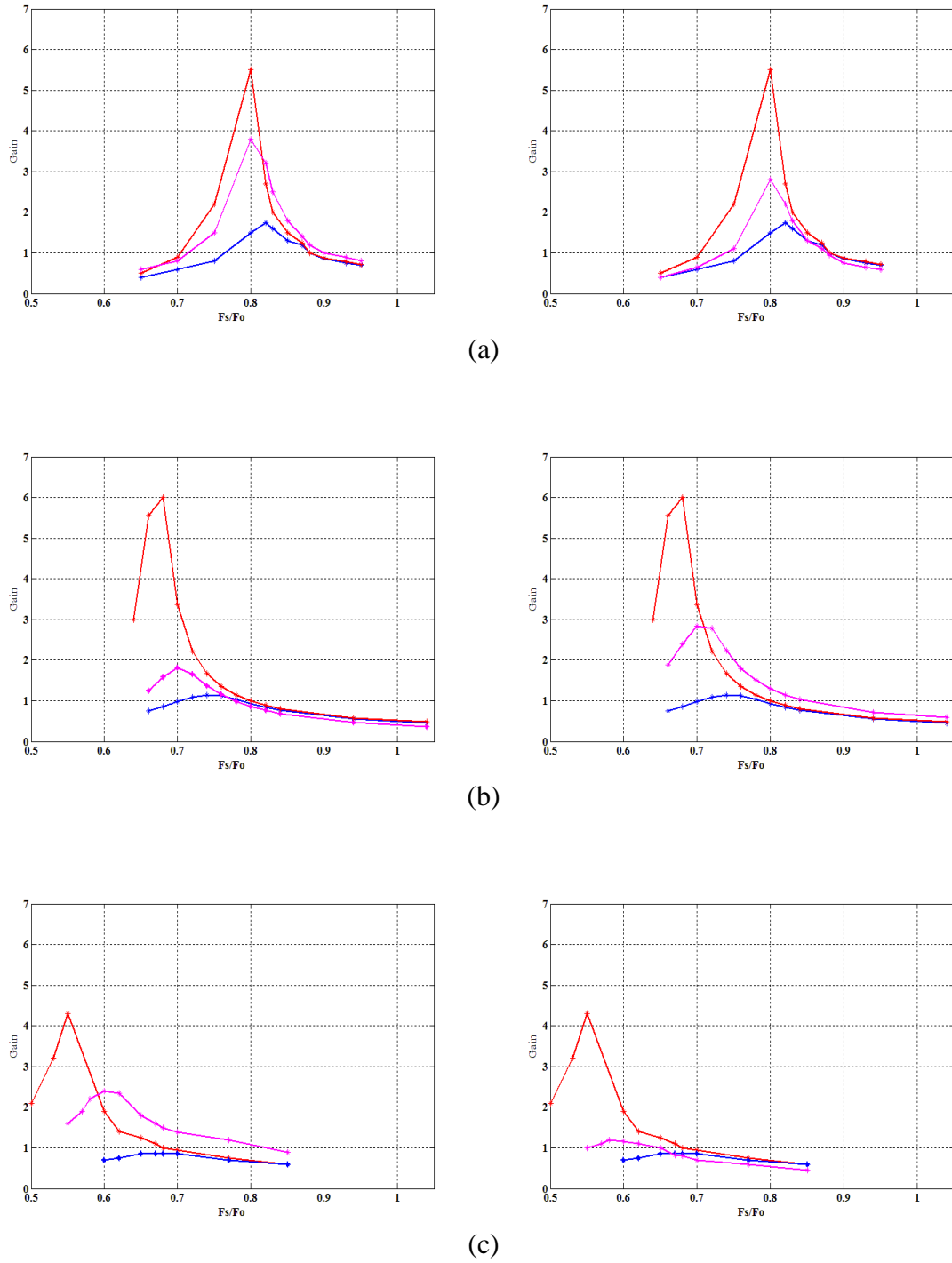


Fig.3.21. Gain curves for different designs of magnetizing inductance and loads. Blue:  $R_{o1}=R_{o2}=176$ , Red:  $R_{o1}=R_{o2}=1760$ , Pink:  $R_{o1}=176, R_{o2}=1760$ .  $v_{o1}$  (left),  $v_{o2}$  (right). (a): design 400k\_025, (b): design 400k\_050, (c): design 400k\_100.

higher efficiency is reached by the design 400k\_Z200. For all these considerations, we can conclude that the high impedance design offers higher quality performance.

Table.3.21. Measured gains and efficiency of the designs with variable magnetizing inductance.

Design	$f_s$ (kHz)	$f_s/f_o$	$R_{o1}$ ( $\Omega$ )	$R_{o2}$ ( $\Omega$ )	$V_{o1}/V_i$	$V_{o2}/V_i$	$\eta$ (%)
400k_025	352	0.88	176	176	0.99	0.99	94.00
	352	0.88	176	1760	0.90	1.24	82.31
	352	0.88	1760	1760	1.03	1.03	60.57
400k_050	320	0.80	176	176	0.92	0.92	98.44
	320	0.80	176	1760	0.85	1.24	85.00
	320	0.80	1760	1760	0.99	0.99	62.32
400k_100	280	0.70	176	176	0.82	0.82	99.08
	280	0.70	176	1760	0.75	1.36	88.15
	280	0.70	1760	1760	0.92	0.92	63.76

 Table.3.22. New designs for several values of the characteristic impedance  $Z_o$ .

Design	$f_o$ (kHz)	$Z_o$ ( $\Omega$ )	$L_p$ ( $\mu$ H)	$C_p$ (nF)	$f_s/f_o$	$f_s$ (kHz)
400k_Z25	400	25	9.95	15.91	0.43	172
400k_Z200	400	200	79.58	1.99	0.80	320

 Table 3.23: Measured gains and efficiency for the designs with variable  $Z_o$ .

Design	$f_s$ (kHz)	$f_s/f_o$	$R_{o1}$ ( $\Omega$ )	$R_{o2}$ ( $\Omega$ )	$V_{o1}/V_i$	$V_{o2}/V_i$	$\eta$ (%)
400k_Z25	172	0.43	176	176	0.914	0.914	91.98
	172	0.43	176	1760	0.858	1.201	79.51
	172	0.43	1760	1760	0.969	0.969	67.12
400k_Z200	320	0.80	176	176	0.93	0.93	98.4
	320	0.80	176	1760	0.86	1.30	85.0
	320	0.80	1760	1760	0.99	0.99	62.3

### 3.7. EVALUATION OF THE TRANSIENT RESPONSE

In this section, the transient response of the complete system is evaluated. Frequency modulation is considered for the resonant transformer due to its simple application and the reaching a unity gain in all the load conditions regardless of the load values.

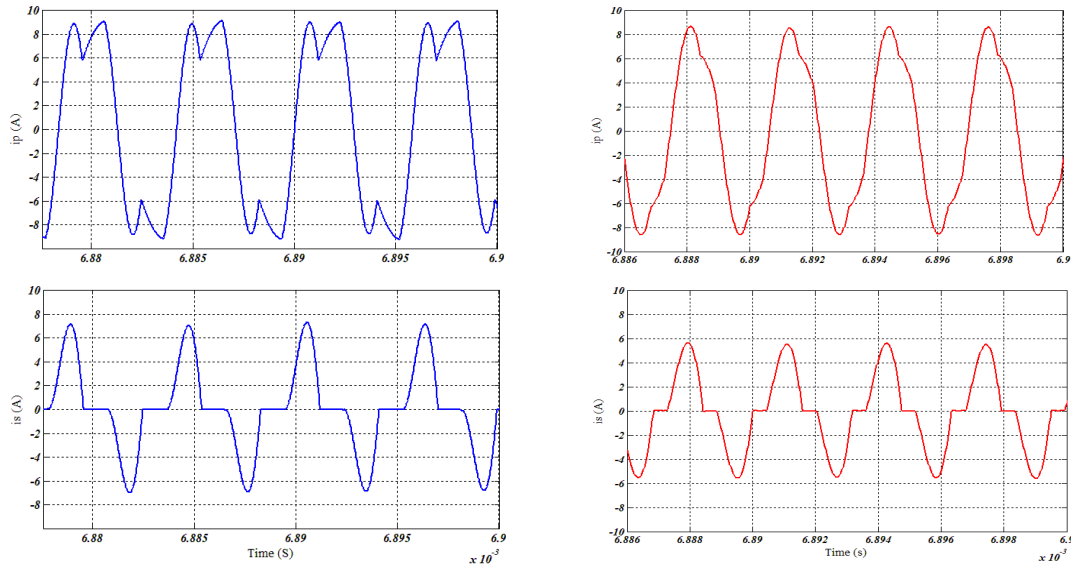


Fig.3.22. Current waveforms for transformer primary-side (top) and secondary-side (bottom). Left: design 400k\_Z25, right: design 400k\_Z200.

Table 3.24: Proposed parameter values for RT system.

Parameter	Symbol	Value	Units
Input voltage	$V_i$	450	V
Resonant inductor	$L_p$	79.5	$\mu\text{H}$
Resonant capacitor	$C_p$	1.98	nF
Parasitic resistance	$R_p$	1	$\Omega$
Parasitic inductance	$L_s$	2.5	$\mu\text{H}$
Characteristic impedance	$Z_o$	200	$\Omega$
Magnetizing inductance	$L_m$	50	$\mu\text{H}$
Transformer ratio	$n$	1	-
Output filter capacitor	$C_o$	10	$\mu\text{F}$
Switching frequency	$f_s$	296	kHz
Resonant frequency	$f_o$	400	kHz

Table 3.24 shows the proposed parameter values for the RT system according to the previous design process. Note that the control input of the SRC topology is reduced from  $f_s/f_o = 0.8$  to  $f_s/f_o = 0.74$ . With this reduction, the minimum value of the boost voltages ( $V_1$ ,  $V_2$ ) is increased in order to guarantee that these voltages are always higher than the output voltages. This is a necessary condition to avoid the control saturation of the output converter.

Fig.3.23 shows the configuration of the control scheme for each of the output inverters (see the diagram of the power circuit in Fig. 3.1). The control has an external voltage loop, that forces the tracking of the reference voltage by the output voltage, an internal current

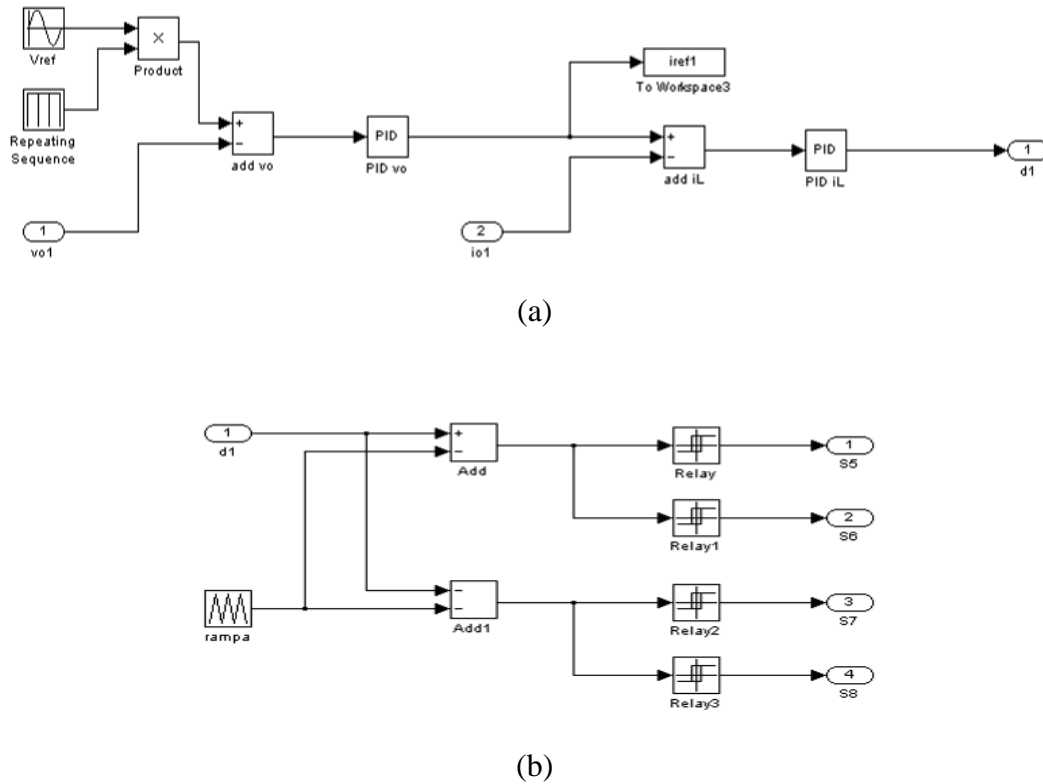


Fig.3.23. The control scheme of the output DC/AC converters shown in Fig. 3.1. (a): control loops. (b): modulator.

loop, that guarantee the correct tracking of the reference current by the inductor current, and a pulse-width modulator. The reference voltage is implemented with a soft-start mechanism to reduce the interaction between the SRC converter and the output converters during the system start-up. Note that the output inverter is viewed from the resonant circuit as a load disturbance. With the soft-start, we reduce the magnitude of this load disturbance. A unipolar modulator is implemented to reduce switching noise at the output of the inverter. The switching frequency is 10 kHz (it could be increased if necessary).

Fig.3.24 illustrates the main waveforms of the ICET system with the proposed design of RT topology. Note that the input current is sinusoidal and it is in phase with the input voltage. It is shown that the power factor of the system is equal to one. According to the figure, the intermediate voltage ( $V_b$ ) and the boosting voltage ( $V_n$ ) are nearly constant in an averaged sense in both load conditions. Only a higher ripple is noticed in these voltages at full load condition because of the second harmonic effect. Also the output voltages of both clamps are perfectly sinusoidal and with constant amplitude (230Vrms). Note that the maximum

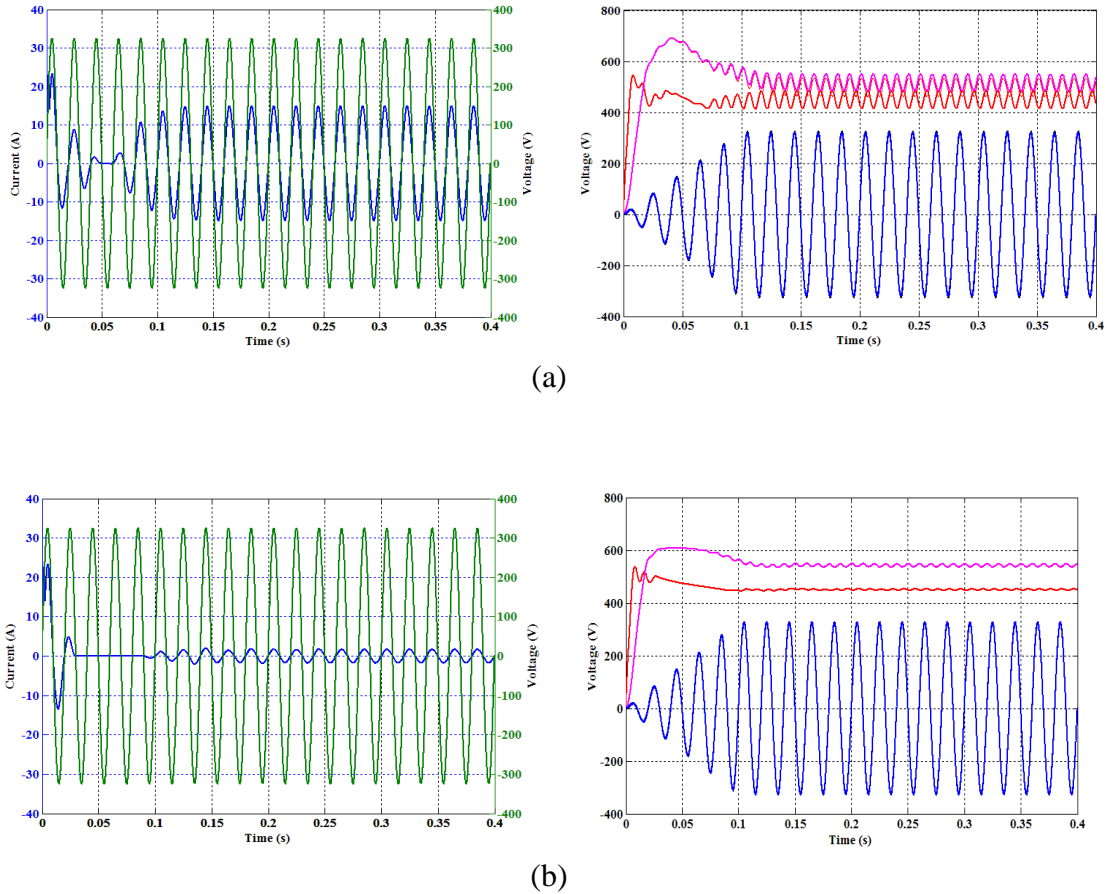


Fig.3.24. Main waveforms of the complete ICET system. (a):  $R_{o1}$ =full load,  $R_{o2}$ = full load ; (b):  $R_{o1}$ =10%full load,  $R_{o2}$ = 10%full load. Left top and bottom: Input current ( $i_i$ : blue) and input voltage ( $V_i$ : green) Right left and bottom: output voltages ( $V_{o1}$ ,  $V_{o2}$ : blue), intermediate voltages ( $V_b$ : pink), boost voltages ( $V_1$ ,  $V_2$ : red). All the mentioned variables are defined in Fig. 3.1

value of the intermediate voltage is only 550 V. The maximum efficiency of the complete system is 91.23%, which in comparison with previous results (Table.3.16) is 7.1 points lower. This phenomenon is mainly caused by the power losses introduced by the input PFC and the two output converters.

Fig.3.25 evaluates the effect of a step load disturbance. Two situations are considered with equal loads ( $R_{o1} = R_{o2}$ , left) and complementary loads (right). This last situation is the worst case condition, in which the resistive load is changed suddenly from minimum to maximum in one clamp and from maximum to minimum in the other clamp. Again, it is possible to observe that the DC values and the AC ripple of the intermediate voltages vary with the load condition while the output voltages are practically independent of the load changes.

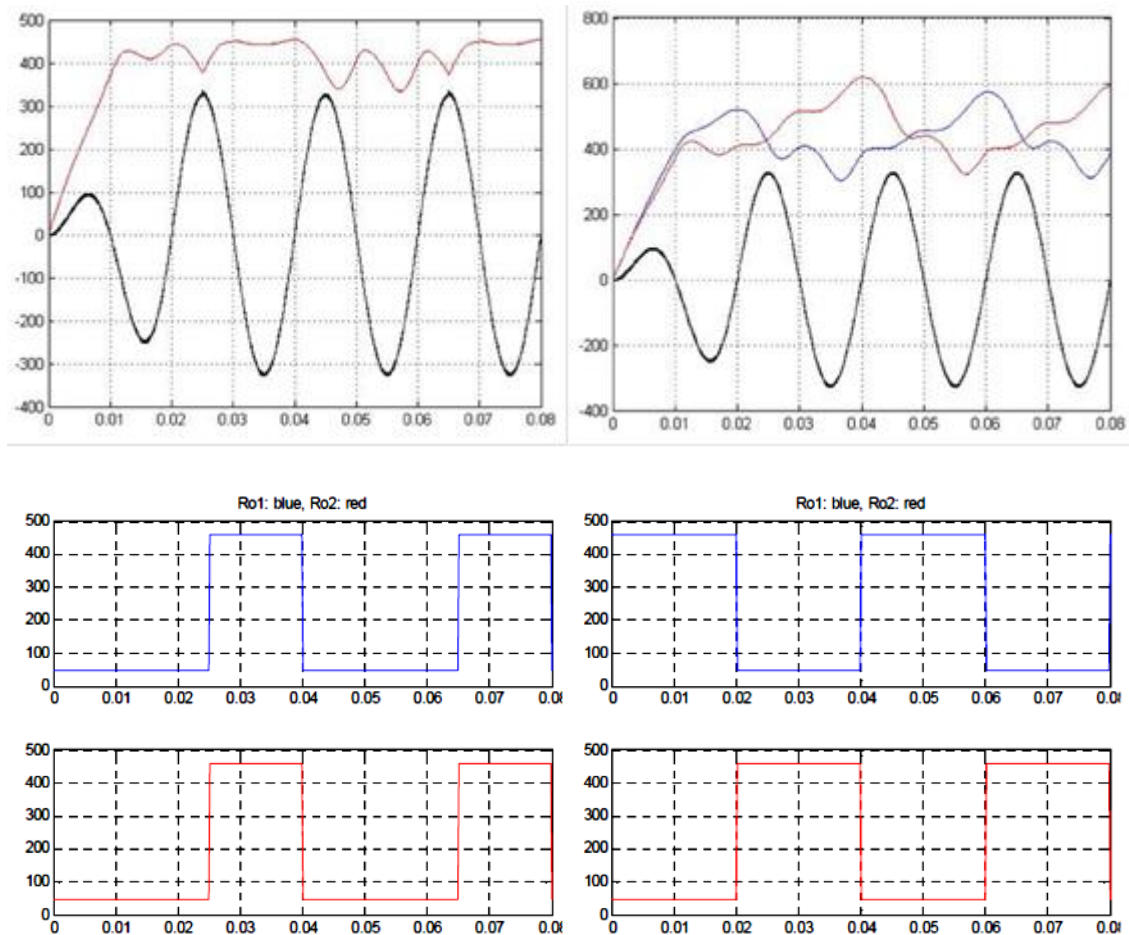


Fig.3.25. Response to step load disturbances in the proposed topology with two high-voltage/high-power clamps. Control input:  $f_s/f_o = 0.8$ . Intermediate voltages:  $V_1$  and  $V_2$ . Output voltages:  $v_{o1}$  and  $v_{o2}$ .

### 3.8. CONCLUSION

This chapter proposed a partially-controlled ICET system formed by an input PFC, an intermediate RT with sliding transformer, and several output inverters to supply the mobile loads. The input and output converters operate in closed loop while the resonant circuit functions in open loop. A comparison between different modulation techniques is presented in order to evaluate which of them allow the resonant converter operate correctly in open loop in this application. The principle of operation and results of each modulation is compared and discussed. From the point of view of control implementation, QM and PM require a complex control system while their efficiency is almost the same as FM. The chapter also presents a detailed design process for the resonant transformer. Variations in the following parameters and their effects have been considered: 1) resonant frequency, 2) magnetizing inductance, 3) characteristic impedance. Measures on the voltage gain and

efficiency have been reported. The transient response of the complete system with frequency modulation is also evaluated. According to the obtained results, it is possible to conclude that the ICET system with multiple clamps has a good performance by using FM in open loop manner. It provides unity power factor, good quality output waveforms with constant rms, nearly constant DC intermediate voltages, and high efficiency.

## CHAPTER 4

---

### Simple and cost effective solution for the partially-controlled ICET system

---

#### Summary

---

4.1 INTRODUCTION .....	79
4.2 PROPOSED TOPOLOGY TO SUPPLY MULTIPLE MOBILE CLAMPS.....	79
4.3 MATHEMATICAL MODELING OF THE PROPOSED TOPOLOGY.....	83
4.4 DESIGN OF THE PROPOSED TOPOLOGY.....	87
4.5 EXPERIMENTAL VALIDATION AND COMPARISON.....	88
4.6 CONCLUSION.....	96

---

This chapter presents the analysis, design and implementation of a simple and cost-effective technique to supply the residential ICET system with multiple mobile loads. The topology is based on the cascaded connection of a closed-loop buck converter and a high frequency resonant inverter operating in closed loop with only a feed-forward term which is loaded by several output passive rectifiers. The proposed system includes a sliding transformer to supply the mobile loads, leading to a safe and flexible location of loads. The theoretical analysis and design of the proposed system is based on a mathematical model derived using the first harmonic approximation. Selected experimental results are included to verify the system features. In comparison with conventional topologies, the proposed system significantly improves efficiency, complexity and cost.



## **4.1. INTRODUCTION**

The purpose of this chapter is to present the analysis, design and implementation of a simple and cost-effective technique to supply the residential ICET system with multiple mobile loads [98]. The proposed topology is based on the cascaded connection of a buck converter operating as a constant current source and a high frequency resonant inverter operating in closed loop with only a feed-forward term and loaded by passive rectifiers. The most promising features of the proposed topology is that the output voltages are nearly constant for all the load conditions even using passive rectifiers at the output side of the proposed ICET system. The drawback of this configuration is the poor transient response. For this reason, the topology is well suited to supply active DC loads with internal post-regulators such as laptops, mobile phones and other loads taking advantage of a flexible location.

The analysis of the proposed topology is carried out with a mathematical model based on the first harmonic approximation. By using the derived model, a systematic design procedure is introduced in order to get constant output voltages in all the loads and also for different load conditions. Moreover, to validate the performance of the proposed system, selected experimental results are compared to those obtained from the conventional topology.

The main contributions of this chapter are: 1) a simple, efficient and cost-effective topology to supply residential loads with multiple clamps, 2) a mathematical model derived by using the first harmonic approximation which includes the effect of magnetizing and leakage inductances, and 3) a systematic design procedure for the resonant components.

## **4.2. PROPOSED TOPOLOGY TO SUPPLY MULTIPLE MOBILE CLAMPS**

In this section the system description and principle of operation of the proposed system are explained.

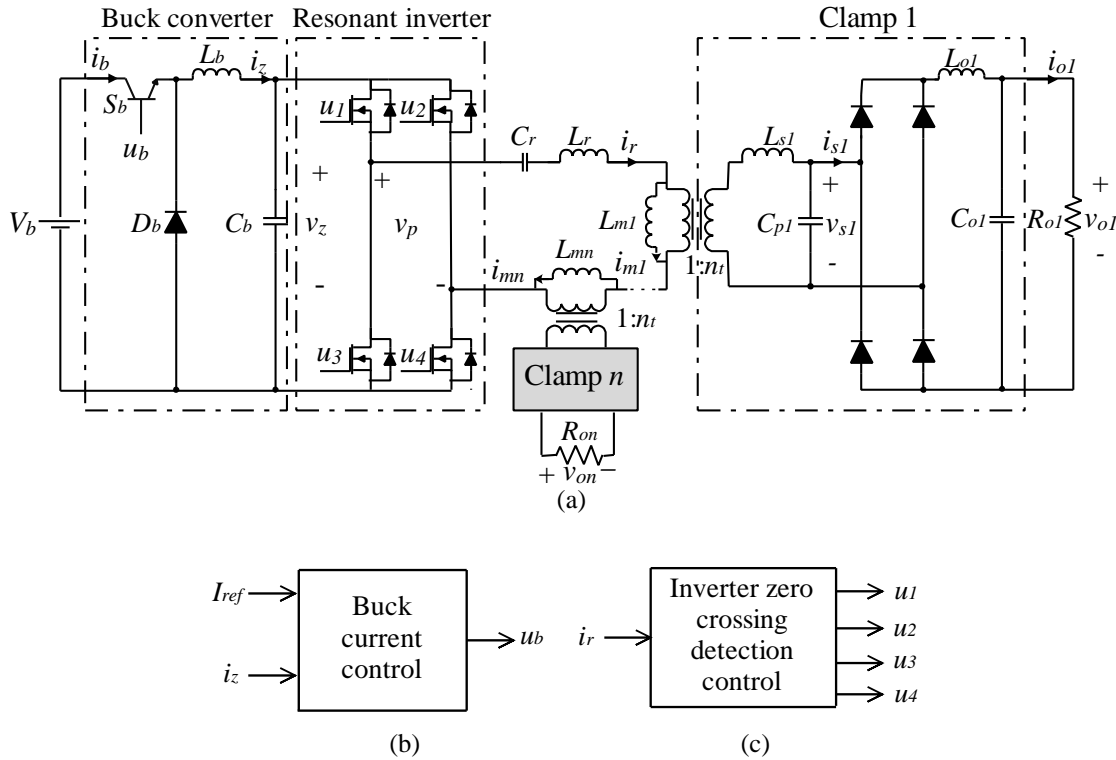


Fig. 4.1. (a) Schematic of the proposed DC/DC converter with multiple mobile clamps, (b) Buck converter current control and (c) resonant inverter control.

#### 4.2.1 DESCRIPTION OF THE PROPOSAL

Fig.4.1.(a) shows the schematic of the proposed topology to supply  $n$  mobile clamps. The topology consists of a buck converter, a full-bridge resonant inverter (RI), resonant elements, a high frequency transformer, and diode bridge rectifiers with low-pass filters. In this system, the buck converter is responsible to inject a constant DC current ( $i_z$ ) to the RI. This constant current is essential to guarantee fixed output voltages ( $v_{o1}, \dots, v_{on}$ ) regardless of the load conditions. In practice,  $i_z$  is fixed by applying a conventional closed-loop control to drive the switch  $S_b$  in accordance with the desired reference current ( $I_{ref}$ ), as shown in Fig.4.1.(b). As a consequence of the constant current, the voltage  $v_z$  changes automatically as a function of the load due to the power matching issue (i.e., the input power is roughly equal to the total output power supplied to the  $n$  loads). Therefore, based on the proposed system, efficiency problem of the conventional fully-controlled ICET system (see chapter 2) is improved even for low load conditions. This property will be validated theoretically and experimentally in the next sections. On the other hand, the inverter operates with the simple zero crossing detection (ZCD) modulation strategy shown in Fig.4.1.(c). From the figure, the resonant current  $i_r$  is used to match the switching frequency  $f_s$  with the resonant frequency  $f_o$  in a feed

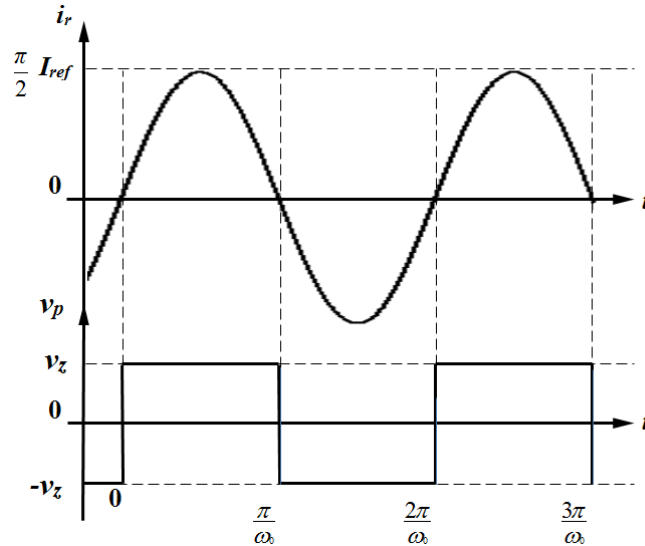


Fig.4.2. Output waveforms of the resonant inverter.

forward way. This control strategy causes constant amplitude in  $i_r$ . By applying ZCD to the inverter on the one side and using a passive diode rectifier on the other side, the input energy is completely transferred to the load as a unidirectional flow (from input side to the output side only).

Moreover, a passive diode rectifier is used for each clamp instead of the controlled rectifier employed in the conventional topology; see chapter 2. Also, a small parallel secondary side capacitor  $C_{pi}$  is included in the proposed topology to fix the output voltages. As a consequence of using diodes instead of switches, the cost and complexity of the proposed topology are reduced particularly in the case of high number of mobile clamps.

#### 4.2.2 DISCUSSION ON THE PROPOSAL

The overall performance of the proposed topology is highly dependent on the buck converter in the first stage. The buck converter is a fundamental element to guarantee a fix output voltage and increase efficiency. This converter in collaboration with resonant inverter is responsible to produce a fix current for the secondary side resonant elements ( $L_m$ ,  $L_s$  and  $C_p$ ). The total impedance of these elements ( $Z_{LC}$ ) is in parallel with load ( $R_o$ ). Therefore, by proper design of  $C_p$  the load effect can be neglected because of dominant value of  $Z_{LC}$  (i.e.  $Z_{LC} \ll R_o$ ), resulting in fix output voltage regardless to the load conditions. The design process of  $C_p$  to obtain a fix output voltage will be explained in section 4.4.

The RI operates in closed-loop with only a feed-forward term to detect the zero-crossing of the resonant current. Fig.4.2 illustrates the output waveforms of the resonant inverter. The sinusoidal waveform is the resonant current  $i_r$  and the square waveform is the voltage  $v_p$ . In steady state, the current  $i_r$  can be expressed as

$$i_r = \frac{\pi}{2} I_{ref} \sin(\omega_o t) \quad (4-1)$$

where  $\omega_o$  is the angular resonant frequency. Note that its amplitude is proportional to the output current of the buck converter. From Fig.4.2, the value of  $v_p$  can be expressed as

$$v_p = v_z \cdot \text{sgn}(i_r) \quad (4-2)$$

According to the figure, the two waveforms are completely in phase. Therefore, circulating reactive current is completely avoided, thus achieving unity power factor operation. Also, at  $f_s = f_o$ , the switches turn on and off at zero current, resulting in nearly zero switching losses [90]. As a consequence of both issues, the efficiency of the proposed topology improves significantly. Also, the principle of operation of the inverter allows that the voltage  $v_z$  automatically changes according to the required output power while the current  $i_z$  is fixed by the buck converter. Therefore, the proposed system can regulate the input power without using a feedback control loop.

It is worth mentioning that a fixed amplitude current can also be obtained in the resonant current using different approaches, for instance with a feedback control system including frequency or phase modulators. In these approaches, the input buck converter can be eliminated. However, in all these cases, the unity power factor provided by the proposed solution cannot be guaranteed, thus forcing the sliding transformer to operate in a more stressing condition. Taking into account the complex structure of the sliding transformer (long primary loop and several mobile secondary sides), the operation of the RI with only a single feed-forward current term is an interesting option to eliminate the flowing of reactive power in the sliding transformer.

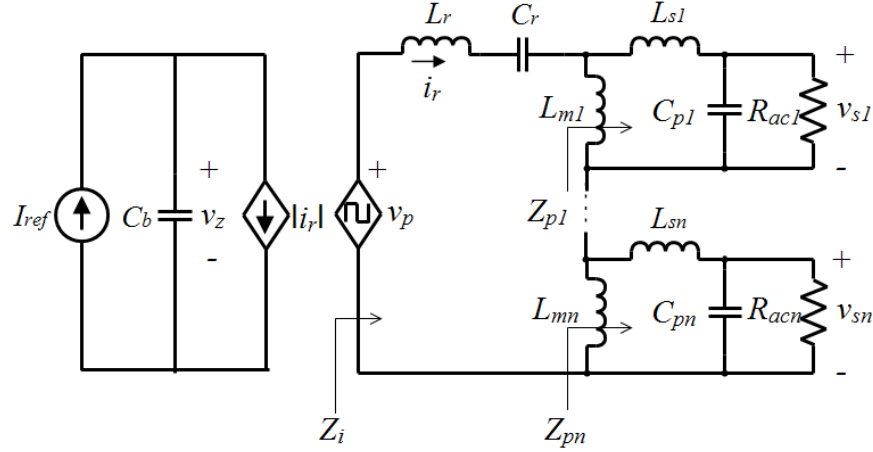


Fig.4.3. Equivalent circuit of the proposed topology.

### 4.3. MATHEMATICAL MODELING OF THE PROPOSED TOPOLOGY

This section presents an equivalent model for the proposed topology. This model is employed to derive the main characteristics of the topology.

#### 4.3.1. MODEL OF THE PROPOSED TOPOLOGY

The proposed topology can be represented by the equivalent circuit model shown in Fig.4.3. The model contains an input current source, two controlled sources, resonant components and equivalent resistors. The current source  $I_{ref}$  represents the operation of the buck converter while the controlled sources characterize the operation of the resonant inverter. Note that the controlled current source reflects the primary side resonant current  $i_r$  to the inverter input side. Besides, the controlled voltage source models the effect of the input voltage  $v_z$  on the inverter output side. For simplicity, the magnetizing inductance, parallel capacitors and leakage inductance are assumed equal in all clamps ( $L_{mi} = L_m$ ,  $C_{pi} = C_p$  and  $L_{si} = L_s$ ). Also, a unity turns ratio is assumed for transformers ( $n_t = 1$ ). Moreover, the loads are modelled by the equivalent AC resistors ( $R_{ac1}, \dots, R_{acn}$ ) which are derived by applying the first harmonic approximation [99]. The value of  $R_{aci}$  under steady state condition can be expressed as

$$R_{aci} = \frac{\pi^2}{8} R_{oi} \quad i = 1, \dots, n. \quad (4-3)$$

where  $R_{oi}$  is the output resistor and  $n$  stands for the number of clamps.

### 4.3.2. ANGULAR RESONANT FREQUENCY

The proposed topology operates at  $\omega = \omega_o$ , where  $\omega$  is the angular frequency. Therefore, to design and analyze the proposed system, an accurate expression for  $\omega_o$  should be obtained as an initial step to calculate the design parameters.

First  $\omega_o$  should be determined by analyzing the total impedance  $Z_i$  marked in Fig.4.3. In fact, the resonant frequency is defined as the frequency when the imaginary part of the total impedance is zero. The total impedance is a function of the series and parallel components which can be represented by the following equation:

$$Z_i = j\omega L_r - \frac{j}{\omega C_r} + \sum_{i=1}^n Z_{pi} \quad (4-4)$$

where  $L_r$  and  $C_r$  are the series components and  $Z_{pi}$  stands for the parallel impedances shown in Fig.4.3. The amplitude of the parallel impedance can be written as

$$|Z_{pi}| = \frac{\omega L_m R_{aci}^2 (\omega^2 L_s C_p - 1) (\omega^2 C_p (L_m + L_s) - 1) + \omega^3 L_m L_s (L_m + L_s)}{R_{aci}^2 (\omega^2 C_p (L_m + L_s) - 1)^2 + \omega^2 (L_m + L_s)^2} \quad (4-5)$$

Note that this amplitude depends on the load by the resistor  $R_{aci}$ . In order to get an impedance independent of the load, the following conditions must fulfill.

$$\omega L_m R_{aci}^2 (\omega^2 L_s C_p - 1) (\omega^2 C_p (L_m + L_s) - 1) \gg \omega^3 L_m L_s (L_m + L_s) \quad (4-6)$$

$$R_{aci}^2 (\omega^2 C_p (L_m + L_s) - 1)^2 \gg \omega^2 (L_m + L_s)^2 \quad (4-7)$$

In this case, the impedance can be expressed as

$$|Z_{pi}| = \frac{\omega L_m (\omega^2 L_s C_p - 1)}{\omega^2 C_p (L_m + L_s) - 1} \quad (4-8)$$

From (4-6) and (4-7), the design conditions for  $C_p$  can be written as

$$C_p \gg \frac{1}{\omega^2(L_m+L_s)} \left[ 1 + \frac{R_{aci}L_m + \sqrt{4L_s^2[2R_{aci}^2 + (L_m+L_s)^2\omega^2 + R_{aci}^2L_m(L_m+L_s)]}}{2R_{aci}L_s} \right] \quad (4-9)$$

$$C_p \gg \frac{1}{\omega^2(L_m + L_s)} \left[ 1 + \frac{\omega(L_m + L_s)}{R_{aci}} \right] \quad (4-10)$$

These two conditions can be expressed as (4-11).

$$C_p \gg \frac{1}{\omega^2(L_m + L_s)} [1 + \text{Max}(a, b)] \quad (4-11)$$

$$a = \frac{R_{aci}L_m + \sqrt{4L_s^2[2R_{aci}^2 + (L_m + L_s)^2\omega^2 + R_{aci}^2L_m(L_m + L_s)]}}{2R_{aci}L_s} \quad (4-12)$$

$$b = \frac{\omega(L_m + L_s)}{R_{aci}} \quad (4-13)$$

In this case, by using (4-4) and (4-8), the input impedance can be expressed as:

$$Z_i = j \left[ \omega L_r - \frac{1}{\omega C_r} + n \cdot \frac{\omega L_m (\omega^2 L_s C_p - 1)}{\omega^2 C_p (L_m + L_s) - 1} \right] \quad (4-13)$$

The resonant angular frequency is obtained by setting (4-13) equal to zero (then by definition  $\omega = \omega_o$ ) and solving for  $\omega_o$ . The expression for  $\omega_o$  is written in (4-14)

$$\omega_o = \sqrt{\frac{L_m(nC_r + C_p) + C_p L_s + C_r L_r + \sqrt{c}}{2C_p C_r (L_m L_r + L_m L_s + n L_r L_s)}} \quad (4-14)$$

$$c = C_p [C_p L_m (L_m + 2L_s) + 2L_m C_r (nL_m - L_r - nL_s) + L_s (C_p L_s - 2C_r L_r)] + C_r^2 [nL_m (nL_m + 2L_r) + L_r^2]$$

### 4.3.3. OUTPUT VOLTAGE

In Fig.4.3, the output voltage  $v_{si}$  is a sinusoidal signal operating at the resonant frequency. Its amplitude relies on the parallel impedance ( $Z_p$ ) and the amplitude of the resonant current

$$V_{si} = (|Z_{pi}| \cdot I_r) \cdot \frac{\frac{1}{C_p \omega_o}}{L_s \omega_o + \frac{1}{C_p \omega_o}} = \frac{\omega_o L_m (\omega_o^2 L_s C_p - 1)}{\omega_o^4 C_p^2 (L_s L_m + L_s^2) + \omega_o^2 C_p L_m - 1} \cdot \frac{\pi}{2} I_{ref} \quad (4-15)$$

From Fig.4.1 and Fig.4.3, the output voltage  $v_{oi}$  is obtained by rectifying and filtering the sinusoidal voltage  $v_{si}$ . Therefore,  $v_{oi}$  can be expressed as

$$v_{oi} = \frac{2}{\pi} v_{si} = \frac{\omega_o L_m (\omega_o^2 L_s C_p - 1)}{\omega_o^4 C_p^2 (L_s L_m + L_s^2) + \omega_o^2 C_p L_m - 1} \cdot I_{ref} \quad (4-16)$$

It must be noticed that the output voltage is independent of the load conditions by assuming that the condition (4-11) is fulfilled.

### 4.3.4. DESIGN CONDITION FOR THE REFERENCE CURRENT

The last step in the mathematical modeling of the proposed topology is to determine a design condition for  $I_{ref}$ . As described above, the voltage  $v_z$  varies as a function of the load. Once the input current to the resonant converter  $I_{ref}$  is constant, the variations in the input power produced by load changes modify the voltage  $v_z$ . In the worst case scenario (i.e.,  $R_{oi} = R_{oimin}$ ), the relation between these variables can be expressed, assuming an ideal efficiency (100%), as:

$$v_z I_{ref} = \sum_{i=1}^n \frac{v_{oi}^2}{R_{oimin}} \quad (4-17)$$

Moreover, to ensure a correct operation of the buck converter, its input voltage  $V_b$  must be always greater (or equal) than the output voltage  $v_z$ . According to this condition, (4-17) can be re-written as follows

Table.4.1. Circuit parameters for the proposed design.

Parameter	Symbol	Value	Units
Input voltage	$V_b$	15	V
Magnetizing inductance	$L_m$	50	$\mu\text{H}$
Leakage inductance	$L_s$	2.5	$\mu\text{H}$
Switching frequency	$f_s$	110	kHz
Minimum load resistor	$R_{oi\min}$	100	$\Omega$
Output voltage	$V_{oi}$	22	V

$$\sum_{i=1}^n \frac{v_{oi}^2}{R_{oi\min}} \leq V_b I_{ref} \quad (4-18)$$

From (4-18), the value for  $I_{ref}$  can be limited as:

$$I_{ref} \geq \sum_{i=1}^n \frac{v_{oi}^2}{R_{oi\min} V_b} \quad (4-19)$$

In practice, the value of  $I_{ref}$  must be slightly over-dimensioned in order to compensate the ideal assumption of 100% efficiency.

#### 4.4. DESIGN OF THE PROPOSED TOPOLOGY

In this section the design procedure for the proposed topology is presented. A topology with two clamps is considered for the design.

The necessary circuit parameters for starting the design process are listed in Table.4.1. Note that these values correspond to a low-power experimental prototype. The design process is based on the worst-case scenario (i.e.,  $R_{oi} = R_{oi\min}$ ) and it is presented in the following steps:

**Step I:** In the first step, the reference current of the buck converter is determined based on Table.4.1 and (4-19). From (4-19), the minimum value of the reference current is  $I_{ref} = 0.64\text{A}$ . This value introduces the minimum current for a correct operation of the buck converter.

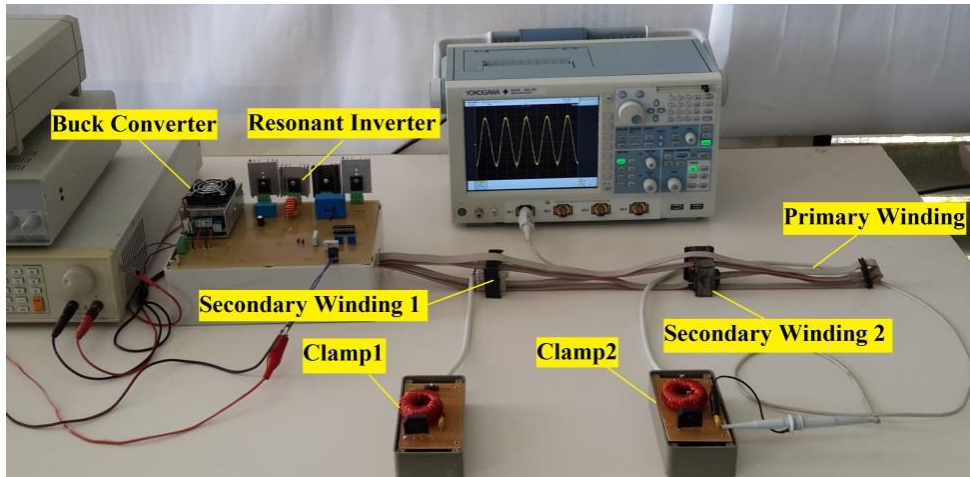


Fig.4.4. Experimental set-up with two mobile clamps.

Step II: The value of the parallel capacitor  $C_p$  for each clamp can be obtained from (4-16) as  $C_p = 80\text{nF}$ . According to (4-11), this value ensures a constant output voltage independent of the load conditions.

Step III: In the final step, the values for  $C_r$  and  $L_r$  are obtained. It should be noted that the primary leakage inductance has a small value. Also, this value may experience some changes during the operation of the system. Therefore, to eliminate the effect of this leakage inductance,  $L_r$  should be chosen noticeably higher. In this example  $L_r$  is chosen equal to  $40\mu\text{H}$  which is drastically higher than  $2.5\mu\text{H}$ . By solving (4-14),  $C_r = 68\text{nF}$  is calculated.

By following these steps a proper design for the proposed topology is reached. The theoretical design is validated experimentally in the next section.

#### 4.5. EXPERIMENTAL VALIDATION AND COMPARISON

The predicted theoretical results are verified experimentally in this section. Also, a comparison between the proposed and conventional topologies is included. A high frequency DC/DC resonant converter prototype with two clamps has been built as shown in Fig.4.4. The main circuit parameters are given in Table4.2. Note that the values are chosen based on the design process explained in the previous section. Moreover, some selected results for the conventional topology will be also presented for comparison purposes. It should be

mentioned that a system with amplitude modulation control technique has been built and tested based on [82]. Table.4.3 lists the main circuit parameters of the conventional topology. To have a fair comparison, the values of this table are selected according to the design process presented in [82] to achieve the same output power, output voltage and switching frequency.

#### 4.5.1. COMPARISON BETWEEN THE CONVENTIONAL AND PROPOSED TOPOLOGIES

Fig.4.5. shows the main waveforms of the conventional and proposed topologies. As shown, the conventional topology has amplitude modulation in the resonant current which produces higher peak value compared to the current of the proposed topology. In the conventional topology, the power flow from the input source to the resonant tank is decided by the closed-loop control system. When the amplitude current increases, the power is

Table.4.2. Circuit parameters for the proposed topology.

Parameter	Symbol	Value	Units
Input voltage of buck converter	$V_b$	15	V
Buck converter inductor	$L_b$	50	$\mu\text{H}$
Buck converter capacitor	$C_b$	22	$\mu\text{F}$
Series resonant capacitor	$C_r$	68	nF
Series resonant inductor	$L_r$	40	$\mu\text{H}$
Magnetizing inductances	$L_{m1}, L_{m2}$	50	$\mu\text{H}$
Leakage inductance	$L_s$	2.5	$\mu\text{H}$
Gap distance	$G_d$	0.1	cm
Transformer turn-ratio	$n_t$	1	-
Parallel resonant capacitors	$C_{p1}, C_{p2}$	82	nF
Output filter inductors	$L_{o1}, L_{o2}$	4	mH
Output filter capacitors	$C_{o1}, C_{o2}$	10	$\mu\text{F}$
Minimum resistive loads	$R_{o1min}, R_{o2min}$	100	$\Omega$
Output voltages	$v_{o1}, v_{o2}$	22	V
Reference current	$I_{ref}$	0.7	A
RI switching frequency	$f_s$	110	kHz
Buck converter switching frequency	$f_b$	50	kHz
Buck converter diode	1N5817		
Buck converter and RI switches	MOSFET IRFP250N		
Driver	HIP4081A		
Diode rectifier	KBU4M		

Table.4.3. Circuit parameters for the conventional topology.

Parameter	Symbol	Value	Units
Input voltage	$V_b$	15	V
Series resonant capacitor	$C_r$	68	nF
Series resonant inductor	$L_r$	40	$\mu$ H
Magnetizing inductances	$L_{m1}, L_{m2}$	50	$\mu$ H
Leakage inductance	$L_s$	2.5	$\mu$ H
Gap distance	$G_d$	0.1	cm
Output filter capacitors	$C_{o1}, C_{o2}$	20	$\mu$ F
Minimum resistive loads	$R_{o1min}, R_{o2min}$	100	$\Omega$
Transformer turn-ratio	$n_t$	1	-
Switching frequency	$f_s$	110	kHz
Output voltages	$v_{o1}, v_{o2}$	22	V

flowing into the resonant tank; when the amplitude current decreases, the input power is zero and the stored energy in the resonant tank is discharged in the loads. This principle of operation produces a higher peak current in all devices (including power switches and diodes). Conversely, in the proposed topology the power flow is continuous and constant, reducing the stress of the devices.

Fig.4.6 shows the output waveforms of the RI (voltage  $v_p$  and current  $i_r$ ) for the proposed topology in two different load conditions. As expected, in the proposed topology, the current has a constant peak value independent of the load. The voltage is a (nearly) square

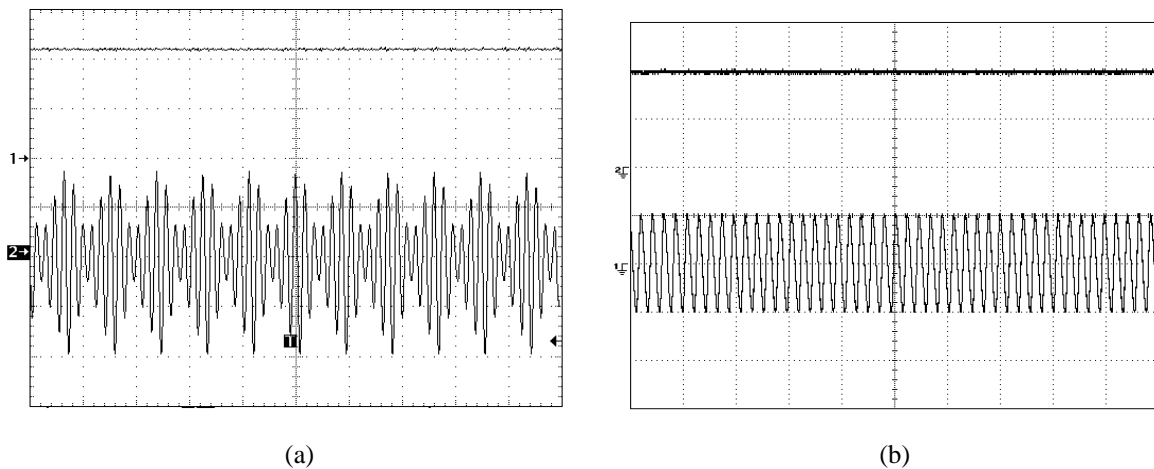


Fig. 4.5. Measured output voltage  $v_{oi}$  (Top, 10V/div) and resonant current  $i_r$  (500 mA, 50 $\mu$ s/div). (a) conventional topology, (b) proposed topology.

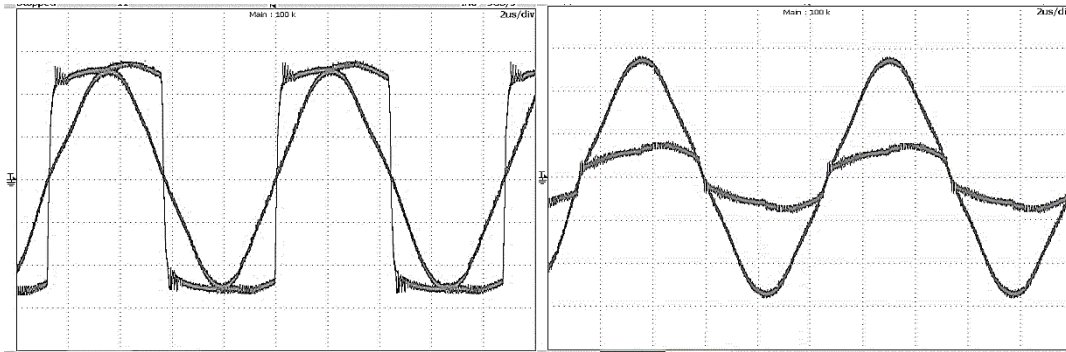


Fig.4.6. Measured resonant current  $i_r$  (sinusoidal waveform, 200mA/div, 2 $\mu$ s/div) and voltage  $v_p$  (square waveform, 5V/div, 2 $\mu$ s/div) in two load conditions for proposed topology. Full load (left) and 10% full load (right).

wave and its amplitude depends on the load condition. As predicted by (4-17) this voltage changes according to the output power.

Fig.4.7 shows the measured efficiency of the conventional and proposed topologies. Note that higher efficiency is obtained in the proposed topology. In particular, at 10 % of full load, the proposed topology improves the efficiency in nearly 25 points compared to the conventional topology result. This increase is a consequence of the input voltage  $v_z$  variation according to the load consumption. In the conventional system there is no adaptation to load condition. The maximum efficiency for the proposed topology is obtained at full load, being 80% in practice. Note that the power losses related to the buck converter are also included in this figure.

#### 4.5.2. PERFORMANCE IN STEADY STATE

Fig.4.8 shows the voltage  $v_z$  as a function of loads. As expected, this voltage changes according to the load conditions. This phenomenon is caused by the fixed input current provided by the buck converter. According to the figure, the maximum  $v_z$  is related to the full load condition where the maximum power is transferred to the loads.

Fig.4.9 shows the experimental results of output voltage as a function of load1 and load2 for the proposed topology. The measures for both output voltages roughly coincide ( $v_{o1} = v_{o2}$ ) and, therefore, only the voltage  $v_{o1}$  is depicted in this figure. The results show that the

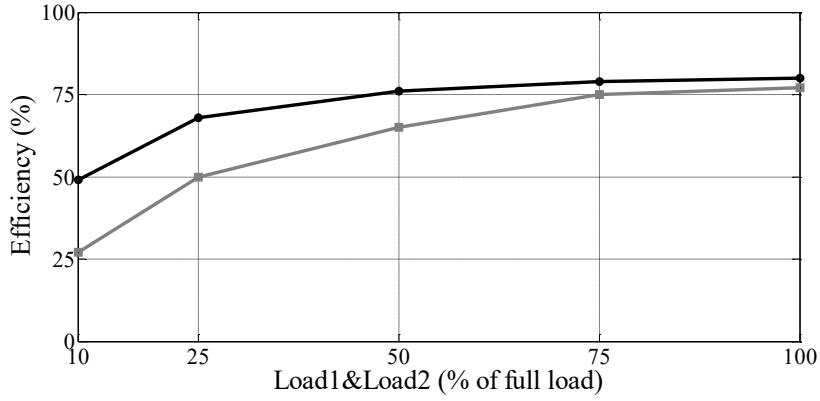


Fig.4.7. Efficiency as a function of load. Conventional topology (grey), proposed topology (black).

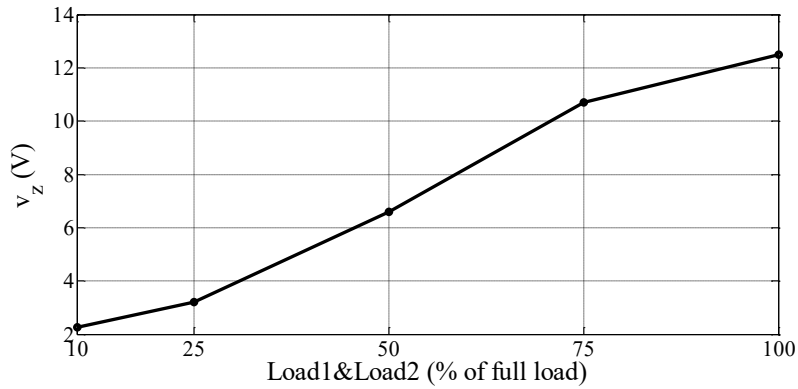


Fig.4.8. Measured input voltage  $v_z$  as a function of load.

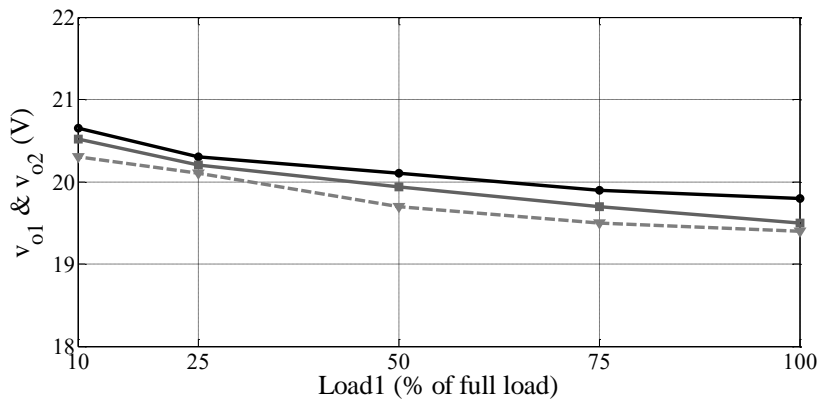


Fig.4.9. Steady state output voltage  $v_{o1}$ ,  $v_{o2}$  as a function of load demand: load2=10%full load and load1 changing (black), load2=load1 both load changing (grey), load2=full load and load1 changing (dash line)

output voltage is approximately constant for all the load conditions when using the proposed topology.

Fig.4.10 illustrates the variation of output voltage  $v_{oi}$  for different clamp position along the primary winding loop. Note that the length of the primary winding loop is 120cm. The experimental measurement for  $v_{oi}$  is obtained alongside the minimum (5cm) to the maximum (60cm) clamp distance from the resonant inverter. As evident, the output voltage is nearly constant in all the clamp positions. This interesting property is achieved due to the constant current  $i_r$  flowing through the primary winding loop.

Fig.4.11 shows the output voltage as a function of air gap variation. It should be noticed that the air gap is defined as the distance between primary and secondary winding. From the figure, by increasing the air gap the output voltage is reduced. As predicted by (4-16), the output voltage depends on the magnetizing inductance and leakage inductance, which vary with the gap distance. Therefore, the mechanism of the clamp connection to the primary winding loop should be considered as an important issue. In fact, a robust mechanical connection to the primary winding loop is necessary to guarantee constant output voltage in the proposed system.

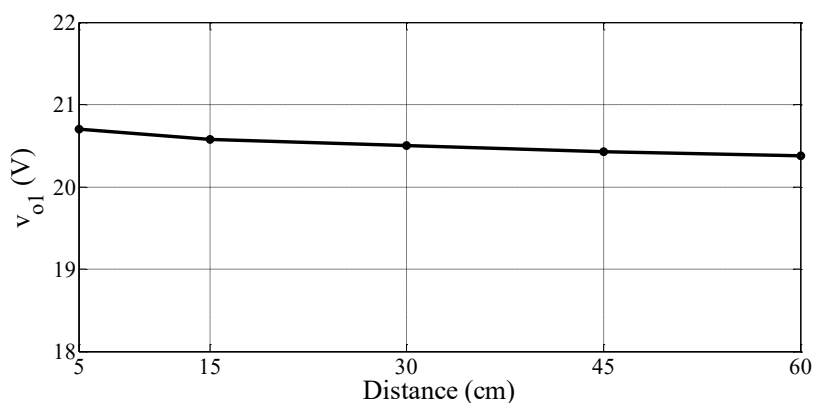


Fig.4.10. Experimental results of the output voltage  $v_{oi}$  as a function of clamp position along the primary winding loop.

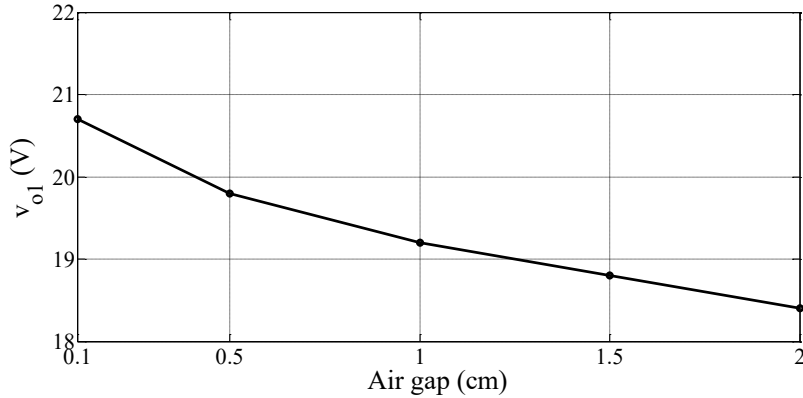


Fig.4.11. Experimental results of the output voltage  $v_{o1}$  as a function of clamp air gap

### 4.5.3. PERFORMANCE IN TRANSIENT STATE

Fig.4.12. shows the main waveforms of the proposed topology in transient state. Fig.4.12. (a) shows the output voltage  $v_{o1}$  and current  $i_{o1}$ , respectively during the step load changes from full load to 10% and return to full load. As predicted theoretically, the output voltage in steady state is independent to the load conditions. As explained before, the proposed system has slow transient response which is expected from a control system without feedback loops. This allows us to identify the practical application of the proposed topology for supplying active DC residential loads with internal post-regulators (laptops, mobile phones, ...). Fig.4.12. (b) illustrates  $i_r$  and  $v_z$ , during step load changes. According to the figure, the input voltage  $v_z$  is automatically changed according to the load conditions. Also, as a consequence of fixed input current provided by buck converter, the amplitude of the resonant current is fixed in all the load conditions.

### 4.5.4. COST COMPARISON

Table.4.4 lists the component count of the conventional and proposed topologies. From the point-of-view of cost, the negative point of the conventional topology is the increasing number of power switches with the number of clamps. In addition, the number of control systems including voltage and current sensors, integrated control circuits and drivers also increase with the number of clamps. In the case of the proposed topology, only the number of power diodes, capacitors and inductors increase with the number of clamps. It is worth mentioning that for a low number of clamps, both topologies have similar cost. However,

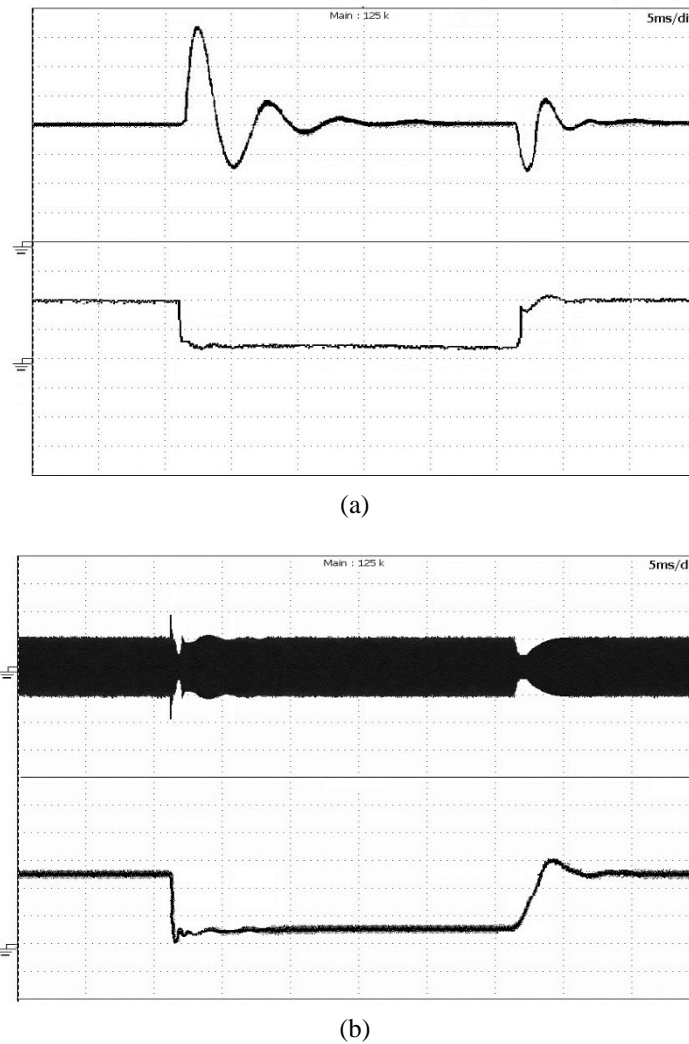


Fig.4.12. Main waveforms of the proposed topology in transient-state. (a) output voltage  $v_{o1}$  and output current  $i_{o1}$ , respectively (5V/div, 100mA/div, 5ms/div). (b) resonant current  $i_r$ , input voltage  $v_z$ , respectively (5V/div, 500 mA/div, 5ms/div).

for a high number of clamps, the cost of the conventional topology increases drastically compared to the cost of the proposed topology. Consequently, the proposed topology is a cost-effective solution when a system with a high number of clamps is required.

Table.4.4. Comparison between conventional and proposed topologies.

Parameters	Conventional	Proposed
	Number of elements	Number of elements
Switch	$4+4n$	5
Diode	0	$1+4n$
Capacitor	$1+n$	$2+2n$
Inductor	1	$2+n$
Transformer	$n$	$n$
Control system	$1+n$	2
Driver	$1+n$	2

## **4.6. CONCLUSION**

A new approach to supply mobile loads with an ICET system has been presented in this chapter. It is based on the cascaded connection of a buck converter operating as a constant current source and high frequency resonant inverter working with only a feed-forward control system. A theoretical tool for the analysis and design of the proposed topology has been introduced. The analysis starts with the development of a static model of the resonant converter based on the first harmonic approximation. The model is simple, predicts accurately the particular properties of the proposed approach, and is useful for the derivation of the design conditions for the converter components. In addition, a systematic step-by-step procedure has been proposed to design the converter components. The theoretical analysis has been practically validated by selected experimental results. The properties of the proposed approach have been compared with the properties of the conventional approach, resulting in higher efficiency and lower cost. In particular, the cost is more competitive as the number of mobile receivers of the system increases.

## CHAPTER 5

---

### Conclusions and future work

---

#### Summary

---

<b>5.1 OVERVIEW.....</b>	<b>99</b>
<b>5.2 MAIN RESULTS AND CONTRIBUTIONS.....</b>	<b>99</b>
<b>5.3 OUTLOOK AND PERSPECTIVES.....</b>	<b>101</b>

---

This chapter presents the overview of the proposed thesis. Also, it has a discussion on the main results and innovative contributions. The main results are classified into the different section according to the objectives of each chapter. Finally, the future works are presented and explained in detail.



## **5.1. OVERVIEW**

This thesis addresses the design, analysis and implementation of the ICET system with multiple clamps in residential areas. As mentioned, the ICET system has been developed and investigated widely. However, few attempts have been made to bring this technology into the residential area which traditionally is supplied with the conventional energy distribution system. The ICET system due to several benefits could be a good alternative to the conventional distribution system.

In the preamble of this thesis, the state-of-the-art and current researches dealing with ICET system have been presented. Also, a classification for the ICET applications are introduced according to power level and place of use. In fact, the current applications are mostly working with single load and often not optimized. Hence, there is an obvious lack of design and optimization methods applicable to an ICET system with multiple clamps. The objectives of this thesis are used to fill this gap. To achieve this goal, the concept of the problem is separated into multiple subsections. These subsections present several solutions from different perspectives for the ICET with multiple clamps. Such as adaptive control algorithm in Chapter 2 which is the key point of this thesis, which give the possibility to have an ICET system with long primary winding loop and always efficient. This algorithm operates without direct information about the load consumption and always update the input current as an optimal value. Moreover, a partially-controlled system has been introduced and compared in Chapter 3. Also, several modulation techniques have been presented and the principle of operation of ICET with them are discussed. Furthermore, from the cost and simplicity point of view, a simple and cost-effective system is presented in Chapter 4 which is operating well and nearly constant output voltage is achieved for all the load conditions. It would be indeed easy to use this information for further research and development by engineers and researchers. In fact, there are several unsolved challengeable problems which could be solved in future works. Finally, to validate the proposed modeling and optimization methods, a low power prototype is designed, built and successfully tested.

## **5.2. MAIN RESULTS AND CONTRIBUTIONS**

The main results and original contributions of this thesis are presented in following points

- *The adaptive control algorithm for ICET system with multiple clamps:* A new control method based on the estimation of the load consumption by using an indirect information from the primary control signal was presented in Chapter 2. The proposed algorithm is applicable to the multiple mobile clamps and it deals with load step changes. The proposed control significantly improves the system efficiency, especially in low load conditions.
- *The partially-controlled system for the ICET applications:* A new partially-controlled system as an alternative to the conventional fully-controlled topology has been presented in Chapter 3. The features of the new topology were obtained by considering several modulation techniques, including frequency modulation, phase modulation and quantum modulation. The performance of the new topology has been evaluated and the best modulation technique has been identified.
- *A simple, efficient and cost-effective topology to supply residential loads with multiple clamps (see Chapter 4):* The new topology was presented based on the cascaded connection of a buck converter and a high frequency resonant inverter loaded by several output passive rectifiers. The proposed system includes a sliding transformer to supply the mobile loads, leading to a safe and flexible location of loads.
- *Mathematical modeling of an ICET system by including the effect of magnetizing and leakage inductance (see Chapter 4):* The analysis of the proposed topology was carried out with a mathematical model based on the first harmonic approximation. By using the derived model, a systematic design procedure was introduced in order to get constant output voltages in all the loads and also for different load conditions.
- *Design procedure for the resonant components of the partially-controlled ICET system (see Chapter 4):* The design process considered the effects of the resonant frequency, magnetizing inductance, and characteristic impedance. By taking into account all these parameters, the component values to have an ICET system with

a fixed output voltage are obtained. Moreover, the effect of each parameter on system performance is analyzed.

- *Implementation of the ICET system with two mobile clamps:* A new prototype to supply two mobile clamps have been built and tested, as shown in Chapter 4. The prototype can supply the movable load such as laptop, grass cutter and tablet. The new system is simple and cost-effective and it is a good alternative to the conventional system. The maximum efficiency of the proposed system is obtained at full load, being 80% in practice.

### 5.3. OUTLOOK AND PERSPECTIVES

Some possible future works related to this thesis are summarized in the following points:

- *Considering the effect of magnetizing and leakage inductance in adaptive control algorithm:* In the proposed adaptive control system the effect of magnetizing and leakage inductance is neglected in order to simplify the mathematical modeling. In future works these elements could be considered in the mathematical model to achieve a high robust control system.
- *Implementation of adaptive control system to validate the theoretical analysis:* In this thesis only theoretical analysis of the adaptive control algorithm has been presented. In future work this algorithm could be tested experimentally. Also the effect of the number of clamps on the system operation should be experimentally tested.
- *Analysis the effect of different resonant tank configurations on ICET topology with multiple clamps:* This thesis only addressed the ICET system with series resonant converter. As we know, several configurations such as parallel or series parallel could be implemented in resonant tank. The analysis of these configurations on ICET system with multiple clamps could be considered for future works.
- *Implementation of current source topology:* This thesis focused in voltage source converters. It is well known that current source converters can provide different

features, but they are not considered for ICET systems. Therefore, the implementation of the ICET system with a current source for future works is recommended.

- *Prototype*: Only a low power prototype has been implemented to validate the theoretical predictions. It could be interesting to realize a large one that integrates the digital control for desired detection and local activation.

Despite these possible improvements, this thesis has successfully proven the feasibility of the ICET system with multiple clamps. Still there are many challengeable problems to solve in ICET systems with multiple clamps. As researchers will solve these problems, then a door will open to future applications for these systems.

In conclusion, the ICET system has been gaining more and more success and reputation in industry and academic area. We strongly recommend this system for residential area due to its especial futures. We hope will see the first commercial product in close future.

## BIBLIOGRAPHY

- [1] Tesla's experiments. [Online], <http://www.neuronet.pitt.edu>, September 2013.
- [2] H. E. S. Jr., J. C. Schuder, and J. W. Mackenzie. "Energy transport through tissue by inductive coupling". *The American Journal of Surgery*, 114(1):87 – 94, 1967.
- [3] A. Ahlbom, U. Bergqvist, J. H. Bernhardt, J. Cesarini, L. A. Court, M. Grandolfo, M. Hietanen, A. F. Mckinlay, M. H. Repacholi, D. H. Sliney, J. A. J. Stolwijk, M. L. Swicord, L. D. Szabo, M. Taki, T. S. Tenforde, H. P. Jammet, and R. Matthes. "Guidelines for limiting exposure to time-varying electric, magnetic, and electromagnetic fields (up to 300 GHz)". *International Commission on Non-Ionizing Radiation Protection. Health Phys*, 74(4):494–522, Apr. 1998.
- [4] The maximum power transfer as a function of the coils size and the frequency with respect to the health restrictions recommended by the international commission on non-ionizing radiation protection. [Online], <http://www.wirelesspowerconsortium.com>, September 2013.
- [5] The wireless power consortium. [Online], <http://www.wirelesspowerconsortium.com/>, September 2015.
- [6] Contactless Energy Transfer, [Online], <http://www.seweurodrive.com>
- [7] Kazmierkowski, M.P. ; Moradewicz, A.J: "Contactless energy transfer (CET) systems -A review", *Power Electronics and Motion Control Conference (EPE/PEMC)*, 2012 15th International, Novi Sad, Sept 2012.
- [8] J. Boys, M. P. Kazmierkowski, E. Lomonova, U. Madawala, G. Covic, Special Section on "Contactless Energy Transfer Systems", *IEEE Transactions on Industrial Electronics*, vol. 60, No. 1, 2013.
- [9] M. G. L. Roes, J. L. Duarte, M. A. M. Hendrix and E. A. Lomonova, "Acoustic Energy Transfer: A Review", *IEEE Transactions on Industrial Electronics*, vol. 60, no. 1, pp. 242-248, Jan. 2013.
- [10] R. M. Dickinson, "Wireless power transmission technology state of the art - The first Bill Brown lecture," *Acta Astronautica*, vol. 53, no. 4-10, pp. 561–570, 2003.
- [11] M. P. Kazmierkowski, A. Moradewicz, J. Duarte, E. Lomonova and Ch. Sonntag, Chapter 35 "Contactless Energy Transfer" in *The Industrial Electronics Handbook, Part II: Power Electronics and Motor Drives*, Second Edition, Edited by B. M. Wilamowski, J. David Irvin, CRC Press, 2011.
- [12] A. Tomaszuk, A. Krupa, "High efficiency high step-up DC-DC converters – a review", *Bulletin of Polish Academy of Science Technical Science*, vol. 59, no. 4, 2011, pp. 475-483.
- [13] E. Waffenschmidt and T. Staring, "Limitation of inductive power transfer for consumer application," in *Proc. European Conf. Power Electronics and Applications*, vol. 1, Sep. 2009, pp. 1–10.
- [14] X. Bao, W. Biederman, S. Sherrit, M. Badescu, Y. Bar-Cohen, C. Jones, J. Aldrich, and Z. Chang, "High-power piezoelectric acoustic-electric power feed thru for metal walls," in *Soc. Photo-Optical Instr. Eng. (SPIE), Conf. Series*, vol. 6930, Apr. 2008.
- [15] Y. Hu, X. Zhang, J. Yang, and Q. Jiang, "Transmitting electric energy through a metal wall by acoustic waves using piezoelectric transducers", *IEEE Transactions on Ultrasonics, Ferroelectrics, and Frequency Control*, vol. 50, no. 7, pp. 773–781, Jul. 2003.
- [16] D. E. Raible, D. Dinca, and T. H. Nayfeh, "Optical frequency optimization of a high intensity laser power beaming system utilizing VMJ photovoltaic cells," in *Proc. Int Space Optical Systems and Applications (ICSOS) Conf*, May 2011, pp. 232–238.

- [17] A. Sahai and D. Graham, "Optical wireless power transmission at long wavelengths," in *Proc. Int Space Optical Systems and Applications (ICSOS) Conf*, May 2011, pp. 164–170.
- [18] C. Liu, A.P. Hu,: "Steady state analysis of a capacitively coupled contactless power transfer system", in *Proc. IEEE Int. Conf. Energy Conversion Congress and Exposition*, San Jose, USA, 2009, pp. 3233–3238.
- [19] C. Liu, A.P. Hu, N.-K.C. Nair, "Modelling and analysis of a capacitively coupled contactless power transfer system", *IET Power Electronics*, vol. 4, Issue 7, 2011, pp. 808-8015.
- [20] M. P. Theodoridis, "Effective Capacitive Power Transfer", *IEEE Transactions on Power Electronics*, vol. 27, No. 12, Dec., 2012, pp. 4906-4913
- [21] A. Esser, H. Ch. Skudelny: "A New Approach to Power Supply for Robots", *IEEE Trans. on Ind. Applications*, vol. 27, No. 5, 1991, pp. 872-875.
- [22] A. Esser: "Contactless Charging and Communication for Electric Vehicles", *IEEE Industry App. Magazine*, Nov./Dec., 1995, pp. 4-11.
- [23] A. J. Moradewicz: "*Contactless Energy Transmission System with Rotatable Transformer – Modeling, Analyze and Design*", PhD-Thesis, Electrotechnical Institute (IEI), Warsaw, Poland, 2008.
- [24] A. J. Moradewicz, M. P. Kazmierkowski: "Contactless Energy Transfer System with FPGA controlled Resonant Converter", *IEEE Trans. on Industrial Electronics*, vol. 57, No.9, 2010, pp. 3181-3190.
- [25] A. J. Moradewicz, M. P. Kazmierkowski: "High Efficiency Contactless Energy Transfer System with Power Electronic Resonant Converter", *Bulletin of the Polish Academy of Sciences Technical Sciences*, vol. 57, No. 4, 2009, pp. 375-381.
- [26] Y. Fujita, A. Hirotsune, Y. Amano: "Contactless Power Supply for Layer-Selection Type Recordable Multi-Layer Optical Disk", *IEEE Optical Data Storage Topical Meeting*, 2006 (CD).
- [27] Dukju Ahn; Songcheol Hong, "Effect of Coupling Between Multiple Transmitters or Multiple Receivers on Wireless Power Transfer," *IEEE Trans. on Industrial Electronics*, vol.60, no.7, pp.2602-2613, July 2013.
- [28] Schmidt, H.-P.; Fuchs, A.; Fuchs, S., "Simultaneous contact less charging of multiple electric vehicles: Contact less power and data transfer for multiple distributed loads," in *Electric Drives Production Conference (EDPC), 2014 4th International*, vol., no., pp.1-3, Oct.2014.
- [29] Ch. Apneseth, D. Dzung, S. Kjesbu, G. Scheible, and W. Zimmermann, "Introduction wireless proximity switches". *ABB Rev.*, 4/2002, pp. 42-49.
- [30] K. O'Brien, G. Scheible, H. Gueldner: "Analysis of Wireless Power Supplies for Industrial Automation Systems". *In Proc. Of IEEE-IECON'03*, (CD).
- [31] G. Scheible, J. Endersen, D. Dzung, J. E. Frey: "Unplugged but Connected: Design and Implementation of a Truly-Wireless Real-Time Sensor/Actuator Interface", *ABB Review*, No. 3 and 4, 2005, pp. 70-73 and 65-68.
- [32] K. D. Papastergiou, D. E. Macpherson: "An Airborne Radar Power Supply with Contactless Transfer of Energy—Part I: Rotating Transformer" and Part II: Converter Design, *IEEE Trans. on Industrial Electronics*, vol. 54, no. 5, October 2007, pp. 2874-2893.
- [33] R. Mecke, C. Rathage: "High frequency resonant converter for contactless energy transmission over large air gap". *In Proc. Of IEEE-PESC*, Aachen 2004, pp.1737-1743.
- [34] J. T. Boys, G. A. J. Elliot: "An Appropriate Magnetic Coupling Co-Efficient for the Design and Comparison of ICPT Pickups", *IEEE Trans. on Power Electronics*, Vol. 22, No. 1, Jan., 2007, pp. 333-335.

- [35] J. Lastowiecki and P. Staszewski: "Sliding Transformer with Long Magnetic Circuit for Contactless Electrical Energy Delivery to Mobile Receivers", *IEEE Trans. on Industrial Electronics*, vol. 53, No 6, 2006, pp. 1943-1948.
- [36] J. Meins, R. Czainski, F. Turki: "Phase characteristics of resonant contactless high power supplies", *Przegląd Elektrotechniczny (Electrotechnical Review)*, Nr 11/2007, pp. 10-13.
- [37] G. A. Covic, J. T. Boys, M. L. G. Kisin, H. G. Lu: "A Three- Phase Inductive Power Transfer System for Roadway-Powered Vehicles", *IEEE Trans. on Ind. Electronics*, Vol. 54, No. 6, 2007, pp. 3370-3378.
- [38] D. C. Erb, O. C. Onar and A. Khaligh: "Bi-Directional Charging Topologies for Plug-in Hybrid Electric Vehicles" in *Proc. IEEE 35-th Applied Power Electronic Conf. and Exposition (APEC)*, Febr., 2010.
- [39] Y-J. Lee, A. Khaligh and A. Emadi: "Advanced Integrated Bidirectional AC/DC and DC/DC Converter for Plug-In Hybrid Electric Vehicle", *IEEE Trans. on Vehicular Technol.*, vol. 58, No. 8, 2008, pp.3970-3980.
- [40] B. Kramer, S. Chakraborty, B. Kroposki: "A Review of Plug-in Vehicles and Vehicles-to-Grid Capability", in *Proc. IEEE 34-th Annual Conf. On Industrial Electronics – IECON'08*, Nov.2008, pp. 2278-83.
- [41] S. Han and D. Divan: "Bi-Directional DC/DC Converters for Plug-in Hybrid Electric Vehicle (PHEV) Applications", in *Proc. IEEE 23-rd Applied Power Electronic Conference and Exposition (APEC)*, Febr., 2008, pp. 784-789.
- [42] The Westinghouse electric corporation website. [Online], <http://www.westinghouse.com>, September 2015.
- [43] Sonicare Philips Toothbrushes. [www.Sonicare.com](http://www.Sonicare.com)
- [44] E. A. Rose, A. C. Gelijns, A. J. Moskowitz, D. F. Heitjan, L.W. Stevenson, W. Dembitsky, J. W. Long, D. D. Ascheim, A. R. Tierney, R. G. Levitan, J. T. Watson, N. S. Ronan, P. A. Shapiro, R.M. Lazar, L.W. Miller, L. Gupta, O. H. Frazier, P. Desvigne-Nickens, M. C. Oz, V. L. Poirier, and P. Meier: "Long-term use of a left ventricular assist device for end-stage heart failure", *New England Journal of Medicine*, 345(20):1435–1443, 2001.
- [45] H. Wu, A. Hu, P. Si, D. Budgett, C. Tung, and S. Malpas: "A push-pull resonant converter with dual coils for transcutaneous energy transfer systems", in *Proc. Industrial Electronics and Applications, 2009. ICIEA 2009. 4th IEEE Conference on*, pages 1051–1056, may 2009.
- [46] H. Matsuki, M. Shiiki, K. Murakami, K. Nadehara, and T. Yamamoto: "Flexible transcutaneous transformer for artificial heart system", *Magnetics, IEEE Transactions on*, 26(5):1548–1550, sep 1990.
- [47] H. Matsuki, M. Shiiki, K. Murakami, and T. Yamamoto: "Investigation of coil geometry for transcutaneous energy transmission for artificial heart", *Magnetics, IEEE Transactions on*, 28(5):2406–2408, Sep 1992.
- [48] T. Sato, F. Sato, and H. Matsuki: "New functional electrical system using magnetic coils for power transmission and control signal detection", *Magnetics, IEEE Transactions on*, 37(4):2925–2928, jul 2001.
- [49] B. Choi, J. Nho, H. Cha, T. Ahn, and S. Choi: "Design and implementation of low profile contactless battery charger using planar printed circuit board windings as energy transfer device", *Industrial Electronics, IEEE Transactions on*, 51(1):140–147, Feb. 2004.
- [50] H. Chung and M. Pong: "Effect of switching frequency and number of winding layers on copper loss of an inductor", In *Power Electronics and Motion Control Conference, 2000. Proceedings. IPEMC 2000. The Third International*, volume 3, pages 1312–1317 vol.3, 2000.
- [51] Inductive powering mouse. [Online], <http://www.a4tech.com/>, September 2015.

- [52] Contactless energy transfer system for a small dockstation. [Online], <http://www.hpwebos.com/us/products...../accessories/touchstone-technology.html>, September 2015.
- [53] Contactless energy transfer of the ecoupled table. [Online], <http://ecoupled.com/>, September 2015.
- [54] Wireless charging platform. [Online], <http://www.qualcomm.com>, September 2015.
- [55] Wireless charging platform. [Online], <http://www.mojomobility.com/>, September 2015.
- [56] Powermat product line. [Online], <http://www.powermateu.com/H>, September 2015.
- [57] La Jamais Contente. <http://www.e-mobile.ch/pdf/2005/Fact-SheetLaJamaisContente>
- [58] Magne Charge. [http://en.wikipedia.org/wiki/Magne\\_Charge](http://en.wikipedia.org/wiki/Magne_Charge).
- [59] Contactless power system. [Online], <http://www.vahleinc.com>, September 2015.
- [60] B. Klontz, K. W., D. Divan, D. Novotny, R. Lorenz: "Contactless Power Delivery System for Mining Applications", *IEEE Transactions on Industry Applications*, vol.31, N°1, pp. 27-35, Jan./Feb. 1995
- [61] Roberts, G., P. Hadfield, M. Humphries, F. Bauder, J. Izquierdo: "Design and Evaluation of the Power and Data Contactless Transfer Device", 1997 IEEE Aerospace Conference Proceedings, vol.3, pp. 523-533, 1997.
- [62] R. P. Twinaime, D. J. Thrimawithana, U. K. Madawala, and C. A. Baguley: "A new resonant bidirectional DC-DC converter topology," *IEEE Trans. Power Electron.*, vol. 29, no. 9, pp. 4733–4740, Sep. 2014.
- [63] S. Aldhafer, P. Luk, and J. Whidborne: "Tuning class E inverters applied in inductive links using saturable reactors," *IEEE Trans. Power Electron.*, vol. 29, no. 6, pp. 2969–2978, Jun. 2014.
- [64] S. Kim, H.-H. Park, J. Kim, and S. Ahn: "Design and analysis of a resonant reactive shield for a wireless power electric vehicle," *IEEE Trans. Microw. Theory Techn.*, vol. 62, no. 4, pp. 1057–1066, Apr. 2014.
- [65] T. Imura and Y. Hori: "Maximizing air gap and efficiency of magnetic resonant coupling for wireless power transfer using equivalent circuit and Neumann formula," *IEEE Trans. Ind. Electron.*, vol. 58, no. 10, pp. 4746–4752, Oct. 2011.
- [66] A. P. Sample, D. A. Meyer, and J. R. Smith: "Analysis, experimental results, and range adaptation of magnetically coupled resonators for wireless power transfer," *IEEE Trans. Ind. Electron.*, vol. 58, no. 2, pp. 544–554, Feb. 2011.
- [67] S. W. Park, K. Wake, and S. Watanabe: "Incident electric field effect and numerical dosimetry for a wireless power transfer system using magnetically coupled resonances," *IEEE Trans. Microw. Theory Techn.*, vol. 61, no. 9, pp. 3461–3469, Sep. 2013.
- [68] M. Q. Nguyen, Z. Hughes, P. Woods, Y.-S. Seo, S. Rao, and J. Chiao: "Field distribution models of spiral coil for misalignment analysis in wireless power transfer systems," *IEEE Trans. Microw. Theory Techn.*, vol. 62, no. 4, pp. 920–930, Apr. 2014.
- [69] M. Kiani, U.-M. Jow, and M. Ghovanloo: "Design and optimization of a 3-coil inductive link for efficient wireless power transmission," *IEEE Trans. Biomed. Circ. Syst.*, vol. 5, no. 6, pp. 579–591, Dec. 2011.
- [70] F. Pijl, P. Bauer, and M. Castilla: "Control method for wireless inductive energy transfer systems with relatively large air gap," *IEEE Trans. Ind. Electron.*, vol. 60, no. 1, pp. 382–390, Jan. 2013.
- [71] U. K. Madawala and D. J. Thrimawithana: "A bidirectional inductive power interface for electric vehicles in V2G systems," *IEEE Trans. Ind. Electron.*, vol. 58, no. 10, pp. 4789–4896, Oct. 2011.

- [72] U. K. Madawala and D. J. Thrimawithana: "A single controller for inductive power transfer systems," in *Proc. IEEE Ind. Electron. Conf.*, 2009, pp. 109–113.
- [73] Z. N. Low, R. A. Chinga, R. Tseng, and J. Lin: "Design and test of a high-power high-efficiency loosely coupled planar wireless power transfer system," *IEEE Trans. Ind. Electron.*, vol. 56, no. 5, pp. 1801–1812, May 2009.
- [74] A. Kurs, R. Moffatt, and M. Soljačić: "Simultaneous mid-range power transfer to multiple devices," *Appl. Phys. Lett.*, vol. 96, no. 4, 2010, Art. ID 044102.
- [75] C.-S. Wang, O. H. Stielau, and G. A. Covic: "Load models and their application in the design of loosely coupled inductive power transfer systems," in *IEEE Int. Power Syst. Technol. Conf.*, Perth, WA, Australia, 2000, vol. 2, pp. 1053–1058.
- [76] B. L. Cannon, J. F. Hoburg, D. D. Stancil, and S. C. Goldstein: "Magnetic resonant coupling as a potential means for wireless power transfer to multiple small receivers," *IEEE Trans. Power Electron.*, vol. 24, no. 7, pp. 1819–1825, Jul. 2009.
- [77] K. K. Ean, B. T. Chuan, T. Imura, and Y. Hori: "Impedance matching and power division algorithm considering cross coupling for wireless power transfer via magnetic resonance," in *IEEE 34th Int. Telecom. Energy Conf.*, Scottsdale, AZ, USA, 2012, pp. 1–5.
- [78] T. Zhang, M. Fu, C. Ma, and X. Zhu, "Optimal load analysis for a two-receiver wireless power transfer system," in *IEEE Wireless Power Transfer Conf.*, Jeju, Korea, 2014, pp. 84–87.
- [79] D. Ahn and S. Hong: "Effect of coupling between multiple transmitters or multiple receivers on wireless power transfer," *IEEE Trans. Ind. Electron.*, vol. 60, no. 7, pp. 2602–2613, Jul. 2013.
- [80] F. Pijl, P. Bauer, J. A. Ferreira, and H. Polinder: "Quantum control for an experimental contactless energy transfer system for multiple users," in *Proc. IEEE PESC*, 2007, pp. 343–349.
- [81] F. Pijl, M. Castilla, and P. Bauer: "Adaptive sliding mode control for a multiple-user inductive power transfer system without need for communication," *IEEE Trans. Ind. Electron.*, vol. 60, no. 1, pp. 271–279, Jan. 2013.
- [82] F. F. A. Van der Pijl, J. A. Ferreira, P. Bauer, H. Polinder: "Design of an Inductive Contactless Power System for Multiple Users", *Conference Record of the 2006 IEEE 41st IAS Annual Meeting*, Vol. 4, pp. 1876-1883, October 2006.
- [83] M. Castilla, L. García de Vicuña, M. López, and V. Barcons: "An averaged large-signal modelling method for resonant converters," in *Proc. IEEE IECON*, 1997, pp. 447–452 Sep. 2009.
- [84] A. Momeneh, M. Castilla, F. F. A. van der Pijl, R. Guzman and J. Morales: "Architecture and design of an inductive contactless energy transfer system with two mobile loads for residential applications," in *Proc. 17th Eur. Conf. Power Electron. Appl.*, pp. 1-10, Sept.2015.
- [85] S. A. Zotov, I. P. Prikhodko, A. A. Trusov, and A. M. Shkel: "Frequency modulation based angular rate system," in *Proc. IEEE MEMS*, Cancun, Mexico, Jan. 23–27, 2011, pp. 557–580.
- [86] T. R. Albrecht, P. Grutter, D. Horne, and D. Rugar: "Frequency modulation detection using high-Q cantilevers for enhanced force microscope sensitivity," *J. Appl. Phys.*, vol. 69, no. 2, pp. 668–673, Jan. 1991.

- [87] A. A. Trusov, S. A. Zotov, and A. M. Shkel: “High range digital angular rate sensor based on frequency modulation,” U.S. Patent pending, UC Case No. 2011-199.
- [88] Hyun-Wook Seong ; Hyoung-Suk Kim ; Ki-Bum Park ; Gun-Woo Moon ; Myung-Joong Youn: “High Step-Up DC-DC Converters Using Zero-Voltage Switching Boost Integration Technique and Light-Load Frequency Modulation Control” *IEEE Trans. Power Electron.*, vol. 27, no. 3, pp. 1383- 1400, July. 2011.
- [89] L. A. Barragan, D. Navarro, J. Acero, I. Urriza, and J. M. Burdio: “FPGA implementation of a switching frequency modulation circuit for EMI reduction in resonant inverters for induction heating appliances,” *IEEE Trans. Ind. Electron.*, vol. 55, no. 1, pp. 11–20, Jan. 2008.
- [90] M.K. Kazimierczuk, D. Czarkowski, Resonat power converters.NewYork, A *Wiley-Interscience*, 1995, pp. 149–199.
- [91] J. T. Matysik: “The current and voltage phase shift regulation in resonant converters with integration control,” *IEEE Trans. Ind. Electron.*, vol. 54, no. 2, pp. 1240–1242, Apr. 2006.
- [92] S. Zheng and D. Czarkowski, “Modeling and digital control of a phase controlled series–parallel resonant converter,” *IEEE Trans. Ind. Electron.*, vol. 54, no. 2, pp. 707–715, Apr. 2007.
- [93] Y. Lu, K. W. E. Cheng, and S. L. Ho: “Quasi current mode control for the phase-shifted series resonant converter,” *IEEE Trans. Power Electron.*, vol. 23, no. 1, pp. 353- 358, Jan. 2008.
- [94] J. Sosa, M. Castilla, J. Miret, L. García de Vicuña, and J. Matas: “Modeling and performance analysis of the DC/DC series-parallel resonant converter operating with discrete self-sustained phase-shift modulation technique”, *IEEE Trans. Ind. Electronics*, vol. 56, no. 3, pp. 697-705, March 2009.
- [95] M. Castilla, L. G. de Vicuna, J. Matas, J. Miret, and J. C. Vasquez: “A comparative study of sliding-mode control schemes for quantum series resonant inverters,” *IEEE Trans. Ind. Electron.*, vol. 56, no. 9, pp. 3487–3495, Sep. 2009.
- [96] D. Cortes, N. Vazquez, and J. Alvarez-Gallegos: “Dynamical sliding-mode control of the boost inverter,” *IEEE Trans. Ind. Electron.*, vol. 56, no. 9, pp. 3467–3476, Sep. 2009.
- [97] L. G. de Vicuna, M. Castilla, J. Miret, J. Matas, and J. M. Guerrero: “Sliding-mode control for a single-phase ac/ac quantum resonant converter,” *IEEE Trans. Ind. Electron.*, vol. 56, no. 9, pp. 3496–3504, Sep. 2009.
- [98] A. Momeneh, M.Castilla, F. F. Van der Pijl, M. Moradi, J. Torres: “New inductive contactless energy transfer system for residential distribution networks with multiple mobile loads,” in *Proc. 17th Eur. Conf. Power Electron. Appl.*, pp. 1-10, Sept.2015.
- [99] R. L. Steigerwald: “A comparison of half–bridge resonant converter topologies,” *IEEE Trans. Power Electron.*, vol. 3, no. 2, pp. 174–182, Apr. 1988.